A STUDY OF METHODS TO MEASURE THE EFFECTS OF A CONTAMINATED ATMOSPHERE ON THE TRANSMISSION OF A HIGH ENERGY LASER BEAM

FINAL REPORT

Prepared by

AVCO MISSILES, SPACE AND ELECTRONICS GROUP
SPACE SYSTEMS DIVISION
201 Lowell Street
Wilmington, Massachusetts 01887

AVSSD-0183-67-RR
Contract DA-18-001-AMC-957(X)

May 1967

Prepared for

BALLISTIC RESEARCH LABORATORIES
UNITED STATES ARMY
ABERDEEN PROVING GROUND
Aberdeen, Maryland

Short Title Ref: AVSSD-0183-67-RR
Avco Doc. Acctg. No. _____
This Document Consists of 152 Pages.

A STUDY OF METHODS TO MEASURE THE EFFECTS OF A CONTAMINATED ATMOSPHERE ON THE TRANSMISSION OF A HIGH ENERGY LASER BEAM

FINAL REPORT

Prepared by

AVCO MISSILES, SPACE AND ELECTRONICS GROUP
SPACE SYSTEMS DIVISION
201 Lowell Street
Wilmington, Massachusetts 01887

AVSSD-0183-67-RR
Contract DA-18-001-AMC-957(X)

May 1967

Prepared for

BALLISTIC RESEARCH LABORATORIES
UNITED STATES ARMY
ABERDEEN PROVING GROUND
Aberdeen, Maryland

SUMMARY

The following report covers the work performed on contract DA-18-001-AMC-957(X), "A Study of Methods to Measure the Effects of a Contaminated Atmosphere on the Transmission of a High Energy Laser Beam." The report contains an analyses of the effects which may be expected, and describes experiments with which these effects may be observed. Breadboard experiments to verify various techniques have been performed, and are included in this report. Finally, the specifications of experimental apparatus in which laser beam experiments (at pressures of up to 10 atmospheres) can be performed are included.

Work on this contract was performed by R. Schlier, R. Penndorf, H. Ceccon, E. Neister, H. Dolazalek, and J. Culbert.

CONTENTS

ILLUSTRATIONS

ILLUSTRATIONS (Concl'd)

ACKNOWLEDGEMENTS

The information which led to the design of an aerosol generator was mainly obtained from Doctors Baust and Rau of the University of Heidelberg and Dr. Jaenicke of the University of Mainz.

1.0 INTERACTION OF LASER RADIATION WITH AEROSOL PARTICLES

1.1 INTRODUCTION

The manner in which intense laser radiation interacts with particulate matter depends upon the type of particles, their size and geometry; upon the intensity and duration of the laser radiation; and upon the wavelength of the radiation. The interaction, in turn, affects the manner in which the radiation is propagated through the atmosphere containing the particles. In the following discussion, various interactions of laser radiation will be described, along with the effects of such interactions on the propagation of the beam. Finally, the experimental methods by which the effects can be observed will be discussed.

The interaction phenomena will be divided into approximate regimes: The low-intensity regime, where the bulk of the phenomena are independent of laser-beam intensity; the intermediate-intensity regime, where heating and perhaps vaporization of the particles can occur; and the high-intensity regime, where the effects are highly intensity-dependent.

1.2 THE LOW-INTENSITY REGIME

At low laser-beam intensities, the dominant phenomena are scattering and attenuation of the beam. Even if the particles can absorb energy from the beam, the temperature rise of the particles is not enough to either affect the optical properties of the particles or, by thermal conduction, to change the temperature of the ambient gas. Investigations in this regime are, consequently, primarily concerned with the measurement of scattering and attenuation.

The major influence of the use of laser radiation, which is coherent rather than incoherent radiation, will be the effect of the coherence of the radiation. Laser radiation, in comparison to ordinary thermal radiation, is characterized by a large "coherence volume", in contrast to the small coherence volume of thermal light.

As a consequence, the laser light irradiating a large number of aerosol particles is in phase, and the scattered light from these various particles has a definite phase relationship. It is no longer sufficient to assume that the total amount of scattered light is the sum of the light scattered by each particle. Rather the amplitude of the light scattered by each particle must be summed, and the intensity determined from the summed amplitude.

In a scattering measurement, a finite volume of scattering centers is viewed, and the total intensity of the scattered radiation is observed. If there are a small number of scattering centers, and the effective aperture of the scattering detector is small, then it could be expected that the observed scattering intensity

would show large variations as the relative positions of the particles changed. If a Q-switched laser pulse was used as the light source, the particles would remain essentially stationary during each pulse, but variations in the scattering from pulse to pulse could be observed.

On the other hand, if there are a large number of scattering centers in the region observed, then the individual light waves, scattered from each particle, arrive at the detector with a random-phase relationship. There is not a complete cancellation, however, because of fluctuations, and the intensity observed in this case should be proportional to the number of scattering centers observed. This has been borne out by the observations of Rayleigh scattering reported by Watson and Clark, who used a Q-switched laser as a light source.

Scattering measurements, then, using laser light sources, must be performed with care. In particular, the number of scattering centers observed must be considered, since a small number will lead to a considerable variation in the observed scattering cross-section.

In an experimental sense, these coherence effects will show up as a departure from the scattering and attenuation expected from a non-coherent source, or calculable from theory. Since theoretical calculations are restricted to a small class of particles -- namely spheres, and the aerosols ultimately studied may not be spherical in shape, it is worthwhile to consider measurements with an incoherent source, as well as measurements with a laser source. An incoherent source can be constructed from a thermal source (i. e., a tungsten lamp) and a suitable filter, operating on the same wavelength as the laser source. The coherence length of a light source is approximately

$$L_{coh} = \frac{\lambda^2}{\Delta\lambda} \quad ;$$

for a ruby laser beam, $\lambda \cong 7 \times 10^{-5}$ centimeters, and $\Delta\lambda = 10^{-9}$ centimeters, so that the coherence length is about 5 centimeters.

To assure that the scattering can have no coherence effects, the coherence length of the radiation should be less than the average particle separation. Thus, since the average particle separation is approximately the inverse cube of the concentration, the band pass of the filter on an incoherent source should be

$$\Delta\lambda \gtrsim n^{1/3} \lambda^2 \quad ,$$

for a wavelength of 7000 Å; $\Delta\lambda$ should be about 5 Å for a concentration of 10^3 particles/cm^3; and 50 Å for a concentration of 10^6 particles/cm^3. For all practical purposes, a 50 Å should be sufficiently wide to ensure a short coherence length, and also be narrow enough so that the individual particle scattering of the incoherent light approximates the scattering of the narrow bandwidth laser light.

The intensity of the light available from the filtered thermal source is quite low. In a 50 Å band about 6943 Å, the brightness of a source at 3000 Å is approximately 0.37 watts/cm^2 steradian. In contrast, a 1-milliwatt gas-laser beam has a brightness of over 3×10^4 watts/cm^2 steradian. The intensity of the beam from the incoherent source is therefore limited to about a factor of 10^5 below that attainable with a 1-milliwatt gas laser, and the techniques used to measure scattering and attenuation must be correspondingly more restrictive.

1.3 THE MODERATE INTENSITY REGIME

1.3.1 Introduction

As the laser intensity and/or pulse direction is increased, the effect of the energy absorbed by the particles in the path of the beam becomes apparent. At relatively low intensities, the particles will be heated, but otherwise unaffected. The increased particle temperature will in turn increase the temperature of the surrounding gas, causing it to expand, with a consequent reduction in density and refraction index. This effect, called the Brueckner effect, will result in a divergence of the beam propagated through the gas.

1.3.2 Particle Melting

First, consider the rate of temperature increase of the particles themselves. The rate of temperature increase of a small particle, in the absence of energy-loss effects, is

$$\frac{dT}{dt} = \frac{3\,\sigma_{abs}\,I}{4\pi\,r_o^{\,3}\,\rho_p\,C_v}\ , \tag{1}$$

if thermal conductivity in the particle itself is neglected. The σ_{abs} is the absorption cross section, I the intensity, r_o the particle radius, ρ_p the particle density, and C_v the specific heat.

The rate of temperature loss of the particle is

$$\frac{dT}{dt} = -\frac{3}{4\pi\,r_o^{\,3}\,\rho_p\,C_v}\left[4\pi\,r_o\,k\,(T - T_o) + 4\pi\,r_o^{\,2}\,\epsilon\sigma\,(T^4 - T_o^{\,4})\right]\ , \tag{2}$$

where ϵ is the thermal emissivity, σ is the Stephan-Boltzmann constant, k is the thermal conductivity of the air, and T_o is the surrounding temperature. The net rate of change of temperature is

$$\frac{dT}{dt} = \frac{3}{4\pi\,r_o^{\,3}\,\rho_p\,C_v}\left[\sigma_{abs}\,I - 4\pi\,r_o\,k\,(T - T_o) - 4\pi\,r_o^{\,2}\,\epsilon\sigma\,(T^4 - T_o^{\,4})\right]\ . \tag{3}$$

In the above equations, thermal diffusivity effects have been neglected. This neglect is justified for laser pulse durations which are large, on the order of 1 millisecond, and particles which are small. It is not justified for laser pulse durations typical of Q-switched devices.

Even under extreme conditions, the third term in the right-hand side of the equation (the radiation loss term), can be neglected for small particles and temperatures under 2000° K. The temperature rate of change equation is then

$$\frac{dT}{dt} = \frac{3}{4\pi r_o^3 \rho_p C_v} \left[\sigma_{abs} I - 4\pi r_o k (T - T_o)\right] , \tag{4}$$

and this can be integrated to give:

$$T = T_o + \frac{\sigma_{abs} I}{4\pi r_o k} \left(1 - e^{-\frac{3kt}{\rho_p C_v r_o^2}}\right) . \tag{5}$$

Now, for most materials, ρC_v is on the order of 1 joule/cm^3 ° K. For air, k is 2.3 x 10^{-4} joules/cm-sec° K. Thus the time required to reach the equilibrium temperature is on the order of 1.5 x 10^3 r_o^2 seconds, for r_o in centimeters. For particles which are much smaller than 10 μ in radius, the equilibrium temperature will be reached in a time which is short compared to the millisecond duration typical of long-pulsed lasers. On the other hand, the particle will not reach the equilibrium temperature in the time typical of a Q-switched laser pulse, unless its radius is less than 0.1 μ. If the particle is larger than 0.1 μ in radius, and the pulse is short, the temperature attained is approximately

$$T = T_o + \frac{3\sigma_{abs} It}{4\pi r_o^3 \rho C_v} \tag{6}$$

Now consider some numerical examples. The absorption cross section of a spherical particle can be calculated from its optical properties. For a particle which is small compared to a wavelength of light, the cross section is

$$\sigma_{abs} \quad \frac{48\pi r^3}{\lambda} (\mu k_o) / [(\mu^2 - k_o^2 + 2)^2 + 4\mu^2 k^2)] . \tag{7}$$

For a particle which is large, it is

$$\sigma_{abs} = \pi r_o^2 (4\mu)/[(\mu + 1)^2 + k_o^2] , \tag{8}$$

μ is the index of refraction, k_o the extinction coefficient, and λ the wavelength. This expression is approximate, but is fairly close to the exact expression. Now, if a copper sphere is chosen as an example (this would be representative of a highly absorbing material), it turns out that, for μ = 0.44 and k_o = 3.26 at 6500 Å,

$$\sigma_{abs} = 2 \times 10^{3} \pi r_o^{3} \quad , \tag{9}$$

for a small particle, and

$$\sigma_{abs} = 0.139 \pi r_o^{2} \tag{10}$$

for a large particle.

$\rho_p C_v$ for copper is about 3.5 joules/cm^3 ° K. Thus the temperature equations are, for a small copper particle,

$$T = T_o + 2.16 \times 10^{6} I r_o^{2} \left(1 - e^{- \frac{1.97 \times 10^{-4} t}{r_o^{2}}} \right), \tag{11}$$

and for a large copper particle,

$$T = T_o + 1.51 \times 10^{2} I_o r_o \left(1 - e^{- \frac{1.97 \times 10^{-4} t}{r_o^{2}}} \right) \quad . \tag{12}$$

Also consider a slightly absorbing dielectric particle. Here μ is about 1.5, and k_o is small. Then, for a small particle,

$$\sigma_{abs} = 6 \times 10^{4} \pi r_o^{3} k_o \quad , \tag{13}$$

$$T = T_o + 6.5 \times 10^{7} r_o^{2} k_o I \left(1 - e^{- \frac{6.9 \times 10^{-4} t}{r_o^{2}}} \right), \tag{14}$$

if $\rho_p C_v = 1$.

The last equation should also be applicable to a large particle, provided that the extinction coefficient k_o is much less than the wavelength divided by the particle radius. Since, in the case of interest, r_o is less than 10^{-3} centimeter, the equation should be applicable for k_o of 10^{-2} or less. A material with a k_o of 10^{-3} is still highly absorbing, since it will absorb the radiation in a distance of about 10^{-1} centimeter. The k_o is the extinction coefficient of the material expressed in units of wavelength, rather than distance in conventional units.

Estimates can now be made of the laser intensity required to cause an appreciable temperature increase in the particle. First, consider a long-pulse laser, which has an upper limit, in the unfocused beam, of about 10^5 watts/cm^2 on the average. For a copper particle of radius 10^{-3} centimeter, and a pulse

duration of 10^{-3} seconds, the temperature increase, according to Equation (12) would be 2700°C. A 10^{-5} centimeter radius particle would attain a temperature of only 21°C, and a 10^{-4} centimeter radius particle would reach a temperature in the vicinity of 2000°C.

For the dielectric particle, the temperature increase for a radius of 10^{-3} centimeter would be 3000°C at a k_o of 10^{-3}, 65°C for a radius of 10^{-4} centimeter, and only 0.65°C at 10^{-5} centimeter.

The above discussion, with numerical examples, indicates that only for large particles (greater than 1 micron) would effects such as melting and vaporization be expected, even for fairly absorbent dielectrics. With particles as small as 0.1 micron, the temperature increase is very small for intensities attainable with unfocused long-pulse lasers.

Except for the largest particles, most of the energy absorbed by the particles is conducted into the gas, during the long pulse. The effect on the optical path, therefore, would be primarily that of a change in index of refraction of the path, rather than a change in the properties of the aerosol particles in the path.

For a Q-switched laser pulse, the time required to attain equilibrium, except for the smallest particles, is longer than the pulse duration. The temperature attained then depends upon the energy-per-unit-area transmitted by the beam, rather than the intensity. For the copper particles, the temperature increase is

$$T = 4.3 \times 10^2 E \quad , \tag{15}$$

for a small particle, and

$$T = 3 \times 10^{-2} E/r_o \quad , \tag{16}$$

for a large particle. For a dielectric particle with extinction coefficient k_o, the increase is

$$T = 4.5 \times 10^4 k_o E \quad . \tag{17}$$

The Q-switched case is clearly different from the long-pulse case. The highest temperatures are obtained with particles which are small compared to a wavelength, in contrast to the long-pulse case in which the high temperatures are associated with larger particles.

Q-switched energy densities, in the unfocused beam, are limited to about 10 joules/cm^2, if damage effects on optical components are to be avoided. It should be noted that 2.5 joules/cm^2 would be required to raise a copper particle to its melting point, if the particle were small. If the particle were large, a correspondingly larger energy would be required, in the absence of thermal

conductive effects to be discussed later.

1.3.3 Thermal Diffusivity Effects

In the preceding discussion, the finite time required to transmit thermal energy in a material was neglected. This neglect is legitimate for small particles and long pulse times, and for slightly absorbing particles, since the latter are more or less uniformly heated. However, for materials with large extinction coefficients, the energy is absorbed in the material in a very short distance, and the surface temperature becomes correspondingly large.

First consider the case in which the particle is large. Then, for short pulse times, only the portion of the particle near the surface is heated during the pulse, and the temperature is the solutions of the heat equation

$$\nabla^2 T = \frac{\rho_p C_{v_p}}{k_p} \partial T/\partial t \tag{18}$$

which is applicable for short times. This solution is

$$T = \frac{2A I \sqrt{t}}{\sqrt{\pi \rho_p C_v k_p}} + T_o \quad , \tag{19}$$

when A is the absorptivity, ρ_p, C_{v_p}, k_p are the densities, specific heat, and conductivity of the particle, respectively.

For copper, $A = 0.139$, $\rho_p C_v = 3.5$ joules/cm^3, and $k_p = 4$ joules/cm sec °K. Thus, for short pulse times, the surface temperature of the copper is, from Equation (19)

$$T = 4.2 \times 10^{-2} I \sqrt{t} + T_o \quad . \tag{20}$$

For the small particles previously discussed, the temperature rise is, from Equation (15)

$$T = 4.3 \times 10^{2} I t \quad ,$$

so that the diffusivity-limited temperature applies for times short compared to 10^{-8} seconds, for very small particles. For large particles, the temperature rise is, from Equation (16),

$$T = 3 \times 10^{-2} I t/r_o$$

and the diffusivity-limited temperature applies to times short compared to $2 r_o^2$ seconds.

For particles larger than 1 μ, the surface temperature is considerably higher than the temperature previously derived. In fact, at an intensity of 10^9 watts/cm^2, the surface temperature of a 10 μ particle would be 4.2×10^3 °K in a 10^{-8} second pulse, whereas the average temperature would be only 300 °K.

The previous conclusion that the smaller particles are heated more, in the short-pulse case, is thus not justified. The surface temperature attained, for a pulse of a given length, approaches limiting values for large and small particles which are not greatly different.

1.3.4 Summary of Particle Heating Effects

For small particles which are heated by a long duration, relatively low intensity (10^5 watts/cm^2) laser beam, the temperature attained is limited by thermal conduction by the ambient gas. The increase in temperature over the surroundings is proportional to the intensity and, except for the most absorbing materials, is small. For particles of about 10^{-5} centimeter in radius, the temperature increase, even with highly absorbing materials, is only a few degrees Kelvin.

Larger particles (10^{-3} centimeters in radius) can be heated sufficiently to attain temperatures at which melting and vaporization can occur.

The temperature attained by particles heated by a short-duration, Q-switched, laser beam is proportional to the energy density in the beam for small particles (10^{-5} centimeters radius), and to the product of intensity times the square root of the pulse duration for large particles. For the case of copper, the temperature attained is relatively independent of particle size. In the Q-switched case, the temperatures attained, for all particle sizes, are sufficient to cause melting and/or vaporization, at energy densities in the vicinity of a few joules/cm^2, provided the particles are absorbing. Weakly absorbing materials will be heated only slightly.

1.3.5 Optical Path Changes

The preceding discussion indicates that, by and large, the major effect of an intense laser beam on an aerosol particle will be to increase its temperature. Except for large particles which are highly absorbing, the temperatures attained by the particles themselves will be insufficient to alter the particles. Only in the case of a high-intensity, Q-switched laser pulse will major effects be expected to occur on small (less than 1 μ) particles.

In most cases, the energy which was absorbed from the laser beam will be conducted to the ambient gas, resulting in a temperature, and consequent density, change. The temperature increase can be estimated to be, if thermal conduction of the energy away from the region of the beam is neglected,

$$\Delta T = \frac{n \sigma_{abs} I t}{\rho_o C_{v_a}} , \tag{21}$$

where n is the aerosol concentration, I the intensity, t the pulse duration, ρ_o the density of the air, and C_{v_a} the specific heat of the air. At first, this increase of temperature will have no appreciable effect on the optical path, because the gas has not had time to expand. If the gas expands adiabatically, however, the density, at the end of the expansion, will be

$$\rho = \frac{\rho_o}{\left(1 + \frac{n \sigma_{abs} I t}{\rho_o C_v T_o}\right)^{3/5}} . \tag{22}$$

Now, the index of refraction of air is

$$\mu = 1 + 2.74 \times 10^{-4} \rho/\rho_o , \tag{23}$$

when ρ_o is the density under normal conditions. Hence

$$\mu = 1 + \frac{2.74 \times 10^{-4}}{\left(1 + \frac{n \sigma_{abs} I t}{\rho_o C_v T_o}\right)^{3/5}} \tag{24}$$

The difference in optical-path length (number of wavelengths) between light passing through the expanded, heated air and the undisturbed medium is then

$$\Delta N = \frac{\mu_o L}{\lambda_o} - \frac{\mu L}{\lambda_o}$$

$$= \frac{L}{\mu_o} (2.74 \times 10^{-4}) \left[1 - \frac{1}{\left(1 + \frac{n \sigma_{abs} I t}{\rho_o C_v T_o}\right)^{3/5}}\right] , \tag{25}$$

where L is the geometrical path length. Now, for a ruby laser, $\lambda_o = 6.94 \times 10^{-5}$ cm, and It is about 10 joules/cm^2. The $\rho_o C_v T_o$ for air is 1.67×10^{-2} joules/cm^3, hence,

$$\Delta N = 4L \left[1 - \frac{1}{(1 + 6 \times 10^2 n \sigma_{abs})^{3/5}}\right] \quad \text{and} \tag{26}$$

$n\,\sigma_{abs}$ depends upon the particle type, size, and concentration.

A change in path length of 1 wavelength is readily observed by interferometric techniques. Thus, in a 1-meter path, a shift of ΔN wavelength would occur when

$$\frac{1}{(1 + 6 \times 10^2\, n\, \sigma_{abs})^{3/5}} = 1 - \frac{\Delta N}{400}$$

or

$$1 + 6 \times 10^2\, n\, \sigma_{abs} = \left(1 + \frac{\Delta N}{400}\right)^{5/3}$$

$$n\, \sigma_{abs} \approx \frac{5\, \Delta N}{3 \cdot 400 \cdot 600} = 7 \times 10^{-6}\, \Delta N\, cm^{-1} \quad . \tag{27}$$

The change in optical path also can cause a divergence of the laser beam emerging from the aerosol-containing region. No change would be expected during a Q-switched laser pulse, because the time required for the heated gas to expand is approximately the transit time of sound across the beam radius. Since sound velocity in air is on the order of 3×10^4 cm/sec, the effect would require about 3×10^{-5} seconds to build up. It would then slowly decay as the temperature and density in the aerosol equalized as a result of thermal conductivity, turbulence, and convection. With a long-pulse laser beam, on the other hand, the time required for the effect to occur would be short compared to the pulse duration. A divergence of the beam would be observed, increasing during the pulse. The amount of this divergence can be estimated, if some assumptions are made about the energy distribution in the beam. If the beam intensity, as a function of radius, follows a parabolic relationship in radius, the intensity is

$$I = I_o\, (1 - r^2/r_o^2) \quad , \tag{28}$$

where I_o is the central intensity, and r_o is the outer radius of the beam. For a weakly absorbing aerosol concentration, the index of refraction can be written as

$$\begin{aligned} \mu &= 1 + 2.74 \times 10^{-4} \left(1 + \frac{n\, \sigma_{abs}\, I t}{C_v\, t_o}\right)^{-3/5} \\ &= 1 + 2.74 \times 10^{-4} - (2.74 \times 10^{-4}) \left(\frac{3}{5} + \frac{n\, \sigma_{abs}\, I t}{\rho_o\, C_v\, T_o}\right) \\ &= 1 + 2.74 \times 10^{-4} - 10^{-2}\, n\, \sigma_{abs}\, I_o\, t\, (1 - r^2/r_o^2) \quad . \end{aligned} \tag{29}$$

Now, the equation of motion of a light beam passing through a medium with an index of refraction gradient is

$$\frac{d^2 r}{dz^2} \simeq \frac{1}{\mu} \frac{d\mu}{dr} \quad , \tag{30}$$

if the beam moves in the r-z plane, and the gradient is radial. If the beam is initially parallel-directed down the z axis, this equation can be integrated to give

$$\left(\frac{dr}{dz}\right)^2 = 2 \ln (\mu/\mu_1) \quad , \tag{31}$$

where μ_1 is the index at the initial radius r_1 .

Thus:

$$\left(\frac{dr}{dz}\right)^2 \simeq 2 \ln \frac{1 + 2.74 \times 10^{-4} - 10^{-2} n \sigma_{abs} l_o t (1 - r^2/r_o)}{1 + 2.74 \times 10^{-4} - 10^{-2} n \sigma_{abs} l_o t (1 - r_1^2/r_o^2)}$$

$$\simeq 2 [- 10^{-2} n \sigma_{abs} l_o t (1 - r^2/r_o^2)$$

$$+ 10^{-2} n \sigma_{abs} l_o t (1 - r_1^2/r_o)^2]$$

$$\simeq 2 \times 10^{-2} \frac{r^2 - r_1^2}{r_o^2} \cdot n \sigma_{abs} l_o t \quad . \tag{32}$$

$$\frac{dr}{\sqrt{r^2 - r_1^2}} = \left(\frac{2 \times 10^{-2}}{r_o^2} n \sigma_{abs} l_o t\right)^{1/2} dz \tag{33}$$

$$\ln \left(r + \sqrt{r^2 - r_1^2}\right)\Big]_{r=r_1}^{r} = \ln \frac{r + \sqrt{r^2 - r_1^2}}{r_1} = \frac{1}{r_o} \sqrt{2 \times 10^{-2} n \sigma_{abs} l_o t} \; L$$

$$r = r_1 \cosh \left[\frac{L}{r_o} \sqrt{2 \times 10^{-2} n \sigma_{abs} l_o t}\right] \quad . \tag{34}$$

L is the path length.

The divergence of the beam, initially at $r_j = r_o$, is then:

$$\frac{dr}{dz} = \sqrt{2 \times 10^{-2}\, n\, \sigma_{abs}\, l_o\, t}\ \sinh\left[\frac{L}{r_o}\sqrt{2 \times 10^{-2}\, n\, \sigma_{abs}\, l_o\, t}\right] ,$$

when (35)

$$\frac{L}{r_o}\sqrt{2 \times 10^{-2}\, n\, \sigma_{abs}\, l_o\, t} \quad \textit{is small, this becomes,}$$

$$\frac{dr}{dz} = \frac{2 \times 10^{-2}\, n\, \sigma_{abs}\, l_o\, t\, L}{r_o} \quad \textit{radians} \quad . \tag{36}$$

For a radius of 1 cm, L of 10^2 cm, $l_o t = 10$,

$$\frac{dr}{dz} = 20\, n\, \sigma_{abs} \quad \textit{milliradians} \quad . \tag{37}$$

Now, previously, it was found that the value of $n\,\sigma_{abs}$ required to give a path difference at Δn wave lengths, to be

$$n\,\sigma_{abs} \cong 7 \times 10^{-6}\, \Delta N, \quad \textit{for a path length of 100 cm}$$

Thus the divergence is related to the path length change by

$$\frac{dr}{dz} \cong 1.4 \times 10^{-4}\, \Delta N \tag{38}$$

for a 1-centimeter radius.

Since most ruby lasers have an inherent divergence of 10^{-3} radian or more, it is apparent that the measurement of optical path-length change will be a more sensitive measurement than the meaasurement of divergence change.

1.3.6 Vaporization Effects

As a result of an extensive series of investigations on the interaction of intense laser radiation with solid targets, a fairly thorough understanding of the interaction phenomena has been developed. This understanding can be summarized briefly, in the following discussion.

At low laser-beam intensities, or at the beginning of a more intense pulse, the laser radiation interacts with the solid target in a conventional manner. If the target is nonabsorbing, the beam is refracted and scattered, in a manner

calculable from electromagnetic theory. If the material is absorbing, energy is deposited in the surface of the target material, and the temperature increases at a rate determined by the geometry, laser intensity, and thermal properties. As the temperature of the particle increases, melting may occur, and ultimately vaporization.

Melting of the particle has effects which are not readily predictable. Once a particle has been melted, it can possibly be fragmented by the pressure of internal gases liberated by the heating. A somewhat fluffy particle could conceivably coalesce. Vaporization, on the other hand, is somewhat better understood. At low laser-beam intensities, the vaporization rate is low, so that the density in the vapor is low. Under these conditions, the vapor is transparent to the laser radiation, except under the special condition that the atomic or molecular absorption lines in the vapor coincide with the laser radiation. At higher intensities, however, the vapor, on leaving the target, is sufficiently dense and sufficiently ionized that it can absorb a portion of the incident radiation. This latter condition has been investigated in a number of experimental programs at Avco and at the Air Force Weapons Laboratory, and has also been the subject of theoretical studies at Avco and General Atomic. The conditions of the experimental investigations have not been directly applicable to the case of present interest, that of small particles. The theoretical studies have been concentrated on a large area targets, and are quite complex, involving extensive computer operations. However, the results of these studies have been used to confirm a simple analytical model of the interaction. The model is discussed in detail in an appendix to this report.

Basically, the assumption used in the model is that the absorption coefficient in the vapor is proportional to the square of the vapor density. This assumption can be expressed mathematically as

$$I = I_0 \exp - \alpha \int_x^\infty \rho^2 \, dx' \tag{39}$$

where I is the intensity at a point a distance x from the surface, I_0 is the intensity at a large distance from the surface, ρ is the density, and α is a coefficient. The beam is assumed to be a plane wave.

It is also assumed that the rate of evaporation from the surface is directly proportional to the intensity at the surface, so that

$$\dot{m}_0 = A I_s \cos\theta / \left(L + \frac{1}{2} v_s^2 \right) \quad , \tag{40}$$

where $\dot{m}_0$ is the mass per-unit-area per-unit-time evaporated, A an absorptivity of the surface, I_s the intensity at the surface, θ the angle of incidence, L the heat

of vaporization per-unit-mass, and v_s the velocity at which the vapor leaves the surface. The v_s is very nearly constant, since it is proportional to the square root of the surface temperature, which in turn is very nearly constant. (The rate of evaporation depends exponentially on temperature.) The above equation implies steady-state conditions in the solid.

A third assumption is that the rate of increase of kinetic energy in the vapor is proportional to the rate of energy absorption by the vapor, or

$$\frac{\partial}{\partial x}\left(\frac{1}{2}\rho v^3\right) = \beta \alpha \rho^2 I \quad , \tag{41}$$

where v is the velocity of the vapor, and β is an efficiency factor. Finally, it is assumed that the mass flow in the vapor is independent of position, although it may be a function of time. Thus

$$\dot{m}_o = \rho v \tag{42}$$

The above equations can be solved analytically, with the result, for a plane wave incident at an angle θ on the surface,

$$\dot{m}_o = 2\beta I_o \cos\theta \Big/ \left[v_m^2 - v_s^2 + (2\beta/A)\left(L - \frac{1}{2} v_s^2\right)\right] \quad , \tag{43}$$

where v_m is obtained from

$$I_o^2 t \cos\theta = (v_m^3 - v_s^3)\left[v_m^2 - v_s^2 + (2\beta/A)\left(L + \frac{1}{2} v_s^2\right)\right] / 6\alpha\beta^2 \quad . \tag{44}$$

For large intensitives and pulse durations, Equation (43) reduces to

$$\dot{m}_o = \frac{2\beta I_o \cos\theta}{v_m^2} \tag{45}$$

and Equation (44) to

$$v_m = (6\alpha\beta^2 I_o^2 t \cos\theta)^{1/5} \quad , \tag{46}$$

from which

$$\dot{m}_o = \frac{0.96\, \beta^{1/5} I_o^{1/5} \cos^{3/5}\theta}{\alpha^{2/5} t^{2/5}} \tag{47}$$

This expression is valid for a large-area target. In the appendix, an expression is developed for a small-area target. In this development, it is assumed that the vaporization follows Equation (47) until the vapor has expanded to a distance equal to the target radius. At this point it is assumed that the vapor has

expanded enough so that it is no longer absorbing. The asymptotic expression for this point is

$$r_o = 1.5\, v_m\, t \quad . \tag{48}$$

Substituting the value of t from this expression into Equation (46), the rate of mass loss in Equation (7) becomes

$$\dot{m}_o = \frac{2^{1/3}\, \beta^{1/3}\, l_o^{1/3}\, \cos^{2/3}\theta}{a^{1/3}\, r_o^{1/3}} \tag{49}$$

The point at which the time-dependent solution crosses over to the steady-state solution is given by equating (47) and (49) and solving for r_o

$$r_o = 2.15\, \beta^{2/5}\, l_o^{2/5}\, \cos\theta^{1/5}\, a^{1/5}\, t^{6/5} \quad . \tag{50}$$

Now, β is an efficiency factor and is greater than 0.1 for most materials. The a can be estimated from the equation for inverse Bremmstrahlung absorption. This equation is, after insertion of numerical values for the physical constants,

$$k_s = a\rho^2 = \frac{1.06 \times 10^{-23}\, n_e^2\, \lambda^2}{T^{3/2}} \left| n \left(\frac{6 \times 10^2\, T}{n_e^{1/3}} \right) \right. \ cm^{-1} \quad , \tag{51}$$

where λ is the wavelength, T the temperature, and n_e the electron density. For an ionised gas of molecular weight M, the electron density is

$$n_e = 6.024 \times 10^{33}\, \rho / M \quad . \tag{52}$$

Hence

$$k_s = a\rho^2 = 3.86 \times 10^{24}\ \frac{\rho^2}{M^2}\ \frac{\lambda^2}{T^{3/2}} \left| n \left\{ \frac{7.07 \times 10^{-6}\, T\, M^{1/3}}{\rho^{1/3}} \right\} \right. \quad . \tag{53}$$

On insertion of typical values of the ionized vapor, $\rho = 10^{-4}$, M = 12, T = 10^5, and $\lambda = 6.943 \times 10^{-5}$ cm, the equation is

$$k_s = a(r_o^{-8}) = 1.43 \times 10^{-1}\ cm^{-1} \tag{54}$$

$$a = 1.43 \times 10^7 \quad .$$

Inserting these values into Equation (50), gives

$$r_o = (2.15)(0.1)^{2/5}\ (1.43 \times 10^7)^{1/5}\, l_o^{2/5}\, \cos^{1/5}\theta\, t^{1/5} \quad ,$$

$$r_c = 23\, l_o^{2/5}\, \cos^{1/5}\theta\, t^{6/5} \quad , \tag{55}$$

for I_o in ergs/cm^2-sec. For I_o in watts/cm^2,

$$r_o = 1.45 \times 10^3 \, I_o^{2/5} \cos^{1/5}\theta \, t^{6/5} \quad .$$

For a Q-switched laser, $t = 3 \times 10^{-8}$ sec,

$$r_o = \frac{1.45 \times 10^3 \, I_o^{2/5}}{(3.3 \times 10^7)^{6/5}} = 1.45 \times 10^{-6} \, I_o^{2/5} \quad .$$

The evaporation, for a particle of radius 10^{-3} cm, will be in the steady state at all intensities above

$$I_o^{-2/5} = (1.45 \times 10^{-3})$$

$$I_o = (1.45 \times 10^{-3})^{-5/2} = 1.25 \times 10^7 \ watts/cm^2 \quad .$$

In the case of a long pulse (10^{-3} second duration), the evaporation will be in the steady state

$$r_o = \frac{(1.43 \times 10^3)}{(10^3)^{6/5}} \, I_o^{2/5} = 0.36 \, I_o^{2/5}$$

$$I_o = (2.8 \times 10^{-3})^{5/2} = 4 \times 10^{-7} \ w/cm^2 \ !$$

The evaporation rate, then, is always steady state. Now, the approximations used give much too high a mass-loss rate at low intensities. At low intensities, the steady-state mass-loss rate is

$$\dot{m}_o = \frac{2A \, I \cos\theta}{L} \quad , \tag{56}$$

when L is the latent heat of evaporation. Equating this with the high intensity evaporation rate, gives

$$\frac{A I \cos\theta}{L} = \frac{2^{1/3} \beta^{1/3} I_o^{1/3} \cos^{2/3}\theta}{\alpha^{1/3} r_o^{1/3}}$$

Hence, the intensity below which the steady-state expression, Equation (49) does not apply is

$$I_o^{2/3} = \frac{2^{1/3} \rho^{1/3} L \cos^{2/3}\theta}{A \, \alpha^{1/3} r_o^{1/3}} \quad .$$

L is on the order of 5×10^{11} ergs/gm for most materials. Using $\alpha = 1.43 \times 10^7$, $\beta = 0.1$, $A = 0.5$, gives

$$I_o = \frac{2^{1/2}\,\beta^{1/2}\,L^{3/2}\cos^{1/2}\theta}{A^{3/2}\,a^{1/2}\,r_o^{1/2}}$$

$$= \frac{1.18 \times 10^{14}}{r_o^{1/2}} \quad ergs/cm^3\,sec$$

$$= 1.18 \times 10^{7}/r_o^{1/2} \quad watts/cm^2 \quad ,$$

as the intensity below which Equation (49) does not apply. For a 10^{-3} centimeter particle, thus, the mass-loss rate does not depend upon vapor absorption, at intensities below about 4×10^8 watts/cm^2. Even at intensities somewhat higher the mass loss will not be greatly different from Equation (49), because that equation shows a mass-loss rate varying as the cube root of the intensity.

The result of the preceeding discussion is that, for all of the cases of interest, the upper limit on mass-loss rate is given by the equation

$$\dot{m}_o \cong A\,I_o \cos\theta \Big/ \left(L + \frac{1}{2}\,v_s^2\right) \quad .$$

A finite time, however, is required for the surface temperature of the particle to reach a value large enough for evaporation at this rate to occur. The surface temperature, corresponding to a given rate of evaporation, can be estimated from the vapor pressure of the material. The rate of evaporation, in gms/cm^2-sec, is related to the vapor pressure, molecular weight, and temperature by the equation

$$\dot{m}_o = 6 \times 10^{-2}\,p\,(M/T)^{1/2} \quad gms/cm^2\,sec \quad , \tag{57}$$

where p is the vapor pressure in torr, M the molecular weight, and T the absolute temperature. In the case of copper, the vapor pressure, as a function of temperature, follows the equation

$$p = 2 \times 10^{12}\,e^{-5.6 \times 10^4/T} \quad torr \quad . \tag{58}$$

For the sake of simplicity, assume that the latent-heat term in the equilibrium equation for mass loss ($L + v_s^2$) is equal to the latent-heat term derived from the vapor-pressure equation

$$L + \frac{1}{2}\,v_s^2 = 5.6 \times 10^4\,R/M \quad , \tag{59}$$

where R is the gas constant in joules/mole, if I_o is in watts/cm^2. The R is 8.31 joules/mol °K, and M for copper is 63.6. Thus the equilibrium mass loss equation is

$$\dot{m}_o = A\, I \cos\theta / 7.3 \times 10^3 , \tag{60}$$

and the rate of evaporation as a function of temperature is

$$\dot{m}_o = \frac{9.6 \times 10^{11}\, e^{-5.6 \times 10^4 / T}}{\sqrt{T}} . \tag{61}$$

The equilibrium temperature versus intensity equation is

$$A\, I \cos\theta = \frac{7 \times 10^{15}\, e^{-5.6 \times 10^4 / T}}{\sqrt{T}} , \tag{62}$$

from this, the approximate answer, valid over the range of intensity from $A\, I_o \cos\theta = 10^4$ to 10^{11}, is,

$$A\, I \cos\theta \approx 5 \times 10^{13}\, e^{-5.4 \times 10^4 / T} , \tag{63}$$

The equilibrium temperature is then:

$$T = \frac{5.4 \times 10^4}{\ln 5 \times 10^{13} - \ln (A\, I \cos\theta)} . \tag{64}$$

If this is equated with the temperature followed by the copper surface, as a function of time, for the large particle, short-pulse case, $A = 0.139$, $\theta = 0°$, the answer is seen as

$$T - 300 = 4.2 \times 10^{-2}\, I \sqrt{t} = \frac{5.4 \times 10^4}{(\ln 5 \times 10^{13} - \ln 0.139\, I)} - 300$$

$$\sqrt{t} = \left(\frac{5.4 \times 10^4}{31.8 - \ln (0.139 I)} - 300 \right) \left(\frac{1}{4.2 \times 10^{-2}\, I} \right)$$

$$I = 10^8 , \quad \sqrt{t} \left(\frac{5.4 \times 10^4}{15.3} - 300 \right) \left(\frac{1}{4.2 \times 10^{-2} \times 10^8} \right)$$

$$t = \left(\frac{3220}{4.2 \times 10^6} \right)^2 = 5.9 \times 10^{-8}\ sec.$$

$$I = 10^7 , \quad t = \left(\frac{5.4 \times 10^4}{17.6} - 300 \right)^2 \left(\frac{1}{4.2 \times 10^5} \right)^2$$

$$= 4.4 \times 10^{-6}\ sec.$$

The time required to reach equilibrium, in the large-particle case, is about $5 \times 10^8 / I_o^2$, in the case of a copper particle. At intensities below 10^8 watts/cm^2, the time required is over 50 nanoseconds, and the particle is not heated enough to evaporate appreciably.

This gives a threshold for a large particle, which is about 10^8 watts/cm^2. For a small particle, the temperature rise is

$$T = 300 + 4.3 \times 10^2 I t \quad .$$

The small particle is uniformly heated, however, although the incident energy arrives on one side

Thus the heat flow is:

$$\pi r_o^3 \times 2 \times 10^3 = 4\pi r_o^2 \dot{m}_o L \quad , \tag{65}$$

and the evaporation rate, for a small particle, is

$$\dot{m}_o = \frac{2 \times 10^3 I r_o}{4 r_o (2.3 \times 10^3)} \tag{66}$$

$$= \frac{9.6 \times 10^{11} e^-}{\sqrt{T}}$$

$$I = \frac{(4)(7) \times 10^{15}}{2 \times 10^3 r_o} \quad \frac{r_o \times p^{-5.6 \times 10^4 / T}}{\sqrt{T}} \tag{67}$$

$$\sim \frac{1.4 \times 10^{13} r_o e^{-5.6 \times 10^4 / T}}{\sqrt{T}}$$

$$I = \frac{10^{11} e^{-5.4 \times 10^4 / T}}{r_o}$$

$$T = \frac{5.4 \times 10^4}{\ln 10^{11} - \ln (I r_o)}$$

$$= 300 + 4.3 \times 10^2 I t$$

$$t = \left(\frac{(5.4 \times 10^4)}{\ln 10^{11} - \ln I r_o} - 300 \right) \Big/ 4.3 \times 10^2 I \quad .$$

For particles of 10^{-5} centimeter radius, the time required for evaporation to occur is then 7×10^{-9} seconds at 10^9 watts/cm^2, and 6×10^{-8} second, at 10^8 watts/cm^2. Again, intensities of over 10^8 watts/cm^2 are required to cause appreciable evaporation.

In the long-pulse case, the intensities are limited to about 10^5 watts/cm^2. The equilibrium temperature, at this intensity, for copper is, for large particles, derived from

$$4\pi r^2 \dot{m}_o = \frac{0.139 \cdot I_o}{7.3 \times 10^3}$$

and

$$\dot{m}_o = \frac{9.6 \times 10^{11}\ e^{-5.6 \times 10^4/T}}{\sqrt{T}} \quad .$$

or

$$I_o = \frac{2 \times 10^{17}\ e^{-5.6 \times 10^4/T}}{\sqrt{T}} \quad .$$

$$I_o \cong 144 \times 10^{15}\ e^{-5.6 \times 10^4/T} \quad ,$$

hence

$$T = \frac{5.4 \times 10^4}{\ln 1.44 \times 10^{15} - \ln I_o} = \frac{5.44 \times 10^4}{\ln 1.44 \times 10^{10}} = 2300^\circ K \quad .$$

However, the maximum allowable temperature for a large particle is

$$T = 300 + 1.51 \times 10^2\ I_o\ r_o\ (1 - e^{-1.97 \times 10^{-4}\ t/r_o^2}) \quad .$$

For $r_o = 10^{-3}$, and an intensity of 10^5 watts/cm^2, the temperature allowable is

$3000^\circ K$ *in* 10^{-3} *seconds.*

However, evaporation would have set in sooner than this, limiting the attained temperature to 2300°K. A particle of this size would thus evaporate at a reasonable rate. However, at 10^4 watts/cm^2, the allowed temperature would be only 570°K, and no evaporation could occur.

With a 10^{-5} cm^2 particle, on the other hand, the allowed temperature would be only 320° K at 10^5 watts/cm^2, and again no evaporation would occur.

It can now be concluded that, for absorbing particles, an intensity of over 10^8 watts/cm^2 is required to cause evaporation in a Q-switched pulse. In a long pulse, the intensity must be in the vicinity of 10^5 watts/cm^2, and the particle size over 10^{-4} centimeters, if evaporation is to occur.

1.4 HIGH INTENSITY REGIME

1.4.1 Introduction

In the discussion of the interaction of laser radiation with small particles, energy density-and-intensity-dependent effects were predicted on the basis of essentially constant material parameters. It has been observed in the Avco laboratory, however, that very marked phenomena occur at laser-beam intensities approaching 10^9 watts/cm^2, even on nonabsorbing materials. For example, a plasma has been observed on the surface of quartz, when it is irradiated in vacuum at an intensity of 10^9 watts/cm^2. When the irradiation takes place in air, the plasma is sufficiently absorbing to considerably attenuate the beam. Observation of the interaction with nonabsorbing plastics indicate a behavior essentially the same as that of graphite at intensities above 10^9 watts/cm^2.

1.4.2 Mechanism of High Intensity Effects

The simplest mechanism of the effects is the semi-classical mechanism of field emission. At an intensity of 10^9 watts/cm^2, the peak electrostatic field associated with the electromagnetic light wave is

$$E_o = 27.6\, I^{1/2} = 8.75 \times 10^5 \text{ volts/cm} \quad . \tag{68}$$

At such a high field, the probability of an internal field emission of a valence electron in a dielectric solid is high. The emitted electron is then free to absorb energy from the electromagnetic wave. In effect, at sufficiently high intensities, the dielectric solid acts as a metallic absorber, and the surface temperature can become quite large. Because the thermal conductivity of the dielectric is small, the approach to an evaporation temperature can be more rapid than it is for the case of a metal. At 10^9 watts/cm^2, the mass-loss rate is dominated by vapor absorption, and the analysis which has been developed for metallic absorbers is applicable, in vacuum.

In air, however, the density of the atmosphere is already higher than the density expected from the evaporated vapor. Thus the absorption by the air surrounding the particle could become quite large, if the air became ionized. If this did occur, a region of considerably larger cross section than the particle could become attenuating, and the overall attenuation of the laser beam would increase.

Whether or not such an effect can occur depends upon the rate at which the electron concentration in the atmosphere can build up. This rate can be estimated by applying a collision hypothesis to the absorption of enery by a free electron in the laser beam.

According to Wright[1], the net rate-of-gain of energy of an electron, in the field of the laser beam in an atmosphere, is

$$\frac{dE}{dt} = N n_\nu \sigma^{5/2} h\nu \left(1 - \frac{2 \nu E m}{n_\nu \sigma^{3/2} h \nu M} \right) \tag{69}$$

where N is the concentration of molecules, σ the electron-atom collision cross-section, n_ν the photon-flux density, ν the frequency, h Planck's constant, v the electron velocity, m the electron mass, and M the molecule mass.

This expression can be rewritten in terms of the laser intensity $I = n_\nu h_\nu$, and the electron energy $E = \frac{1}{2} m v^2$, as

$$\frac{dE}{dt} = N I \sigma^{5/2} \left[1 - E^{3/2} (8m)^{1/2} / \sigma^{3/2} M I \right] . \tag{70}$$

Now, the electron can gain energy in the field of the laser until it either reaches the maximum energy

$$E_{max} = \sigma (M^2 I^2 / 8m)^{1/3} , \tag{71}$$

or makes an exciting collision with the molecule. Once this happens, the excited molecule can be readily ionized by photon absorption. For air, we can use about 5 electron volts as the necessary electron energy. The electron-molecule collision cross-section[2], for air, is about 6×10^{-16} cm^{2*} at energies under 5 electron volts. If numerical values are substituted in the above equations, they become, using $I = 10^7 I_o$ ergs/cm^2 sec, for I_o in watts/cm^2; $m = 9.1 \times 10^{-28}$, $M = 4.81 \times 10^{-23}$ gm, $N = 3 \times 10^{19}$ particles/cm^3,

$$\frac{dE}{dt} = 2.7 \times 10^{-12} I_o \left[1 - (E/E_{max})^{3/2} \right] \text{ ergs/sec} , \tag{72}$$

or

$$\frac{dE}{dt} = 1.69 I_o \left[1 - (E/E_{max})^{3/2} \right] \text{ ev/sec} ,$$

and

---

*American Institute of Physics Handbook, p. 7–174.

$$E_{max} = 1.17 \times 10^{-5}\ l_o^{2/3}\ ev. \tag{73}$$

The equation for dE/dt can be integrated, to give

$$E = 1.69\ l_o\ t, \qquad \text{for } E/E_{max} < 0.1,$$

$$t = (0.59\ E/l_o)\left[\frac{\ln\left(1 + \sqrt{\frac{E}{E_{max}}} + E/E_{max}\right)\Big/\left(1 - \sqrt{\frac{E}{E_{max}}}\right)^2 - 2\sqrt{3}\ \tan^{-1}\left(\frac{\sqrt{3}\ \sqrt{\frac{E}{E_{max}}}}{2 + \sqrt{E/E_{max}}}\right)}{3\ E/E_{max}}\right] \tag{74}$$

The term in brackets is approximately 1.2 when $E/E_{max} = 0.5$.

The energy E which the electron attains is the average. If the energy distribution is Gaussian, the fraction which has an energy E_i or more is exp - E_i/E. The rate of collision between electron and molecule is $N\sigma v$, so that the rate of increase of electron concentration can be written as

$$dn_e/dt = n_e\ N\sigma v\ exp - E_i/E. \tag{75}$$

If numerical values are now substituted for N, σ, and $v = 5.93 \times 10^7 E^{1/2}$ cm/sec for E in ev, the equation becomes

$$(1/n_e)\ dn_e/dt = 1.38 \times 10^{12}\ (l_o\ t)^{1/2}\ exp - E_i/1.69\ l_o t. \tag{76}$$

as long as E is less than 0.5 E_{max}, approximately. On making the substitution $x = 1.69\ l_o t / E_i$, the equation is

$$ln\ n_e/n_o = (6.3 \times 10^{11}\ E_i^{3/2}/l_o) \int_0^{1.69\ l_o t/E_i} x^{1/2}\ e^{-1/x}\ .\ dx. \tag{77}$$

The time required to increase the electron concentration by a factor of e is then obtained from

$$1.59 \times 10^{-12}\ l_o/t_i^{-3/2} = \int_0^{1.69\ l_o t/E_i} x^{1/2}\ e^{-1/x}\ . \tag{78}$$

For all reasonable values of E_i and I_o, the term on the left is much less than unity. If the substitution of $x = 1/y$ is made it becomes

$$\int_0^{1.69\, I_o t/E_i} x^{1/2}\, e^{-1/x}\, dx = \int_{\frac{E_i}{1.69\, I_o t}}^{\infty} y^{-5/2}\, e^{-y}\, dy\,, \tag{79}$$

where y is always much greater than unity. In such a case, the integral is dominated by the exponential, and has the value

$$\int_0^{1.69\, I_o t/E_i} x^{1/2}\, e^{-1/x}\, dx = (1.69\, I_o t/E_i)^{5/2}\, \exp - E_i/1.69\, I_o t \tag{80}$$

$$= 1.59 \times 10^{-12}\, I_o/E_i^{3/2}\,.$$

Now, on solving this equation, it is found that, for most practical cases, $1.69\, I_o t/E_i$ is on the order of 0.2. Thus the time required to increase the electron concentration by a factor of e is approximately

$$t = 0.1\, E_i/I_o\,. \tag{81}$$

Assuming, pessimistically, that E_i is about 10 electron volts, then the time at 10^9 watts/cm^2 is about 10^{-9} seconds. At this intensity, then it appears highly probable that the electron concentration can increase by several orders of magnitude during a short laser pulse, and that air-breakdown effects can be triggered. At 10^8 watts/cm^2, on the other hand, the required time is 10 nanoseconds, and the concentration would increase only slightly (a factor of 10) in a short laser pulse.

2.0 INTERPRETATION OF EXPERIMENTAL MEASUREMENTS

In the preceeding sections of this report, the phenomena which might be expected to occur in the various intensity regimes have been discussed. The results of this discussion will now be applied to the design and the interpretation of experiments.

2.1 LOW INTENSITY REGIME

At low-laser-beam intensities no effect on the particle occurs, and heating of the particle is not sifficient to cause appreciable changes in the optical path. The effect of the aerosol on the beam is therefore primarily that of scattering and attenuation. However, the possibility of coherence effects should be investigated. Such experiments require the comparison of scattering and attenuation between a coherent laser beam and an incoherent beam of approximately the same wavelength. For the purpose of these measurements, the coherent beam can be either the continuous-wave beam derived from a gas laser, in which case the observation of scattering and attenuation will be time averaged, or a pulsed beam derived from a Q-spoiled laser. In order to ensure coherence and minimize thermal and other effects, the beam from the Q-switched laser should be reduced in intensity by selection of only a small portion of the beam and subsequent magnification. This procedure will also ensure a minimum divergence beam.

The incoherent beam can best be derived from an incandescent source and a suitable filter. The bandpass of the filter should be on the order of 10 and 50 angstroms, in order to make the coherence length of the radiation small compared to the average separation of the particles. If line radiation is used, the coherence length will be large compared to the separation, and coherence effects might be observed.

2.2 MODERATE INTENSITY REGIME

At moderate intensity levels, which may be crudely defined as below 10^8 watts/cm^2 for a Q-switched laser, above 10^2 watts/cm^2 for a long-pulsed laser, thermal effects will occur. At low intensity levels, these effects will appear as a change in the temperature of the ambient gas, with consequent expansion and reduction of refractive index. The scattering and attenuation will not be expected to change significantly. However, beam divergence will increase, as a result of the reduction in index. Thus increase in divergence can result in a spurious measurement of the attenuation, if the field-of-view of the detector for attenuation is initially small.

The most important measurement for the index of refraction effects will be that of optical interferometry along the path traversed by the laser beam. This measurement will indicate refractive index changes and will be more sensitive than the measurement of the beam divergence.

In the case of a long-pulse-laser beam, the refractive index in the path irradiated during the pulse will change during the duration of the pulse, so that interferometric measurements will show a decrease in index as the pulse continues. Time-resolved measurements, in this case, can be readily made by using the laser beam itself as a light source, and resolving the index changes by means of an image-converter camera. In the case of a Q-switched laser, the pulse duration is too short to allow the density change to occur, and the index measurements, again time resolved, require the use of a second light source.

At higher beam intensities, the particles themselves may be partially melted, vaporized, or fragmented. These effects would all cause a change in the scattering and attenuation. If the particles are initially small, the effect of a reduction in particle size, as a result of vaporization, melting, or fragmentation, would be a reduction in the scattering cross section. If the particles were initially large compared to a wavelength of light, the effect would be for an individual particle, a fluctuation in the scattering cross section.

Both the scattering and the attenuation would be expected to show time variations in this case, and the measurements should be made on a time-resolved basis.

In addition to the scattering and attenuation changes, the particles themselves might be heated sufficiently to radiate thermally. It is, therefore, useful to include the measurement of radiation at other than the laser wavelength, to the measurements of scattering. Because nonlinear effects in the aerosols themselves may also contribute other wavelengths, these measurements should be spectrally resolved. The best experimental approach would be to first, determine the total spectral radiation, using photographic techniques, and then to make time-resolved measurements using a monochromater and photo detector. The wavelength selected would be chosen to separate thermal radiation from nonlinear effects.

2.3 HIGH INTENSITY REGIME

In the high-intensity regime, particle vaporization may occur for all materials. In addition, the atmosphere surrounding the particle may itself become appreciably absorbing. If such occurs, the attenuation of the beam will change drastically, being appreciably greater. Because the air is absorbing to the laser light, it would be expected that the laser light scattered would also be reduced. Also, the air would be heated to a much greater extent than would otherwise occur, so that index-of-refraction effects would be greatly enhanced. If the air were appreciably ionized, the index of refraction would be reduced even below unity, as a result of the free electrons present. This effect, an index reduction because of free electrons, would occur immediately, and would not require time to build up. Furthermore, the radiation from the heated air would be appreciable. Again, a measurement of the spectral distribution of the radiation would serve to show the presence of radiation from excited air, as well as from particle vapors, and would clearly indicate the presence of these high-intensity effects.

2.4 ADDITIONAL MEASUREMENTS

The types of measurements briefly suggested above are optical in nature. They include the measurements of attenuation and scattering, reradiation, and wavefront changes by means of index-of-refraction and beam-divergence measurements. In addition, it would be useful to include a pressure measurement in the test chamber. The thermal effect of the radiation in heating the air, either directly or by conduction from the particles, can introduce a sound wave into the chamber. The measurement of the magnitude of this wave would be additional information on the process which took place.

It is also possible to directly measure the increase in air temperature in the chamber. However, because the time response of the detector would be slow, such a measurement would not be meaningful, and it would be better to infer the temperature from the index-of-refraction change.

The electron density in the chamber can also be measured. One can either use collecting electrodes, and measure the total charge collected from a given volume in the aerosol containing gas, or use a microwave technique and measure the electron concentration directly. The latter technique has the advantage of being unaffected by electron-ion recombination, and the disadvantage of a relatively low sensitivity. The charge collection method would be particularly appropriate for the detection of electrons thermionically emitted from the heated aerosol particles.

3.0 EXPERIMENTAL INVESTIGATIONS

3.1 LASER SYSTEM

The laser system used in these investigations is composed of an oscillator-amplifier system. The oscillator utilizes a 5/8 x 6 inch, flat-ended, ruby rod pumped by four EG&G FX 47 flash lamps in a multielliptical cavity. The flash lamps are energized by a pulse-shaping network that shapes the input electrical energy. A 11,500 joule capacitor bank supplies the flash-tube energy. The optical resonator is formed by a totally reflecting prism at one end, and the polished face of the output end of the ruby rod which acts as a Fresnel reflector. Q-switching is accomplished by a rotating-plane dielectric reflector which folds the optical cavity by its position between the ruby rod and the reflecting prism. The reflector rotates at 200 rps, but the folded optical path doubles the effective switching rate at 400 rps.

The resonant cavity can be varied from 1/2 to 1 1/2 meters long. Changing the cavity length serves two purposes. Lengthening the cavity increases the output pulse width and decreases the beam divergence. A 1 1/2-meter cavity normally produces a pulse whose width at points of half maximum is approximately 70 nanoseconds long. The 1/2-meter cavity length and the addition of an optical cell, containing cryptocyanine in methanol in the resonant cavity, decreases the pulse width to 35 nanoseconds (FWHM), and also prevents any pulsing before and after the main pulse. The energy output of the oscillator is approximately 1 1/2 to 2 joules in the Q-switched mode. This system is cooled by dry nitrogen, and has a repetition rate of 1 shot per 3 minutes. The dry nitrogen provides an inert atmosphere in the cavity and prevents oxidizing of the metal end caps and trigger wires.

The laser amplifier was constructed by Electro-Powerpac of Cambridge, Massachusetts. The single-pass amplifier head is composed of a 5/8 x 12 inch, Brewster-angled ruby rod. The Brewster angle prohibits any internal reflection and is one means of allowing the oscillator-polarized beam to single pass through without introducing any multiple pulsing at this wavelength. The rod is pumped by four modified EG&G FX47 flash lamps, mounted in a multielliptical cavity. The flash lamps are energized by a capacitor bank capable of storing up to 60,000 joules. Since the oscillator output is kept constant, all the energy-output control of the system is provided by the amount of energy fed to the amplifier flash lamps. The output of the amplifier ranges from 0 to 20 joules with a pulse width identical to that of the oscillator. The output is normally kept below 10 joules to prevent damage to the output end of the amplifier ruby rod and other optical components in the laser-beam path. The amplifier head is cooled by compressed air and has a repetition rate of 1 shot per 4 minutes.

The system is arranged so that the output of the amplifier passes through a diverging plano-concave lens of focal length - 20 centimeters and then a converging plano-convex lens of focal length 100 centimeters. The lenses are separated by approximately 80 centimeters to produce a nearly parallel output beam of 5 times the original beam dimensions. The flat side of the lenses is placed toward the laser. This orientation minimizes spherical aberation in the combination and also prevents a secondary focus in the vicinity of the concave lens. The flat surfaces of the lenses are slightly tilted to prevent any direct reflection back into the laser amplifier. This tilt is necessary to prevent oscillation in the amplifier and does not introduce any serious distortion. The parallel beam leaving the lens combination is directed the length of the laboratory. A series of stations with removable, dielectric-coated mirrors is located so that the laser beam can be deflected into experimental chambers at various points along the beam.

3.2 CHAMBER DESIGN

3.2.1 Laboratory Aerosol Generator

In order to determine the efficacy of various window and chamber configurations, and in order to carry out some preliminary, laser-interaction experiments, a laboratory source of aerosols was needed. At first, it was contemplated that smoke (cigarette or cigar) would be adequate for this purpose. However, after a more careful investigation, the tar and other contaminants were found to coat the chamber walls and surfaces. This meant that the system would continually have to be broken down, cleaned, and reassembled, causing more time than usual to be spent for realignment of the system before firing operations could be resumed. Hence, this means was abandoned.

A simple aerosol generator was developed that was quick, easy to start, and left much less residue in the experimental chamber. This system uses concentrated hydrochloric acid and ammonia hydroxide. By mixing these vapors, ammonium-chloride salt is formed consisting of fairly uniform particles of sizes normally under a micron. A schematic of the generator is shown in Figure 1. Air flows into separate flasks containing the acid and the base, picks up the HCl and NH_3 vapors, and then passes into a mixing chamber where formation of the small particles takes place. The size of the particles can be controlled to some extent by the ratio of the flow of air through the two flasks. The concentration can be varied by changing the flow of air through the generator chambers and through the air-bypass line. It must be remembered, however, that the mixing of these two liquids produces a violent reaction. Therefore, precautions must be made to ensure that accidents with this combination are reduced to a minimum.

This device can be operated continuously with reasonably stable aerosol concentration. When this smoke was allowed to flow into the test chamber, it was

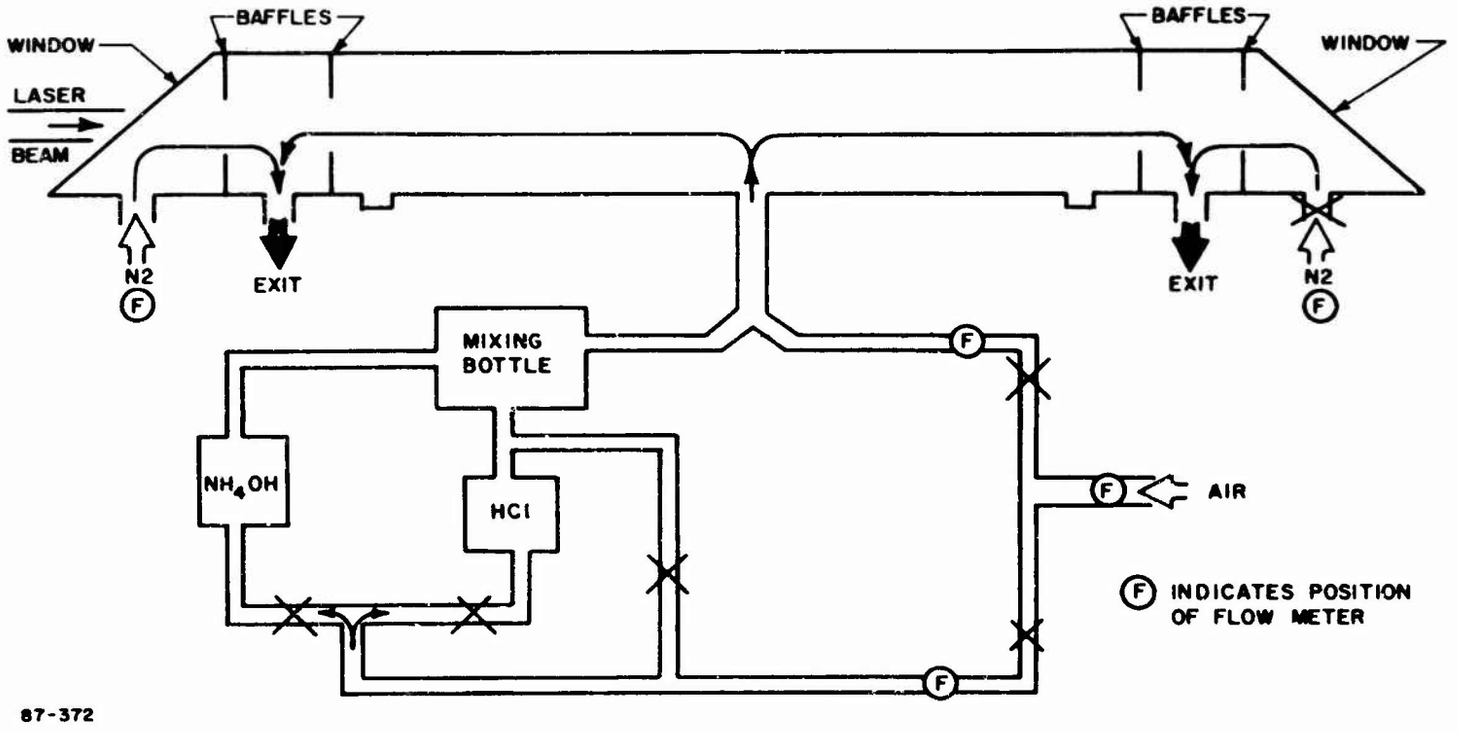

Figure 1 SCHEMATIC FOR AEROSOL GENERATOR

found possible to obtain a reasonably-uniform particle distribution (as determined by visual observation of the light scattered from a gas-laser beam) in the chamber, and at the same time prevent any aerosol particles from reaching the windows at each end of the chamber. This was done with the aid of a gas flow into the chamber in baffled regions near the windows. The aerosol mixture leaves the chamber in the baffled region.

Because of the continued use of the aerosol-generation system for long periods of time, minor problems developed. This led to modifications of the aerosol mixing bottle (Figure 2). To ensure continuous and uniform mixing, a baffle six inches high had to be placed between the two gas-input tubes, both of which entered in a 2-liter filter flask. The exit nozzle had to be replaced with a 13 millimeter glass tube to prevent salt formation. The bottom of the input tubes had to be flared out to prevent salt formation on the ends causing irregular flow. The position of the tube openings was found to be best at 2 inches from the top of the baffle--too low, and salt formed at the outlet opening of the flask; too high, and salt formed inside the flare on the HCl tube.

It has been found that for continued operation, more air had to flow through the HCl bottle than through the NH_4OH bottle, to maintain a balanced concentration. As the concentration of one to the other becomes unbalanced, the salt "smoke" formation is drastically reduced, and after about an hour the particle concentration in the tube thins out to almost nothing.

3.2.2 Window Design

The major problem associated with the design of the windows by which the laser beam enters and leaves the scattering chamber is that of prevention of aerosol particles from accumulating on the windows. If such occurs, and the particles are at all absorbing to the intense laser light, inevitable damage to the windows will result, and, perhaps more importantly, a significant amount of attenuation will occur at the windows. The window protection method adopted consisted of a gas baffle. The design is shown in Figure 3. Here dry nitrogen (chosen because the compressed-air supply available contained contaminating oil particles) passes into the baffle chamber containing the window, and exits through an export chamber into which the aerosol-containing gas also flows. The regions between the window and the export chamber, and the test chamber and the export chamber, are separated by baffles whose size can be selected. O-ring seals are used in the assembly of the various parts. The chambers themselves were constructed of Pyrex, and were epoxied to the metal flanges. The window is constructed of optically-flat glass and is epoxied at the Brewster angle (approximately 33 degrees) to the line-of-sight of the laser beam. No coatings were used, since the transmission for the proper plane of polarization (E-vector parallel to the plane of incidence) is essentially unity. If there is a component of light which is polarized in the direction parallel to the surface (perpendicular to the plane of incidence),

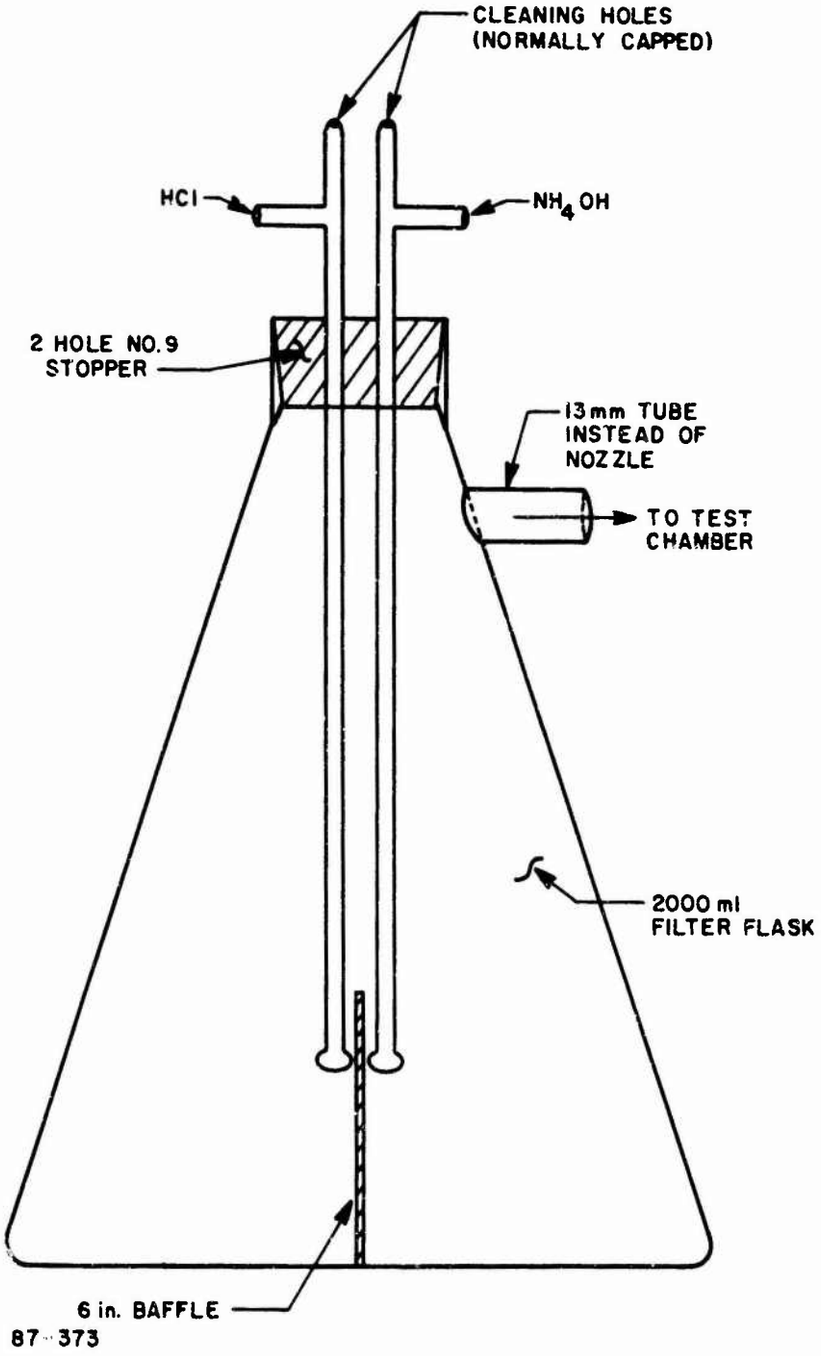

Figure 2 AEROSOL MIXING BOTTLE

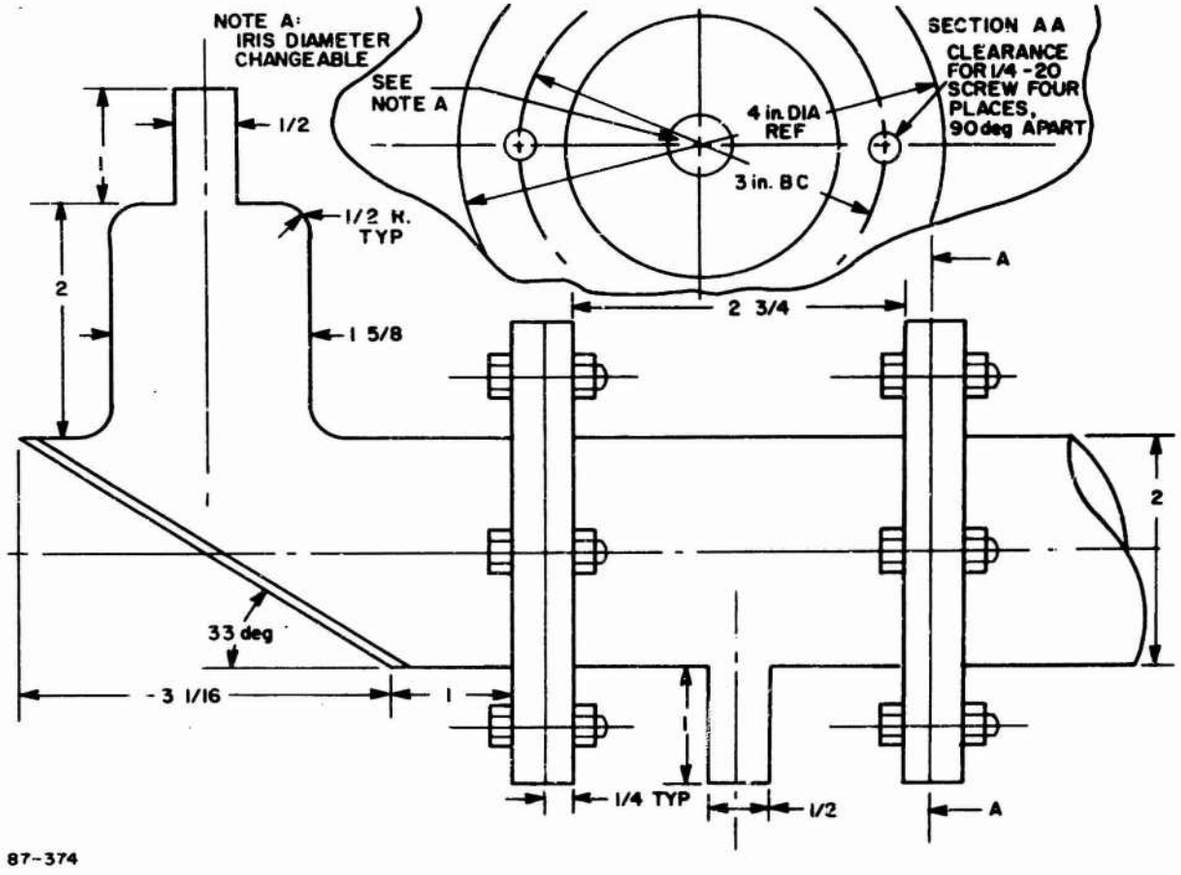

Figure 3 WINDOW PROTECTION METHOD

approximately 74 percent of this light will be transmitted, and 26 percent reflected. The reflected portion is trapped in the side arm of the chamber, which can be blackened if desired.

3.2.3 Chamber Design

All of the experimental chamber designs have been constructed of 2-inch-diameter Pyrex tubing of various lengths. The first work was done with a tube 1 meter long, with an aerosol inlet at the center consisting of a single 16-millimeter-diameter side tube. When this chamber was used in conjunction with window chambers and export chambers of the type described, with baffle openings of 1-inch diameter, it was found relatively straightforward to adjust the gas flow so as to prevent the accumulation of aerosol particles at the windows. However, the mixing at the center of the chamber, where the aerosol entered, was not complete, and the observed concentration varied, in a fluctuating manner, in the region near the inlet.

The gas flows required for window protection also varied with chamber length. With the 1-meter length, the flow of nitrogen (total) required to protect the windows against an aerosol-containing air flow of 1.75 liters/min was approximately 2.5 liters/min. With a shorter chamber (aerosol length 21 centimeters), higher flow rates were needed (5.5 liters/ min of N_2 versus 2.5 liters/min of air).

The procedure used to adjust the flow rates into the various portions of the chamber was to first establish a flow in the window-protection region. Then, aerosol was admitted to the chamber, and the aerosol concentration was visually observed by observing the scattering from a gas laser beam passing through the chamber. The scattering was sufficiently strong that individual particles could be discerned. The gas flows could then be adjusted so that the aerosol-containing region could be made to terminate approximately at the baffle separating the test chamber from the export chamber.

The visible scattering from the beam also indicated the degree of homogeneity in the concentration. With a small entrance tube, the region near the center, where the gas entered, was clearly inhomogeneous. The small tube was replaced with a larger diameter (2-inch) tube, and it was found that the gas-inlet rate could be adjusted so that the aerosol distribution was very nearly homogeneous throughout the length of the tube.

The air- and nitrogen-flow rates are fairly critical. If the air (aerosol) inlet rate is too low, the aerosol cannot be made to fill the test chamber. If the rate is too high, a severe turbulence develops in the export chamber, and some of the aerosol reaches the window. If the nitrogen flow is too high, the turbulence reaches back into the test chamber, causing a nonuniform distribution. The values of flow rate given above are those which appear to give the best results, for the particular chamber and window used.

Conventional glass stopcocks were used to control the flow rates in the aerosol-generating and window-protection system. These stopcocks are not sufficiently precise for all purposes (in particular, it is difficult to obtain very slow rates), and should be replaced by needle valves that are more easily adjusted. The flow meters used were the 990 series, No. 2135, manufactured by Hoke & Co. These meters serve primarily as indicators, since the actual flow conditions are best found by experiment.

3.2.4 Chamber Length Limitations

The chamber length that can be used depends upon the divergence of the laser beam, the diameter of the beam desired, and upon whether or not inhomogeneities in the beam are considered to be significant. The allowable chamber length also depends upon the aerosol concentration being investigated, and whether or not a reasonably uniform intensity is desired throughout the length of the beam.

3.2.4.1 Beam Homogeneity

One of the problems that will be encountered in conducting any careful research on the effects of a high-intensity laser beam on a contaminated atmosphere is that of "hot spots" and other inhomogeneities in the laser beam. Hot spots are inherent in a particular laser system, since they are related to the imperfections in the laser materials and to the manner in which the laser is pumped. Another source of nonuniformity is due to the divergence of the beam. This divergence limits the path length over which a beam of uniform intensity can be propagated.

It is obvious that the presence of inhomogeneities renders the interpretation of intensity-dependent effects considerably more difficult, particularly if the effects occur at only a few places in the beam. Because such effects are complex, every effort should be made to produce as uniform an intensity distribution in the laser beam as possible, prior to actual experimentation. In the work at Avco, such an effort has not been made as part of this contract, partially because of time limitations, but primarily because of the material expense involved in the selection of the highest-quality laser materials.

The beam profile of the oscillator-amplifier combination at Avco has been examined, however. Two types of inhomogeneities have been observed. First, if the profile is observed by focusing an image of the output end of the laser amplifier rod, horizontal striations (perpendicular to the plane of polarization of the output light) are observed. Those striations also appear if a continuous gas laser beam is passed through the unpumped rod. The striations are believed to be a result of imperfections in the rod, which result from the method of growth (Verneuil method for the Avco rod).

Linde has recently announced that all of their ruby laser materials are now being produced by the Czochralski technique (pulling from the melt). Such rods should be considerably improved in their optical quality.

Inhomogeneities are also observed if the laser beam is made parallel by means of an optical system. Although the striations are not apparent, a more or less random inhomogeneity occurs. Again, this is believed to be related to the imperfections in the laser rod. Measuring of the divergence of the laser rod, by measurement of the minimum-focal-spot size at a large distance (10 meters) indicates that the divergence is largest in the direction normal to the direction of the striations mentioned above.

A third type of inhomogeneity can also exist. When a long-pulse laser beam is varied by time-resolved photography, it has been observed that, on imaging the end of the laser source, only small areas of the source emit at any given time. In the near field (close to the source), the intensity of any given part can therefore be much higher than the average.

Avco has examined the time dependence of the Q-switched laser output as a function of position, by using a restricted aperture photodiode as a probe. No serious time versus position effect was observed, except that there was a slight shift in the time of maximum intensity as the probe was moved across the beam. This shift amounted to about ten percent of the laser pulse width (between half-power points).

3.2.4.2 Minimization of Inhomogeneities

The inhomogeneities in the laser beam should be as small as possible in a system intended for careful research. As a first step, the laser materials should be selected for the highest optical quality. Second, the system should be operated in a single-axial mode, or at least have the transverse modes suppressed. Such mode selection, unfortunately, leads to a loss in output energy. Some of this loss can be regained by increasing the gain of the amplifier in an oscillator-amplifier combination. Mode selection will produce a significant improvement of the output-beam profile only if the materials are of near-diffraction-limited quality.

The optical system used to direct the beam is also of major importance. If the direct beam is used, without optics, then the near-field inhomogeneities will persist for a long distance. A simple example of this can be presented. Suppose the output beam has a total divergence of 4 milliradians (typical of most available ruby lasers). Further, assume that, in the near field, the scale of inhomogeneities is on the order of 1 millimeter, and that the beam for each of the inhomogeneities also has a total divergence of 4 milliradians. Then, if the laser beam has a diameter d, then individual beams will not overlap until the diameter of the beam from each inhomogeneity is on the order of the diameter of the laser rod, or a distance from the rod of

$$z = \frac{d}{4 \times 10^{-3}} \quad 250 \ dcm \quad . \tag{82}$$

The greatest homogeneity therefore occurs in the far field of the radiation pattern from the laser rod. If an optical system is used, this is at the focus of the radiation from the rod. In most cases, an optical system will be necessary, in order to produce the high beam intensity or energy density necessary to produce intensity-dependent effects. However, in order to minimize intensity variations due to the geometry of the system, it is necessary to limit the path length in the aerosol-containing region.

3.2.4.3 Minimum Path

This limiting path length can be estimated by assuming that the laser beam consists of initially parallel light, with which there is associated a divergence angle (half angle) a. If the beam has an initial radius, r_o, and is focused with a focal length f, then the beam radius, as a function of distance from the focal point is:

$$r = af + \left(a + \frac{r_o}{f}\right) x \qquad x > 0 \tag{83}$$

for positions beyond the focal point,

and

$$r = af - \left(\frac{r_o}{f} - a\right) x \qquad x < 0 \tag{84}$$

for positions short of the focal point, in order to have a focus, $r_o > af$. Now, if the permissible variation in r is limited to some factor, F times the minimum radius, $r_{min} = af$, the equation is

$$Faf = af + \left(a + \frac{r_o}{f}\right) x_1 \qquad x > 0 \tag{85}$$

$$Faf = af - \left(\frac{r_o}{f} - a\right) x_2 \qquad x < 0 \quad , \tag{86}$$

then:

$$x_1 = \frac{Faf - af}{a + r_o/f} = \frac{af(F-1)}{a + r_o/f} \tag{87}$$

$$x_2 = \frac{Faf - af}{\left(\frac{r_o}{f} - a\right)} = \frac{af(F-1)}{a - r_o/f} \quad . \tag{88}$$

The path length is

$$L = x_1 - x_2 = af(F-1)\left(\frac{1}{a + r_o/f} \quad \frac{1}{a - r_o/f}\right) \tag{89}$$

$$= \frac{af(F-1)(-2r_o/f)}{(a^2 - r_o^2/f^2)} \tag{90}$$

$$L = \frac{2ar_o(F-1)}{r_o^2/f - a^2} = \frac{2ar_o f^2(F-1)}{r_o^2 - a^2 f^2} .$$

In the special case in which $r_o = af$,

$$x_1 = \frac{af(F-1)}{2a} = \frac{f(F-1)}{2}$$

$$x_2 = -f,$$

$$L = f + f\frac{(F-1)}{2} \tag{91}$$

and since $r_{min} = af$,

$$\frac{L}{r_{min}} = \frac{1}{a} + \frac{F-1}{2a} = \frac{F+1}{2a} . \tag{92}$$

Now, if an optical system is used, the divergence angle is $a = \frac{a_L r_L}{r_o}$ where a_L is the divergence of the output from the laser, r_L the output-beam radius, and r_o the radius of the beam as it energizes from the system. Then,

$$\frac{L}{r_{min}} = \frac{r_o}{a_L r_L}\left(\frac{1+F}{2}\right) \tag{93}$$

and since $r_{min} = af = r_o$,

$$L = \frac{r_o^2}{a_L r_L}\left(\frac{1+F}{2}\right) = \frac{r_o^2}{a_L r_L} . \tag{94}$$

A typical beam divergence for a laser beam is 2×10^{-3} radians, and a typical laser-beam radius is 0.625 millimeter (1/4 inch),

hence

$$L = \frac{r_o^2}{1.25 \times 10^{-3}} = 800\, r_o^2 \text{ cm.} \tag{95}$$

Thus, with a beam of 1 centimeter radius, an 8-meter chamber length can be used to maintain a nearly uniform intensity. However, many experiments will require a higher intensity than attainable with a 1-centimeter beam. To increase the intensity by a factor of 10 reduces r_o^2 by a factor of 10, to an 80-centimeter path length.

Increasing the intensity also poses a window problem, since the chamber window cannot withstand a flux of larger than 10^9 watts/cm^2. In many cases the size of the minimum spot must be less than r_o, and the special case cannot be used.

Then

$$L = \frac{2\, a\, r_o f^2 (F-1)}{r_o^2 - a^2 r^2} , \tag{96}$$

now, $af = r_{min}$,

$$L = \frac{2\, r_{min}\, r_o f\, (F-1)}{r_o^2 - a^2 f^2} \tag{97}$$

$$\text{but } f = \frac{r_{min}}{a} = \frac{r_{min}\, r_o}{a_L\, r_L} \tag{98}$$

$$\therefore L = \frac{2\, r_{min}^2\, (F-1)}{a_L\, r_L \left(1 - \frac{r_{min}^2}{r_o^2}\right)} \tag{99}$$

since $a_L\, r_L$ for a typical case is 1.25×10^{-3} cm,

$$L = \frac{1600\, r_{min}^2\, (F-1)}{\left(1 - \frac{r_{min}^2}{r_o^2}\right)} \tag{100}$$

Note that this cannot exceed the value for $r_{min} = r_o$,

$$L = 400\, (1+F)\, r_{min}^2 . \tag{101}$$

Now, the above equations can be used to determine the maximum allowable path length, as a function of minimum beam radius, for an F of 1.1, corresponding to a 20 percent intensity change over the path length, if r_o cannot be less than 1.0.

The results are shown below:

r_{min}	10 cm	1	0.5	0.2	0.1
L	8.4×10^4	8.4×10^2	5.4×10^1	6.6 cm	1.60 cm

For certain types of measurements, in which the effect to be observed is not a function of beam size, but only of beam intensity, it is possible to perform the experiment with only a portion of the beam. At this focus of the beam, as has been previously discussed, inhomogeneity is minimized. If an aperture is placed at the focus, a homogeneous region of the beam can be selected and imaged by a lens. With a slight demagnification, the same intensity can be obtained at the image of the aperture as was obtained at the primary focus, and this image will contain a very nearly homogeneous intensity distribution.

With this approach, the allowable path length is not reduced, because the portion of the beam selected by the aperture at the primary focus has a restricted divergence. The major difficulty that would be encountered with this approach would be vaporization of the aperture. However, the primary focus can be made as large as desired, so that the intensity on the aperture material is less than that required to damage it.

The focal-point-selection technique can be applied in all cases in which the effect to be observed occurs during the laser pulse. This will include vaporization and fragmentation of the aerosol particles, with consequent changes in scattering and attenuation. It will also include the measurements of wave-front changes during the pulse, including intensity-dependent effects such as the Townes effect. However, this technique would reduce thermal effects, such as the Brueckner effect, because the beam size is reduced. It would also reduce the magnitude of a scattered signal, but this latter should not be significant, since the signal is expected to be quite large.

3.2.4.4 Multiple Paths

The length limitations of the chamber given above will also apply if flat mirrors are used to reflect the beam back through the chamber. No additional path length can be gained by such a technique, and the total path length traversed by the beam, including the additional length made necessary by the use of mirrors outside the aerosol-containing region, is given by the limitations above.

It is possible to use focusing mirrors to increase the effective path length, however. Suppose, for example, the path length allowable in the aerosol is 100 cm, as a result of divergence and inhomogeneity limitations. Then, by using a focusing mirror outside the chamber, such that the radiation from the center of the path is focused back at the same region (but offset to prevent overlap), the path length in the aerosol can be effectively doubled without introducing any addition divergence. With the addition of a second mirror, the path length can be tripled, and so on.

This method is, of course, limited in extent, if we specify that the various beams are not to overlap in the aerosol region or on the mirror surfaces.

3.3 EXPERIMENTAL MEASUREMENTS

3.3.1 Scattering Measurements

Figures 4 and 5 show the design of a simple scattering-chamber photomultiplier mount, suitable for use with the glass-test chamber that was constructed for the evaluation of the window-protection method. It is designed to allow an undistrubed aerosol to flow through with easy insertion into the regular, chamber baffle system. It has a mount for the photomultiplier tube at 90 degrees and at 45 degrees measured with the forward reflection as 0 degree, and can be reversed for measurements at 135 degrees. It can also be rotated at 360 degrees about the cylindrical axis in order to investigate a possible angular dependence on polarization. Directly opposite these two mounts are light traps. All four mounts are protected by a baffle system that keeps the aerosol from the windows and does not distrub the main flow. In front of the photomultiplier is a collimater that will allow only a known specific volume of aerosol to be observed. There is a polarizing film in front of the multiplier to ascertain whether the scattered light in any position is polarized in any preferred direction.

The phototube used is an RCA-6810. However, this is not the one recommended. The reason is that the 6810 has an S-11 response curve, and a gain of 6×10^5 with a 3-nanosecond rise time. The recommended tube is the RCA-4459. It has an S-20 spectral response, a gain of 6.6×10^6, and a rise time of 2 nanoseconds when operated at 2300 volts.

With the photomultiplier in position, the laser can be fired through the chamber with only air flowing through. Any problems involving fluorescence and reflected light are then overcome by use of filters. When a null is achieved when the laser is fired, then scattering experiments can be undertaken.

The experimental scattering chamber shown in Figures 4 and 5 has been tested with generally good results. With no aerosol in the chamber, it was possible to increase the gain of the photomultiplier tube to the point of instability and still observe no background scattering. With the system used, it was not

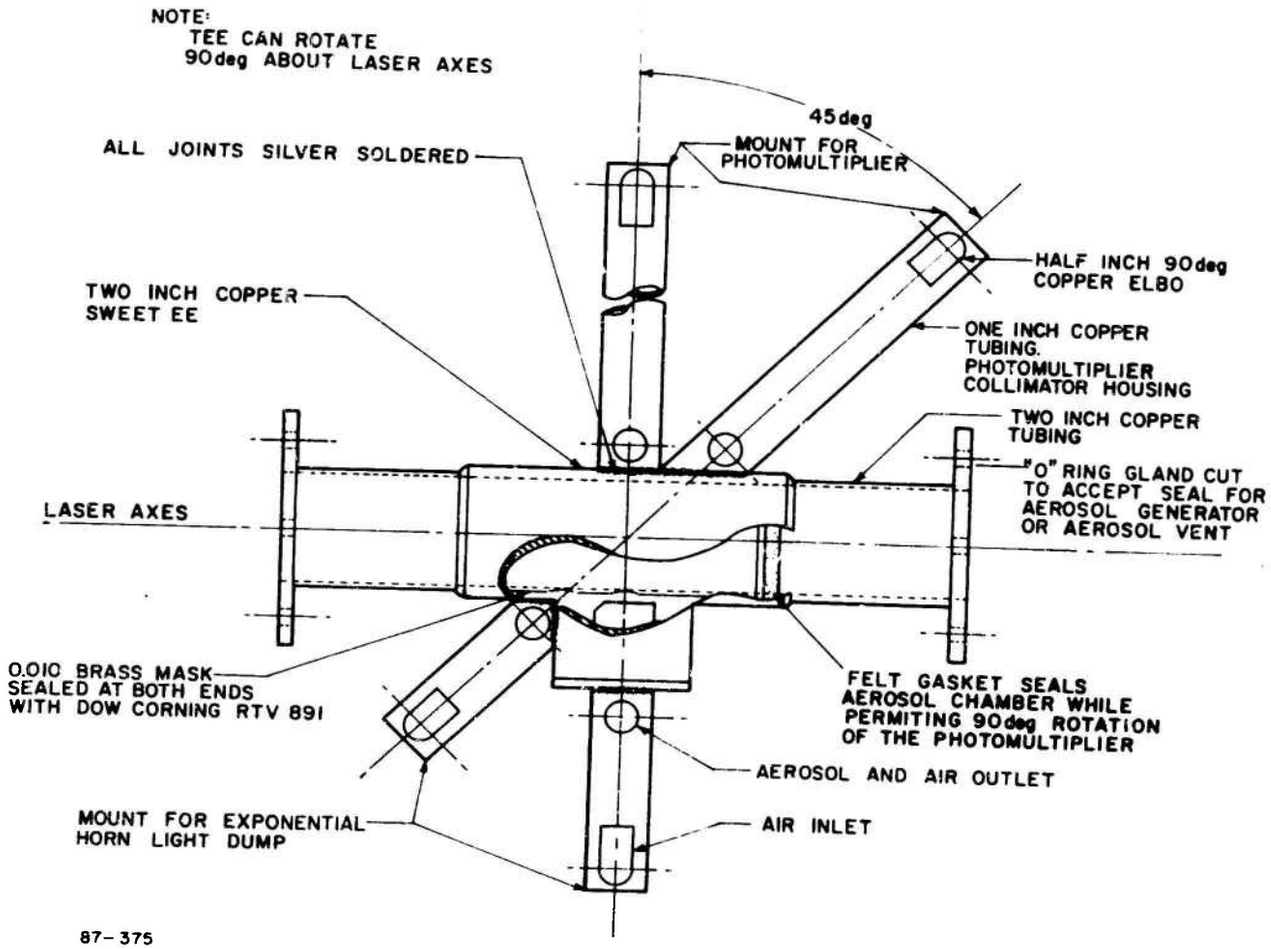

Figure 4 AEROSOL SCATTERING CHAMBER

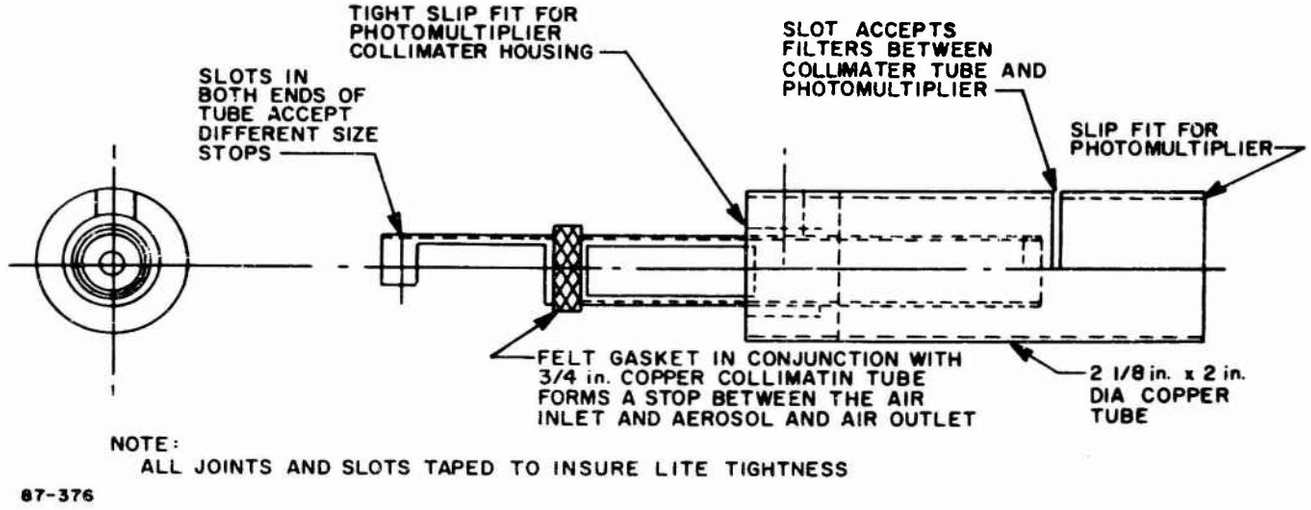

Figure 5 PHOTOMULTIPLIER MOUNT

possible to observe Rayleigh scattering, however. This was because the gain on the multiplier could not be increased sufficiently before an instability set in. Upon addition of the ammoniun-chloride aerosol to the chamber, very large scattered signals could be observed.

It has been found, however, that the photomultiplier system must be calibrated against a known light source of the same intensity and duration as the laser radiation scattered into the chamber, if quantitative results are to be obtained. The manufacturer's specifications on the multiplier tube, both in gain and frequency response, are only indicative. A means of absolute calibration of the entire system -- which includes the photomultiplier, any filters, and the collimation system -- is required.

A simple method of calibration has been adopted. This consists of the arrangement shown in Figure 6. The electron multiplier and collimater are allowed to view a diffuse reflecting surface which is illuminated by the direct high-power laser beam. If the reflectivity of the surface is nearly unity, and the detection system is placed at a sufficiently large distance that the entire illuminated area is within its field of view, then the power received by the detector is

$$P = R \cos\theta \, (r_1/r)^2 \, P_o \qquad (102)$$

where r_1 is the radius of the aperture limiting the collected radiation (the aperture nearest the multiplier tube), r the distance of the diffuse reflector to the aperture, and θ the angle between the line-of-sight between the detector and the reflector and the normal to the reflector. By varying the angle θ the reflector can be checked to show that it is truly diffuse. R is the diffuse reflectivity at the ruby-laser wavelength, and P_o is the laser-beam power at the reflector. P_o can be determined by focusing the radiation arriving at the position of the detector into a suitable monitor. The procedure Avco used is to measure the energy content of the beam at this point with a calorimeter and to determine the instantaneous power from a simultaneous observation of the pulse shape using a beam-splitter and photo-diode combination.

The diffuse reflector should be coated with magnesium oxide, which has a diffuse reflectivity of 0.98 at 0.7 microns. The calibration should be done at several gain settings of the multiplier, in order to ensure that a suitable sensitivity range can be selected.

Some care must be taken in the geometrical set up used for the scattering measurements. It is important that the field of view of the detector be larger than the laser beam, if a complicated analysis is to be avoided. Consider the schematic arrangement shown in Figure 7. The detector phototube views the laser-beam region through two collimating apertures of radius r_1 and r_2, separated by a distance L. The r_1 is the aperture nearest the detector and should be no larger than r_2. If the distance between the second aperture, r_2, and the center

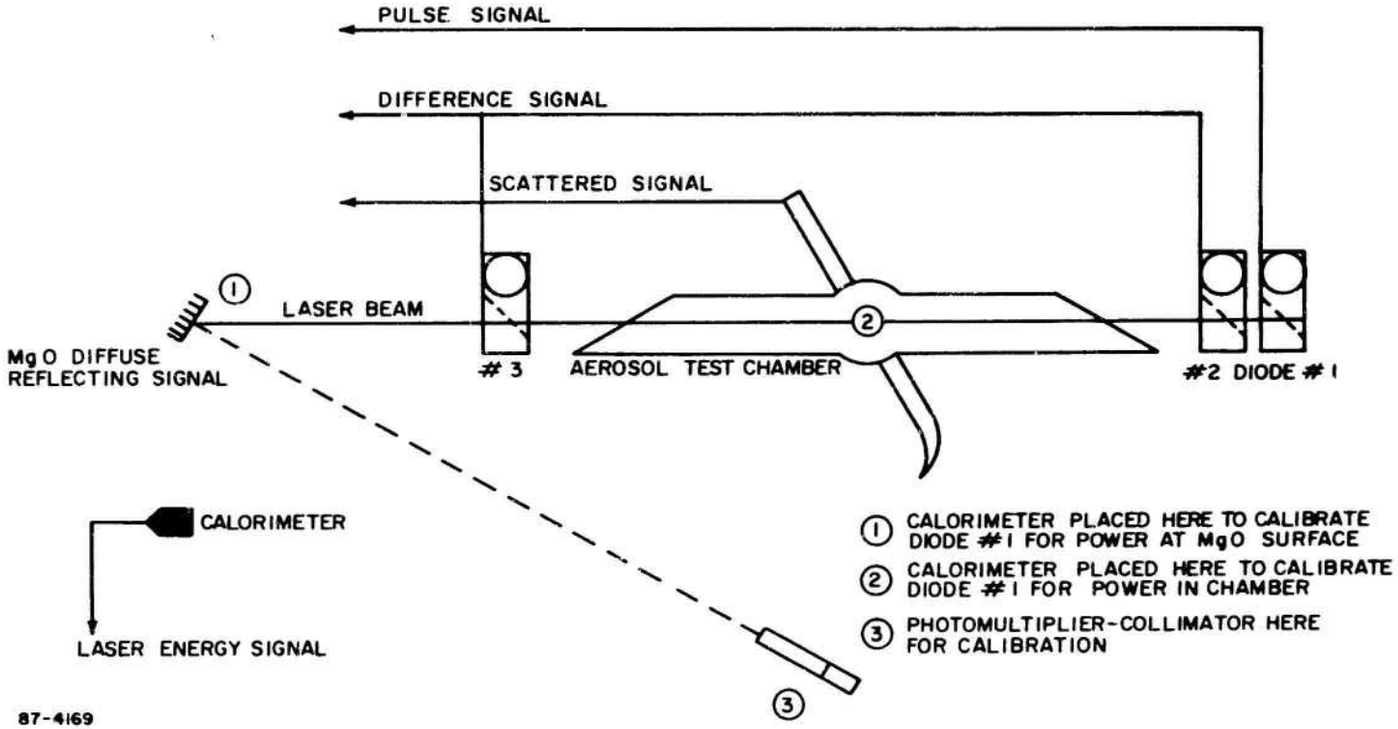

Figure 6 SCATTERING AND ATTENUATION MEASUREMENT

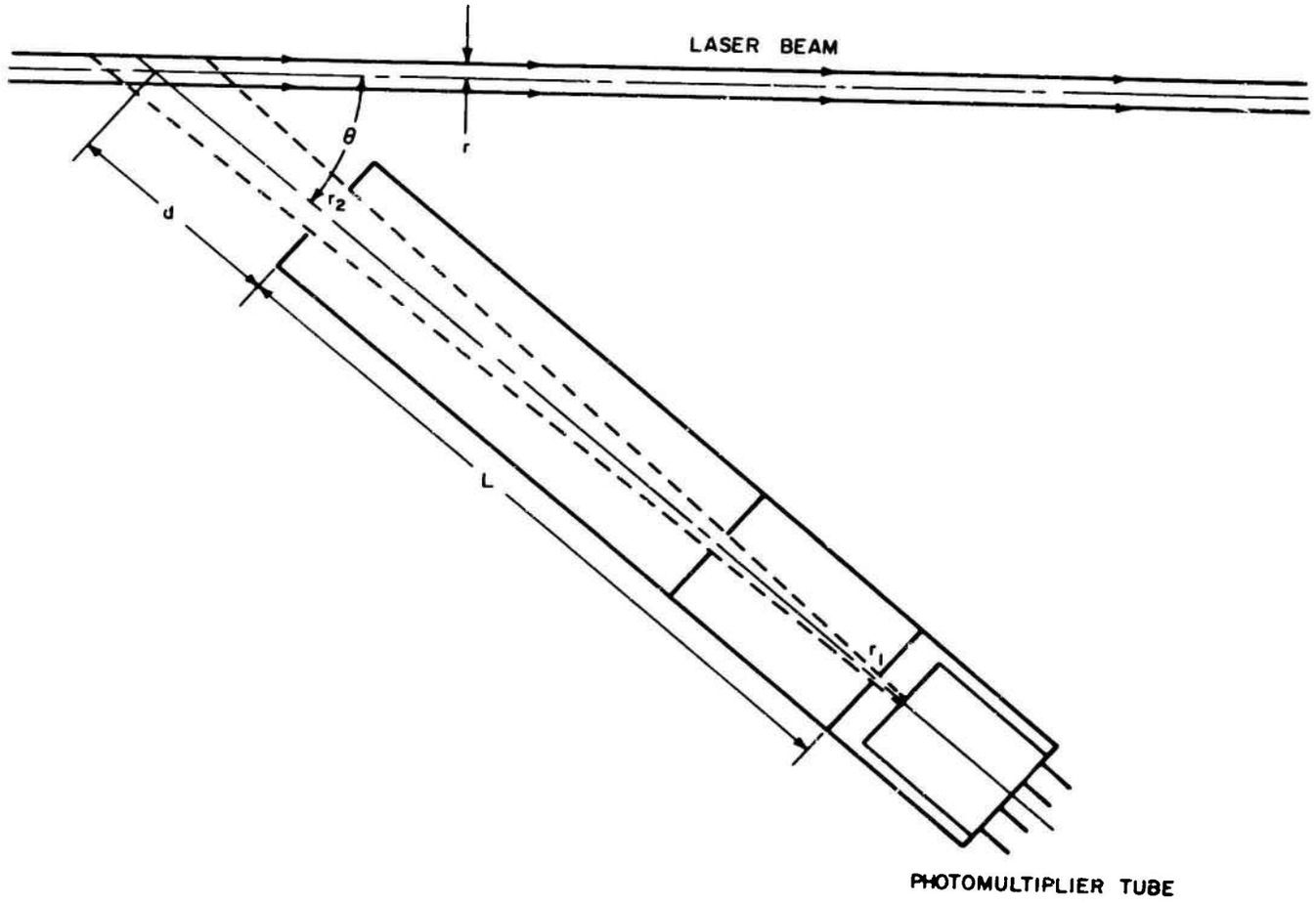

Figure 7 SCATTERING MEASUREMENT GEOMETRY

of the laser beam is d, and the scattering angle is θ (the angle between the beam axis and the line-of-sight of the detector), then the power scattered through the aperture r_1 into the detector is

$$P_d = \frac{\pi r_1^2 r_2}{L(L+d)\sin\theta} P_o \qquad (103)$$

where P_o is the laser-beam power at the point of scattering, and P_d is the differential-scattering cross-section-per-unit volume (the sum of the individual particle cross sections over the particle distribution). This equation should be accurate to better than 10 percent if the beam radius r is less than 22 percent of the linear field of view $2(L+d)\, r_2 / L$, and to better than 3 percent if the radius r is 1/8 of the total linear field of view.

If, on the other hand, the radius r is comparable to the field of view, or larger, the scattered power depends upon the intensity distribution in the beam. Although it is, in principle, possible to compute the signal received for a given measured distribution and cross section, there is nothing to be gained, since the scattering cross section can be measured easily with a beam of smaller diameter.

3.3.2 Attenuation Measurements

The measurement of attenuation of the laser beam poses unique problems. In the first place, in order to have a situation as interpretable as possible, it is desirable that the intensity over the aerosol path traversed by the beam be as nearly constant as possible. Otherwise, the effects of the beam on the aerosol, and consequent effects on the optical path, will be a function of position along the path. Thus it is desirable to keep the total attenuation of the beam below about 10 to 20 percent.

A change in attenuation cross section of 10 percent would then appear, in a measurement, as a change in attenuation of only 1 to 2 percent. Consequently, the maximum precision is desired.

With a continuous light beam, it is possible to use conventional spectrophotometer techniques. The laser beam can be split, so that a portion passes through the aerosol, and a second portion used as a reference. With the aid of of a chopper, both beams can be alternately brought to the same detecting surface, and ac-amplification techniques used to determine the degree of attenuation with a high degree of precision. However, with the short pulse durations attainable with high-power lasers, such mechanical chopping is not feasible.

The problem is particularly acute with a Q-switched laser pulse. Here the pulse lasts a few tenths of nanoseconds, and any effects of the beam may be manifested as a time-dependent change in the attenuation. In order to observe this effect, it is thus necessary to be able to measure the pulse shape to a precision of 1 percent or more, a procedure which is difficult with the resolution and linearity of present oscilloscopes.

3.3.2.1 First Approach

The approach that has been adopted is to mix the electric signals from two photodetectors, one before and one after the attenuating regions, and to measure the difference signal. The first experimental arrangement is shown in Figure 8. The optical detectors are planar diodes, ITT type 114. A schematic of the diode and the diode holder are shown in Figure 9, which is a manufacturer's brochure. The 114 diode has an S-4 response, which is very insensitive to ruby-laser light. However, the magnitude of the signal available is large (about 2×10^{-4} amperes per watt of incident light) so that the more sensitive FW 4000 (S-1 response) is not necessary, and would require additional attenuation of the light entering the detector. In the first set up, one of the diodes was operated with a positive anode, and the signal was obtained from the cathode current. The other diode was operated with a negative cathode, and the signal was obtained from the anode current. The two currents were then mixed in a resistive network, and the difference signal (the signal from each diode was of opposite sign) fed to a conventional oscilloscope.

This approach was unsuccessful. The response of the two diodes, when operated in the manner described, was sufficiently different, especially in time response, that a balance between the two signals could not be obtained. It is believed that this difficulty is inherent in the construction of the diodes. The cathode is a large-area plate, whereas the anode is a grid which is in contact with the entrance window of the diode. Thus it would be expected that space charge effects would interfere with the time response when the anode current is measured.

Some typical diode-response characteristics are shown in Figure 10. The upper traces are for the A and B diodes at different operating voltages. Output of the diodes are plotted against transmission. The lower traces show a comparison between the responses of the two diodes. The A diode was operated with a negative cathode and shows a relatively decreasing response, which is to be expected, since the anode current was measured and was probably space-charge limited.

3.3.2.2 Second Approach

A second approach, that of operation of both diodes so that the cathode current from each was fed into a differential amplifier, after passing through a 50 ohm impedance, also failed. Here the difficulty is believed to be associated with both nonlinearities in the amplifier, and time-response effects. The experimental arrangement for this approach is shown in Figure 11. This circuit used the ITT diode circuit shown in Figure 9.

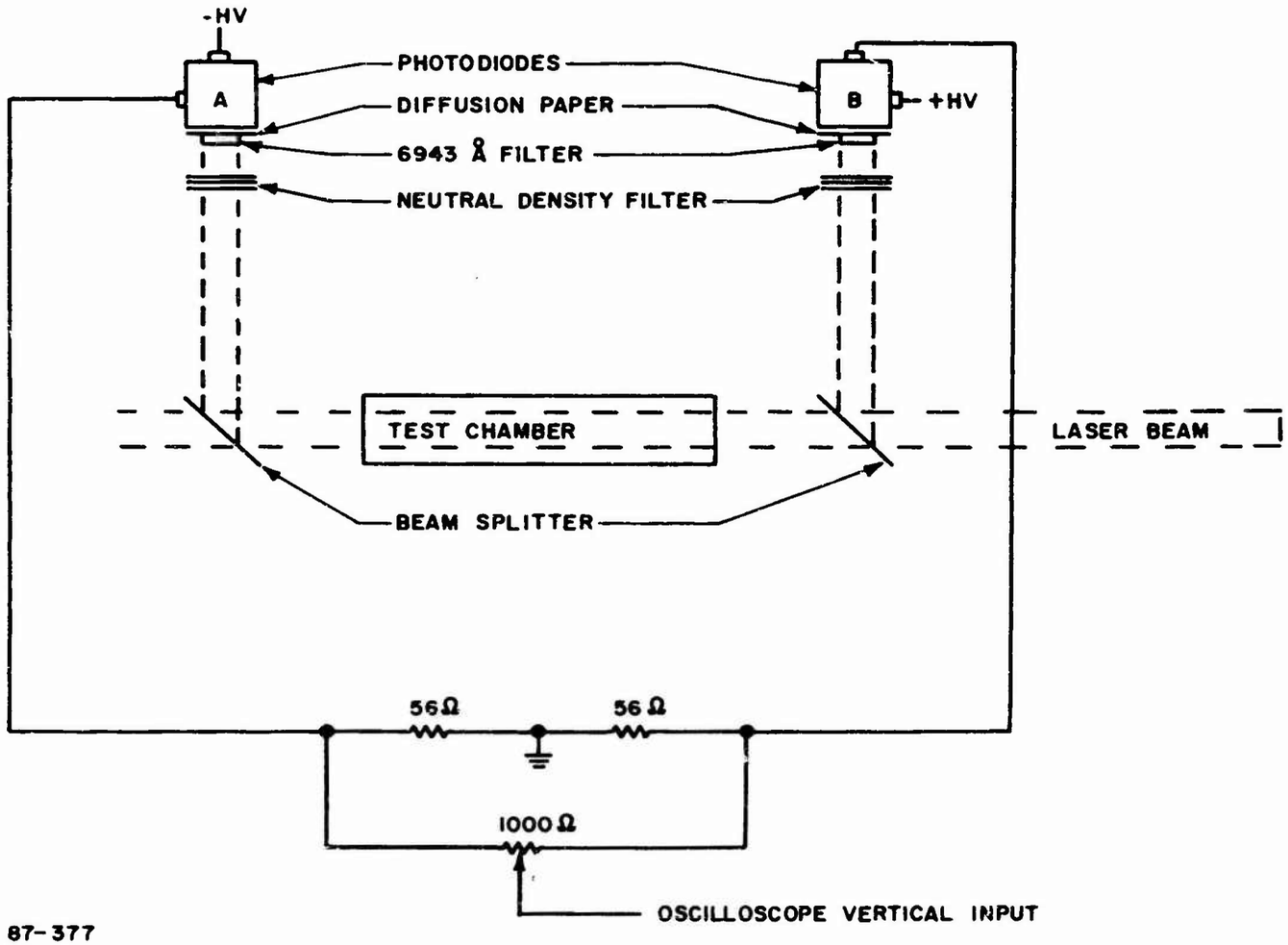

Figure 8 ORIGINAL EXPERIMENTAL ARRANGEMENT

Type F4502

The F4502 photodiode holder is designed to accommodate the 2-1/4 inch diameter series of biplanar photodiodes, such as the FW114, FW114A, and F4000 (S1). The F4502 provides a means of coupling these tubes to a coaxial cable; however coupling capacitors are not provided.

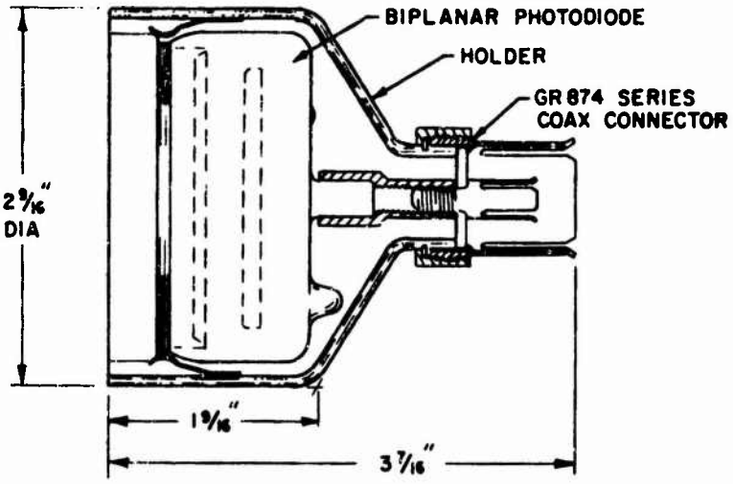

SUITABLE BIPLANAR CIRCUIT

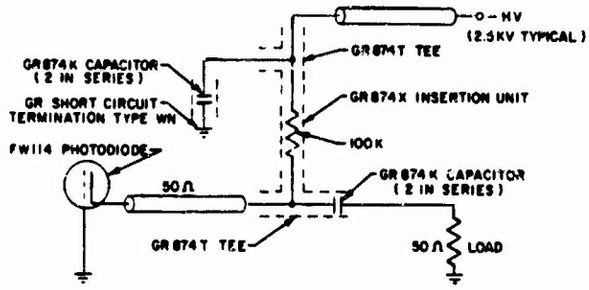

5KV MAXIMUM VOLTAGE

Figure 9 PHOTOTUBE HOLDER

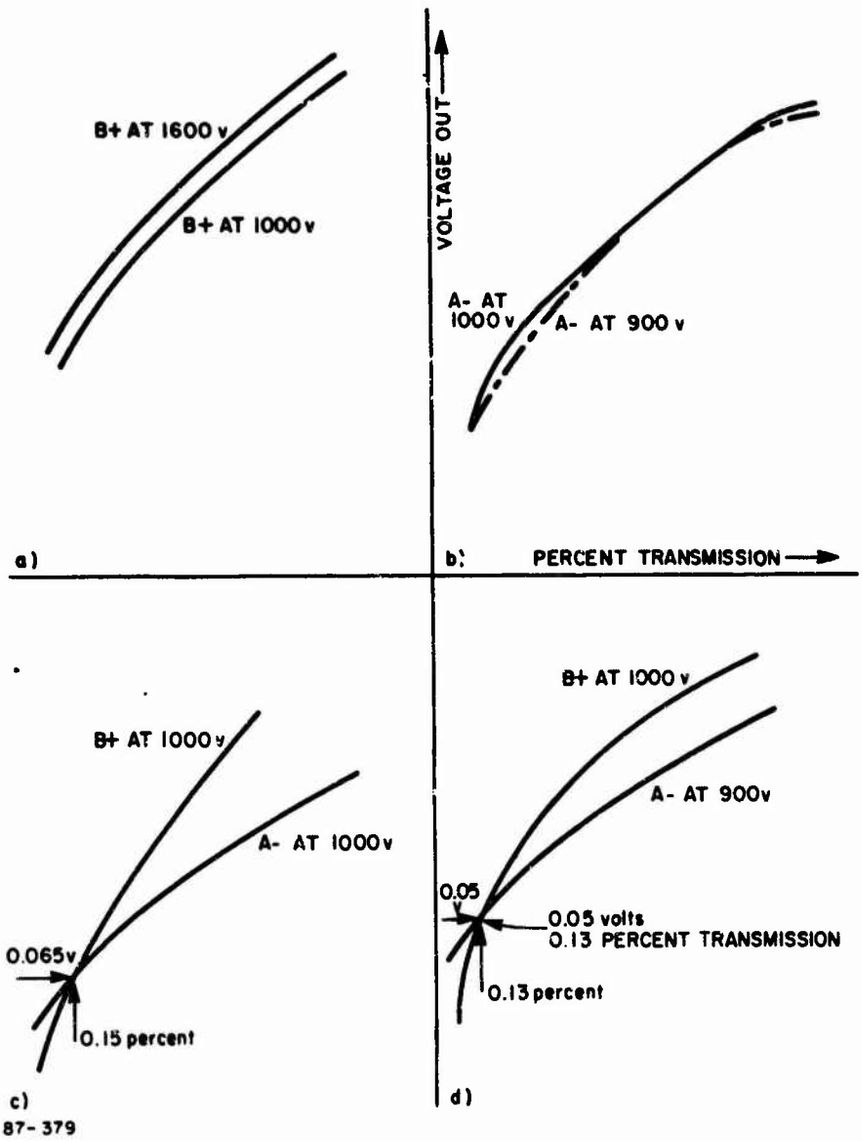

Figure 10 DIODE RESPONSE CHARACTERISTICS

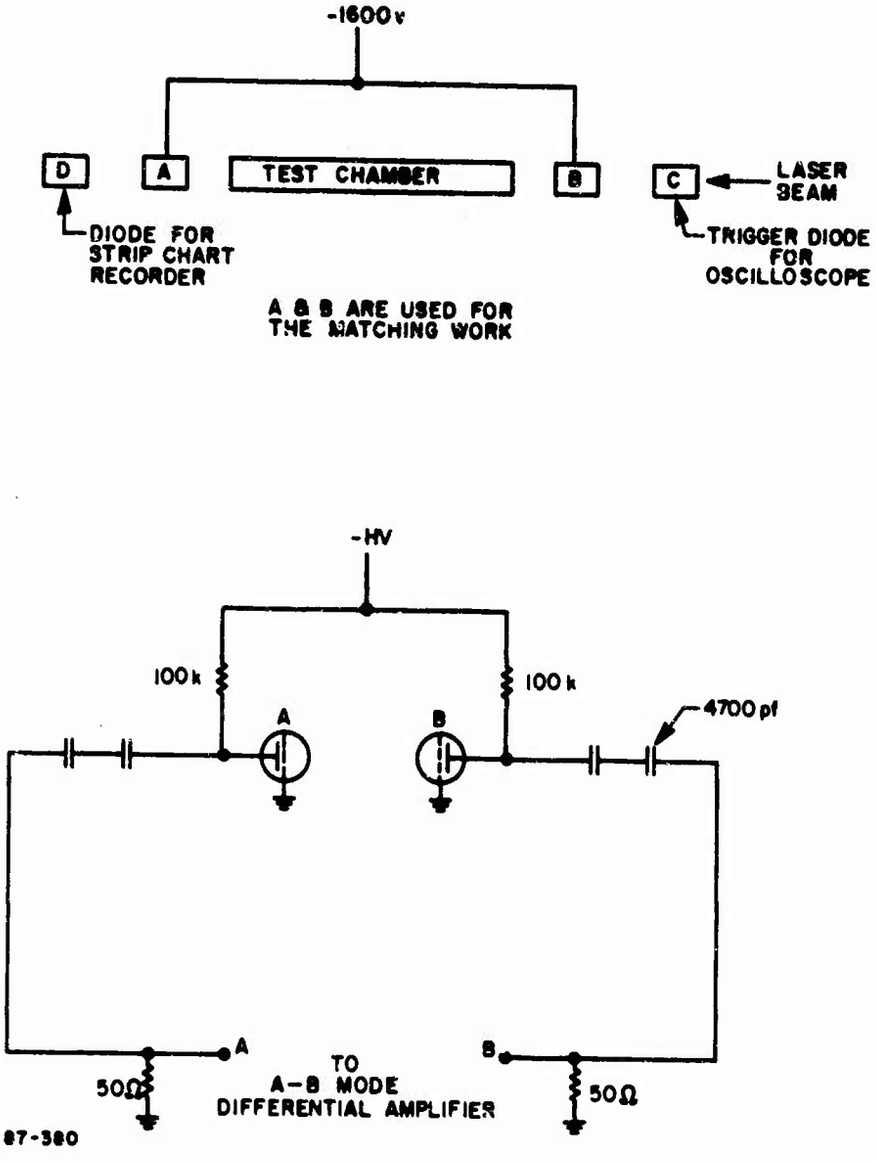

Figure 11 ORIGINAL ELECTRICAL ARRANGEMENT

At this time, the beam-splitter design was improved to allow for the insertion (in an easily controlled manner) of neutral density filters. It should be mentioned that, for quantitative work, the manufacturer's specification of the optical density (optical density is defined as the logarithm to the base 10 of the reciprocal of the transmission) is not accurate, especially at the laser wavelength of 6943 Å. For balancing purposes, this error is not significant, but can be important in calibration and diagnostics. The design used is shown in Figure 12. This mounting has a single beam splitter. Because the light is not necessarily plane polarized, a more sophisticated beam splitter should be used for careful experiments. This should contain an additional 45 degree glass plate, located at right angles to the first, in such a manner that a polarized light beam makes two reflections, and the effect of the two reflections removes the dependence of the signal arriving at the detector on the polarization of the light. The insertion of the additional beam splitter reduces the signal by a factor of 5, and can be compensated with a more sensitive photodetector (S-1 response).

3.3.2.3 Main Problem

Following these two unsuccessful approaches, it was decided that the main problem lay in the electronics, rather than in the photodetectors. It was also apparent that both photodetectors had to be operated in an identical manner. The approach then adopted was to apply the signal from each phototube directly to the plates of the oscilloscope. The circuit for this is shown in Figure 13. Again, the ITT-suggested diode circuit is used. The circuit was then successively revised to eliminate unwanted signal reflections, and to improve the time response, Figures 14 and 15. First, a 100-foot length of RG-58U cable was added to delay the signal enough to permit triggering of the oscilloscope with a trigger pulse derived from the laser-monitor detector. (The direct application of the signal to the detector plates bypasses all internal delays.) The 50 ohm terminating resistor was moved and finally placed on both ends of the 100-foot delay line.

The arrangement, as shown in Figure 16, was capable of at least a 1-percent balance However, it was found that as the output intensity of the laser was increased, a large unbalance signal appeared, which behaved as if the high-voltage supplied to one of the diodes had somehow become depleted. In order to elminate this, the ITT circuit was abandoned. In its place the diode circuit shown in Figure 17 was used. The ITT holders were adapted by removing the spring holder from the case, inserting a Teflon insulator, and soldering a high-voltage lead to the anode ring of the diode. The high voltage to the diodes was now ballasted with separate capacitors, to prevent depletion of the supply. Finally, the 4700 picofarad condensors in the plate-deflection circuit were replaced by 470 pf, and a variable-delay line was added to one of the two signal lines. The final arrangement is shown in Figure 18.

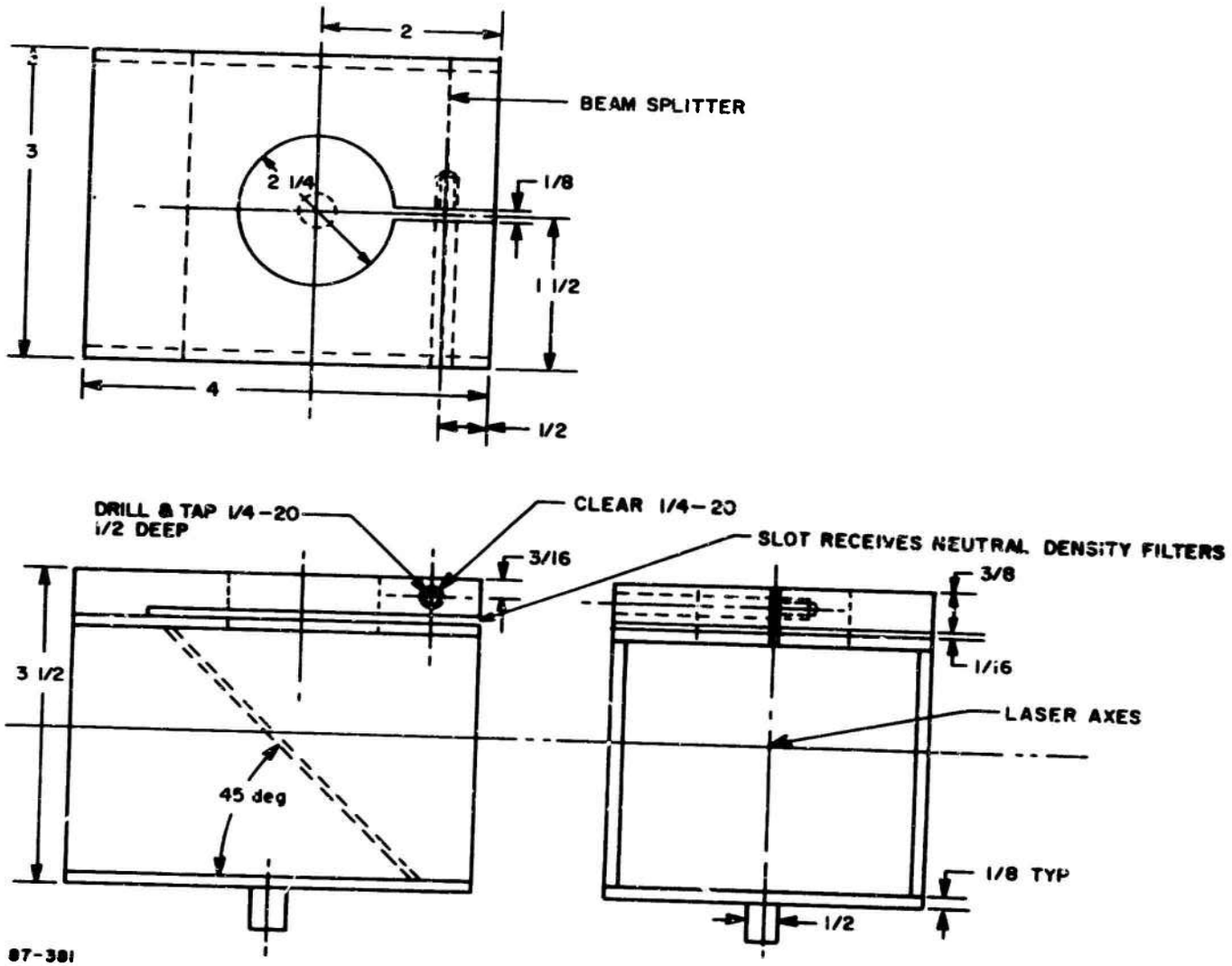

Figure 12 BEAM SPLITTER

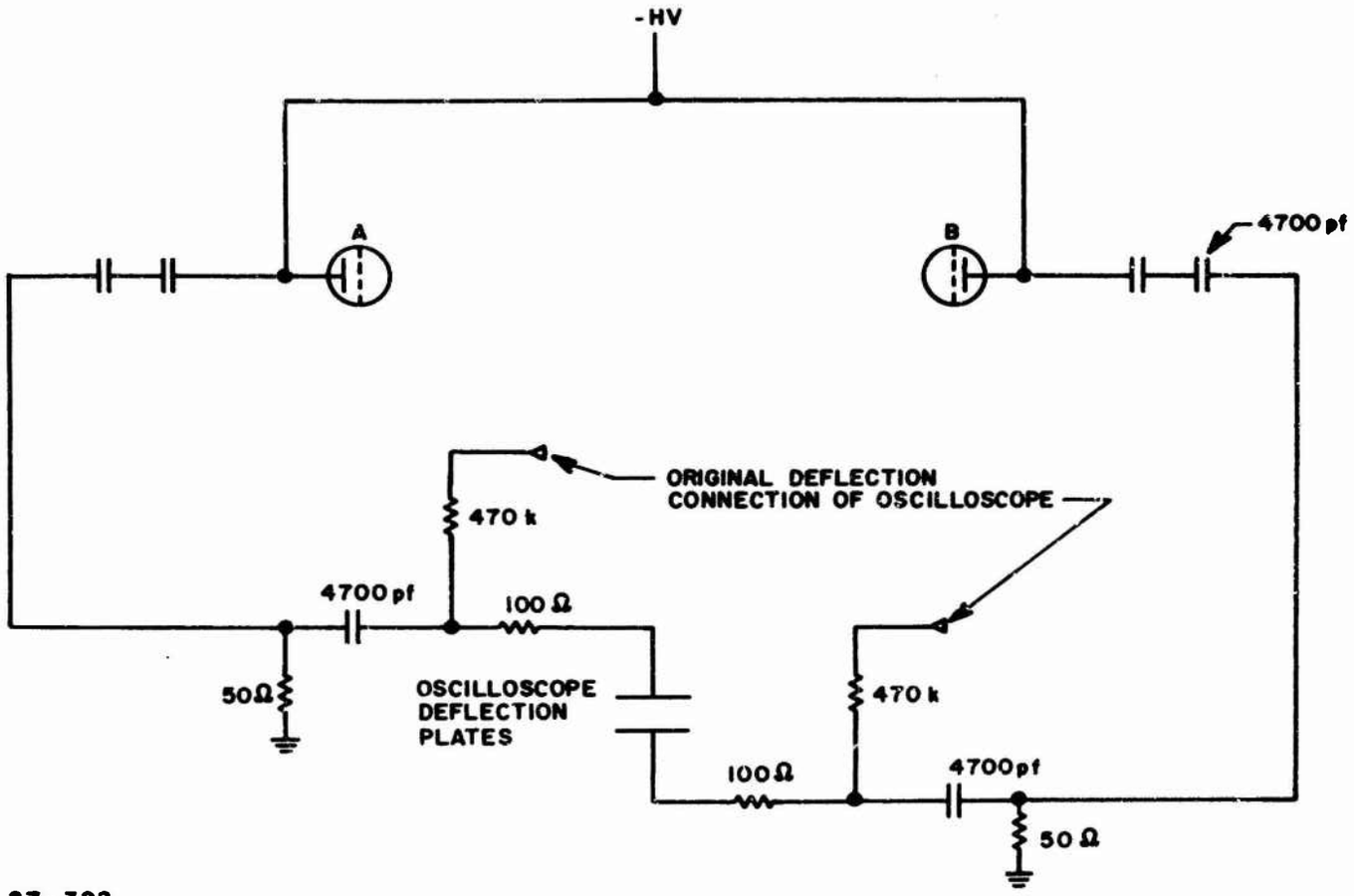

Figure 13 MODIFIED CIRCUIT A

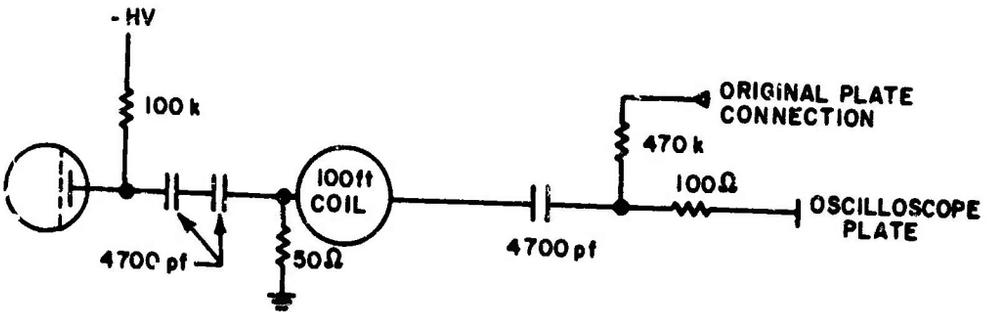

Figure 14 MODIFIED CIRCUIT B

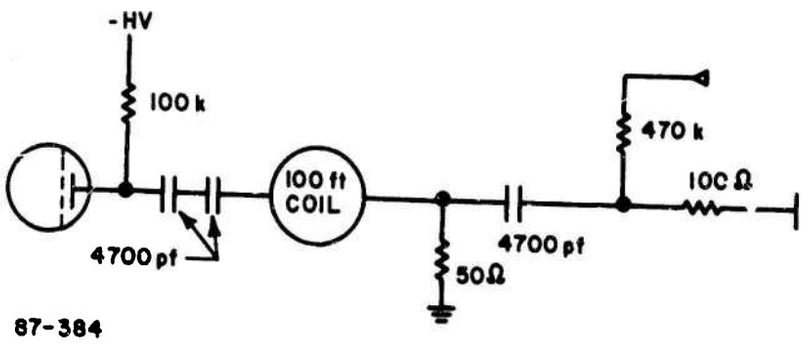

Figure 15 MODIFIED CIRCUIT C

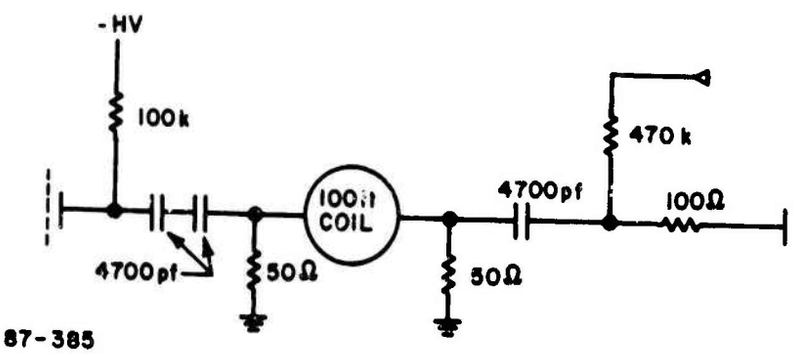

Figure 16 MODIFIED CIRCUIT D

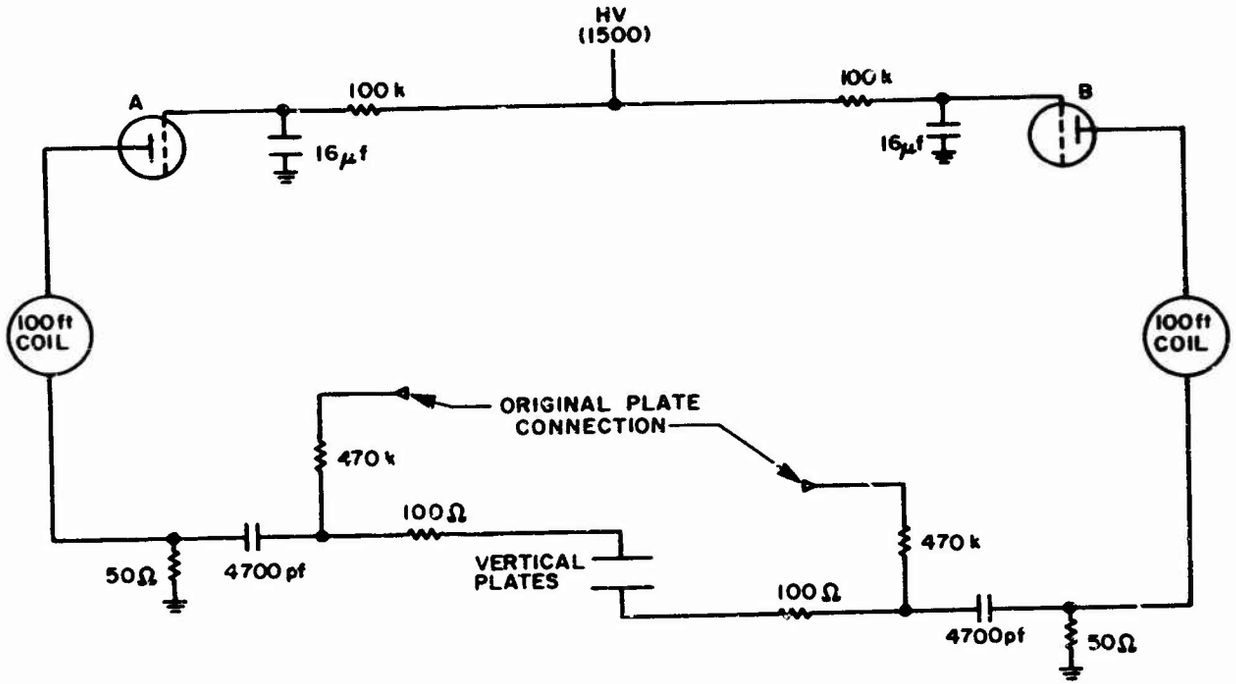

Figure 17 MODIFIED CIRCUIT E

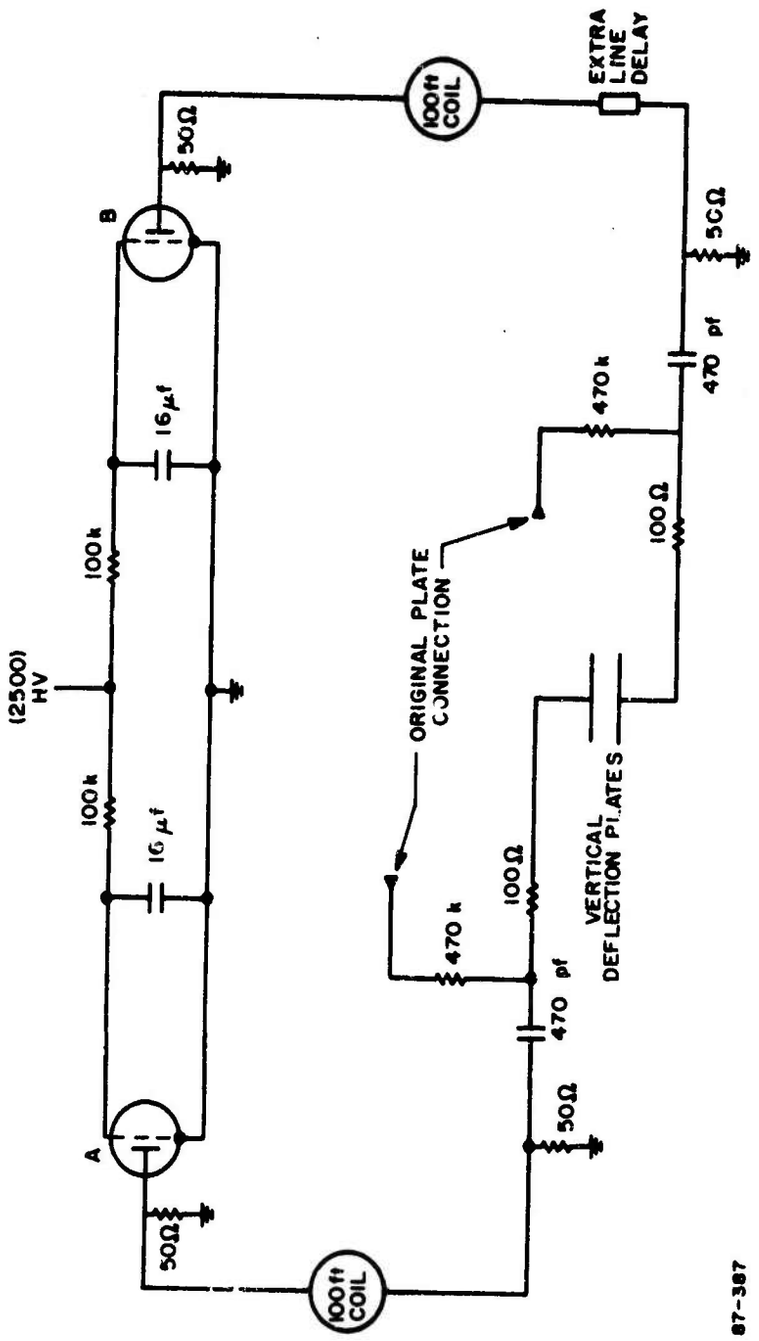

Figure 18 MODIFIED CIRCUIT F

This circuit was capable of balance to at least 1 percent. However, it did develop a major difficulty. At very-high signal levels (corresponding to nearly 50 volts applied to each plate) the electron beam in the oscilloscope defocussed. Thus, although the balance could be maintained at high signal strengths, the signal could not be observed. This effect also limits the sensitivity, since it limits the magnitude of the signal which can be applied.

It was hoped that a better oscilloscope (Tektronix 519) could be adapted to the above circuit. However, the construction of the oscilloscope is such that a major design alteration is required. It is not possible to apply the signals to both deflection plates.

Following these attempts to obtain a balance technique to better than 1 percent, a novel approach was investigated. This consists of reversing the phase of the signal through one cable by connecting the central conductor of the cable at the output end to ground, and obtaining the signal from the outer conductor. The two signals are now of opposite sign, and can now be directly mixed, and applied to one plate of the oscilloscope. The circuit for this is shown in Figure 19. This method is successful because the cable length is such that the transit time is longer than the pulse length. As a consequence, the signal loses its reference to ground and reversal of signal is possible. The method will not succeed for pulses longer than the transit time, which is approximately 150 nanoseconds in the 100-foot cable. The method also allows a balance to be obtained, to about 0.5 percent, and is therefore an improvement over the earlier technique. It also is not affected by the magnitude of the signal. Finally, it can be applied to a 519 oscilloscope, which has extremely good (less than 1 nanosecond) time response.

The time response obtained by applying the signal directly to a 545 oscilloscope has also been investigated with the same type of circuit as shown in Figure 19. This response is approximately 2 nanoseconds, which is considerably better than the response of the internal circuitry in the oscilloscope.

Figure 20 shows a schematic of the suggested arrangement for short-pulse attenuation measurements. Each monitor, which will be described later in detail, provides an output signal which is proportional to the light power arriving at the monitor position. The signal from the two monitors is mixed, as previously discussed, and used as a measure of the difference between the light power entering the test chamber and leaving the test chamber. This difference can then be compared to the actual signal entering the chamber to provide a precise measurement of the effect of the aerosol in the chamber on the attenuation.

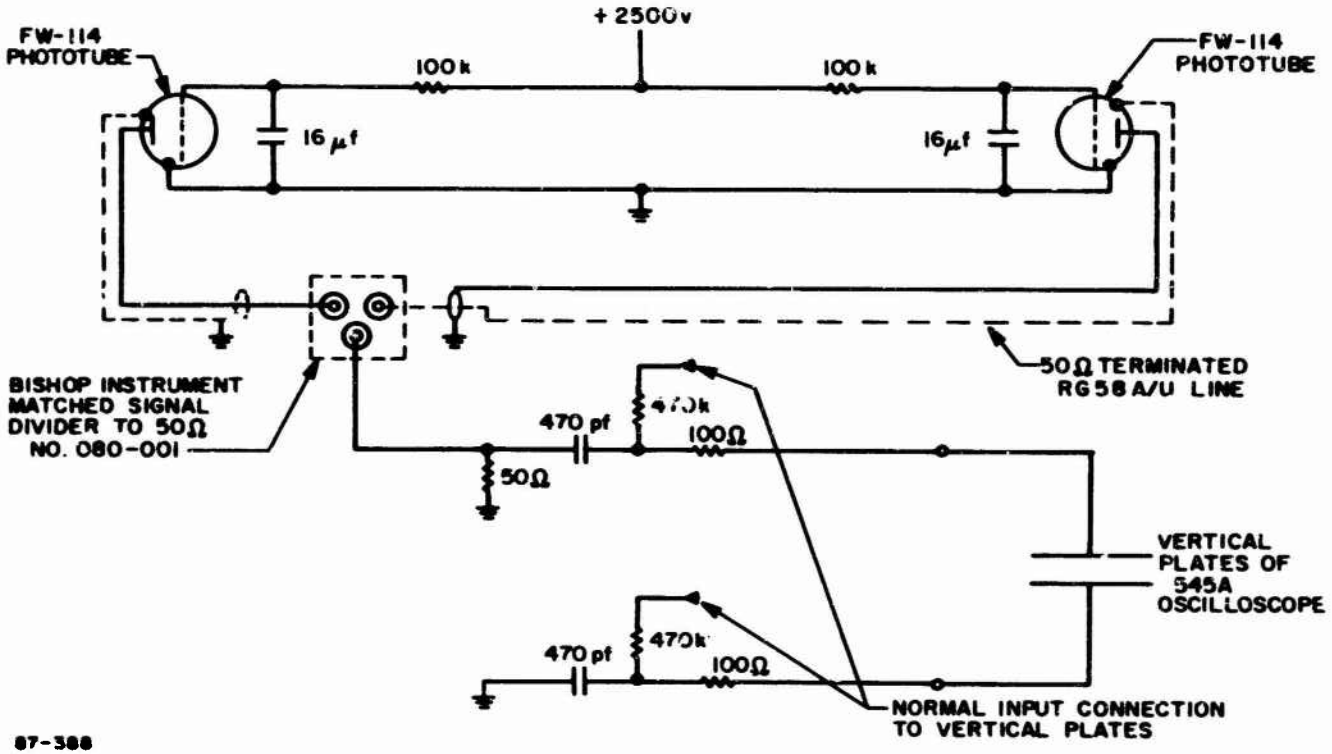

Figure 19 FINAL BALANCING NETWORK

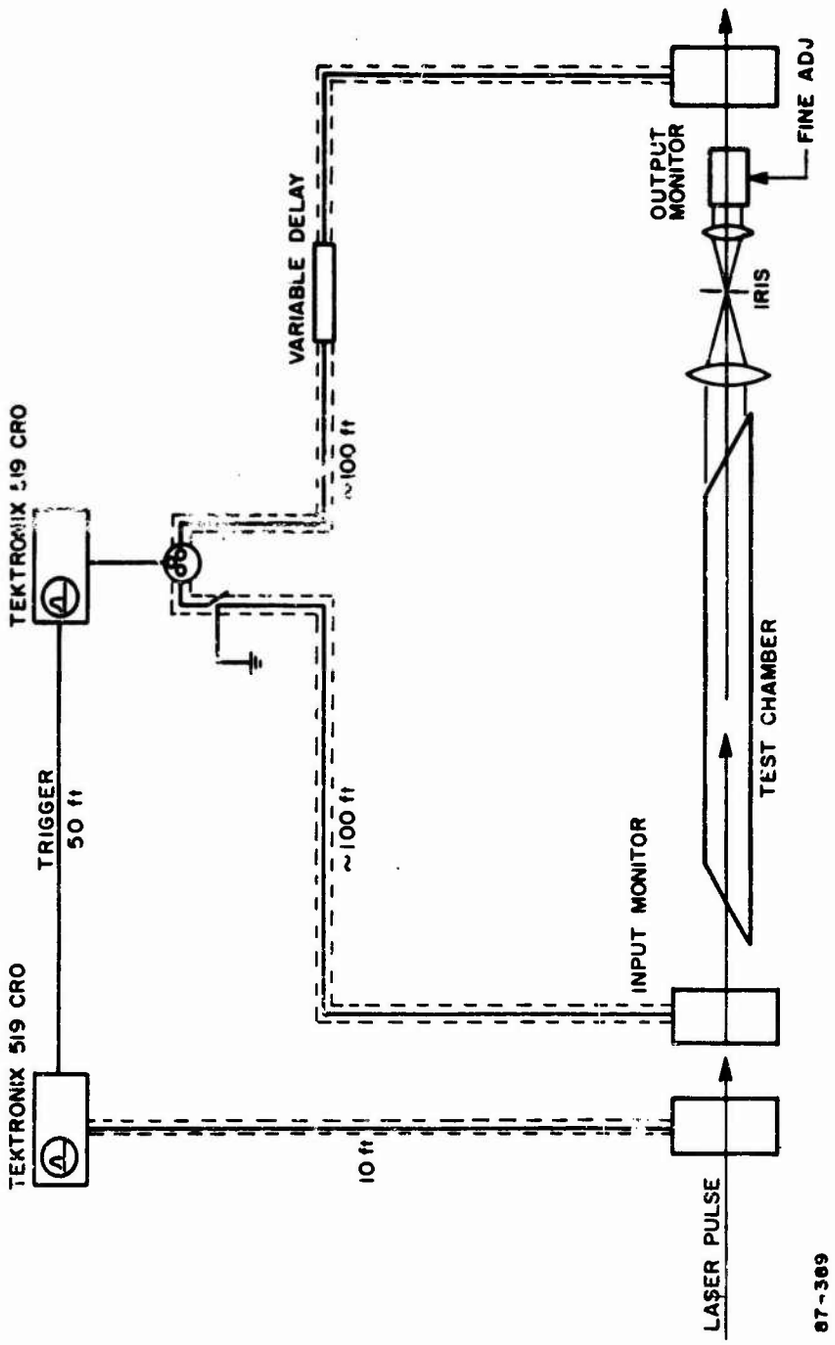

Figure 20 ATTENUATION MEASUREMENT

3. 3. 2. 4 Suggested Procedure

The suggested procedure is the following. The signal corresponding to the incoming laser pulse is fed directly to a Tektronix 519 oscilloscope, operating in the single sweep, internal-trigger mode. Care must be taken to ensure that the signal arriving at the oscilloscope is not too large, since the internal resistance of the oscilloscope can be destroyed by a short-pulse signal exeeding 100 volts. By starting with a large attenuation (a neutral-density filter of high value) in the path to the monitor phototube, the amount of attenuation can be successively reduced at each firing until an approximately full-scale signal is obtained. This corresponds to approximately 20 volts with an impedance of 125 ohms, or a photo-current of 0. 16 amperes. Such a photocurrent corresponds to a power, at the detector, of 2. 7 x 10^5 watts, for the S-4 FW114ITT planar diode. Since a 10^9 watt laser pulse would provide about 2. 7 x 10^6 watts at the monitor photosurface (as will be discussed later), an attenuation of a factor of 10 is required. If a more sensitive photodiode (S-20 response) is used, a factor of nearly 1000 would be required. Neutral-density filters are available which can allow a selection of attenuation factors from over 10^4 (ND = 4) to as little as 0. 80 (ND = 0. 1), so approximate selection of the necessary attenuation requires only a few firings.

The trigger pulse from the oscilloscope is now used to trigger a second oscilloscope which displays the difference signal from the two monitor diodes. Because of the delay introduced in the difference signal by the presence of the 100-foot cable lengths, the trigger signal may also require a delay. This can be accomplished with a long cable length, selected after determining the actual delay.

The signal from the two monitors depends upon the degree to which a balance is attained. First, a very large, neutral-density filter is placed in the output monitor, so the signal observed is essentially that of the input monitor. A large enough filter is placed in the input monitor so the signal observed corresponds to about a full-scale deflection. The delay between the oscilloscope trace of the pulse shape and the trace of the unbalance signal can be accurately measured. If now the attenuation in the output monitor is decreased until an approximate balance is attained, it will be possible to further reduce the attenuation in both the input and output monitor, without obtaining an excessive signal. At this time it will also be important to adjust the variable-time delay, which should be in the line of the output signal, so as to ensure that the signals coincide. The difference signal is then made as small as possible, by means of neutral-density filters, until the nearest balance is attained, with the remaining signal corresponding to a slight deficiency in the input. Fince balance can be achieved by adjustment of the angle of incidence to the output beam of two pellicles or beam splitters. Two are required to make the adjustment independent of plane of polarization.

Once a fine balance has been achieved, the unbalance signal is calibrated by the insertion of a calibrated, neutral-density filter into the input-beam monitor. In the absence of any aerosol particles in the chamber, the unbalance signal in the oscilloscope is now proportional to the signal in the pulse-shape-monitor oscilloscope:

$$V = A(T - 1) V_s \tag{104}$$

where V is the observed difference voltage (or deflection), and V_s is the voltage (or deflection) of the actual pulse. T is the transmissivity of the added filter, A is a proportionality constant, which is evaluated by this technique. The delay between the two oscilloscope signals must be taken into account in making this calibration. The constant A should be independent of pulse shape or magnitude. Now, if an aerosol is added to the test chamber, of transmissivity T_a, the signal observed will be, if the filter in the input side is not removed.

$$V_a = A(T - T_a) V_s \tag{105}$$

from which

$$T_a = T - V_a / A V_s . \tag{106}$$

Since the individual signals from the input and output monitors can be quite large (only the difference is recorded), the factor A is large. As a consequence, a small change in transmission can be readily observed. It is estimated that this change can be as little as 1/2 percent. The limitation here is primarily that of time response in the mixing circuit. Some improvements may be possible. The factor A can be as much as 10. An ultimate limitation would be the accuracy to which the oscilloscope trace can be measured. This is about 0.1 millimeter. With a full scale deflection of 20 millimeters, the precision attainable would then be about 1 part in 2000, or 0.05 percent.

3.3.2.5 Long-Duration Laser Pulses

For long-duration laser pulses, the above technique is not suitable. In the first place, the phase-reversal method does not work if the overall pulse duration is large. In the second place, the magnitude of the signal is such that some amplification is necessary. On the other hand, a rapid time response is also not necessary. In fact, since there is no reason to expect that changes in attenuation will occur during the individual pulses which form the output of a long, or multiple-pulsed, laser burst, the time response of the system need only be enough to permit the evaluation of the average power. A simple integrating circuit is sufficient for this. Also, because high time response is not important, the detectors can be operated in the manner first used. One can be operated with the cathode at a negative high potential, and the signal be obtained from the anode current. The other can be operated with the anode at a positive high potential, and the signal obtained from the cathode current. The two signals are then used to charge condensers, and the

oscilloscope is used to record the integrated difference in the two output currents. The circuit for this is shown in Figure 21. The balancing procedure is precisely the same as that used in the short-pulse case and, since the same diodes can be used will not involve greatly differing values of attenuation. The only difference will be that the signal observed on the oscilloscope will be the integral of the laser power, rather than the power itself.

The monitors for the laser-beam power are shown schematically in Figure 22. These consist of a first beam splitter, oriented so that a small portion of the beam is deflected at right angles onto a second beam splitter, and thence is reflected through filters and other optical elements onto the photo-surface of an ITT planar diode. For minimum loss of energy, the first beam splitter should be be such that the beam is reflected in a direction parallel to the direction of polarization of the laser beam. In order to eliminate the effect of polarization, the second splitter should be such that the reflection is at right angles to the plane of polarization. With such a system, if the splitters are uncoated glass flats, or pellicles, about 1.65 percent of the beam will be reflected by the first reflector, and 16.7 percent of this will be reflected by the second reflector, for a net power to the filters and diode of 0.275 percent of the incident power.

The construction of the monitor includes the ability to place neutral-density filters or other filters in the path between the second reflector and the planar diode. These filters can be used to control the power arriving at the diode, to select the plane of polarization desired, and to select the wavelength range over which the detector is to be sensitive. A diffusing plate should also be used close to the diode, to reduce the intensity on the diode photosurface, minimize "hot-spots", and reduce the effect of a non-uniform photo-response if the beam profile is altered.

The ITT planar diodes, which were shown in Figure 9, are particularly well adapted to the measurement of intense-laser-light beams. They have extremely fast-time response, since the photoelectrons need travel only about 1 centimeter. They are constructed to withstand high voltages (as much as 5000 volts applied potential), so the space-charge limitation on photocurrent is very large. In fact, under usual operating conditions, the signal necessary to drive a 519 oscilloscope to a full-scale deflection (about 0.16 amperes) is nearly three orders of magnitude less than the space-charge-limited photocurrent. Given an adequate light source (and laser beams are adequate), they are far superior to photomultipliers in both time response and tolerable output current.

The only major difficulty that may be encountered when planar diodes are used to monitor the short-duration laser pulse is that of an excessive noise signal radiated by the diode circuitry. The noise occurs because the photocurrent emitted by the laser pulse is on the order of a tenth of an ampere, with a rise-time of a few nanoseconds. As a consequence, an electromagnetic signal is radiated by the diode and any unshielded leads to it. This signal can be picked up by other detectors in the vicinity. A particularly bad offender is the photomultiplier used for observing scattered signals. Care must be taken to adequately shield the anode lead of the photomultiplier from pick up from the dynode leads. The noise from the photodiodes can can also be minimized by diode design as will be discussed later.

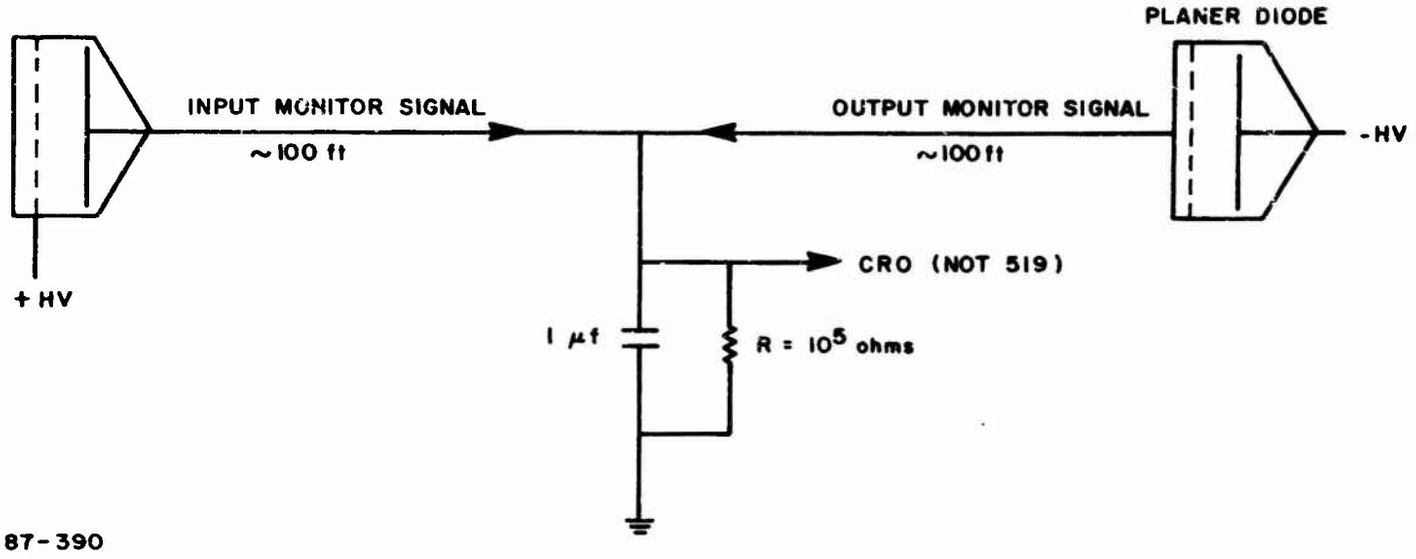

Figure 21 INTEGRATING CIRCUIT

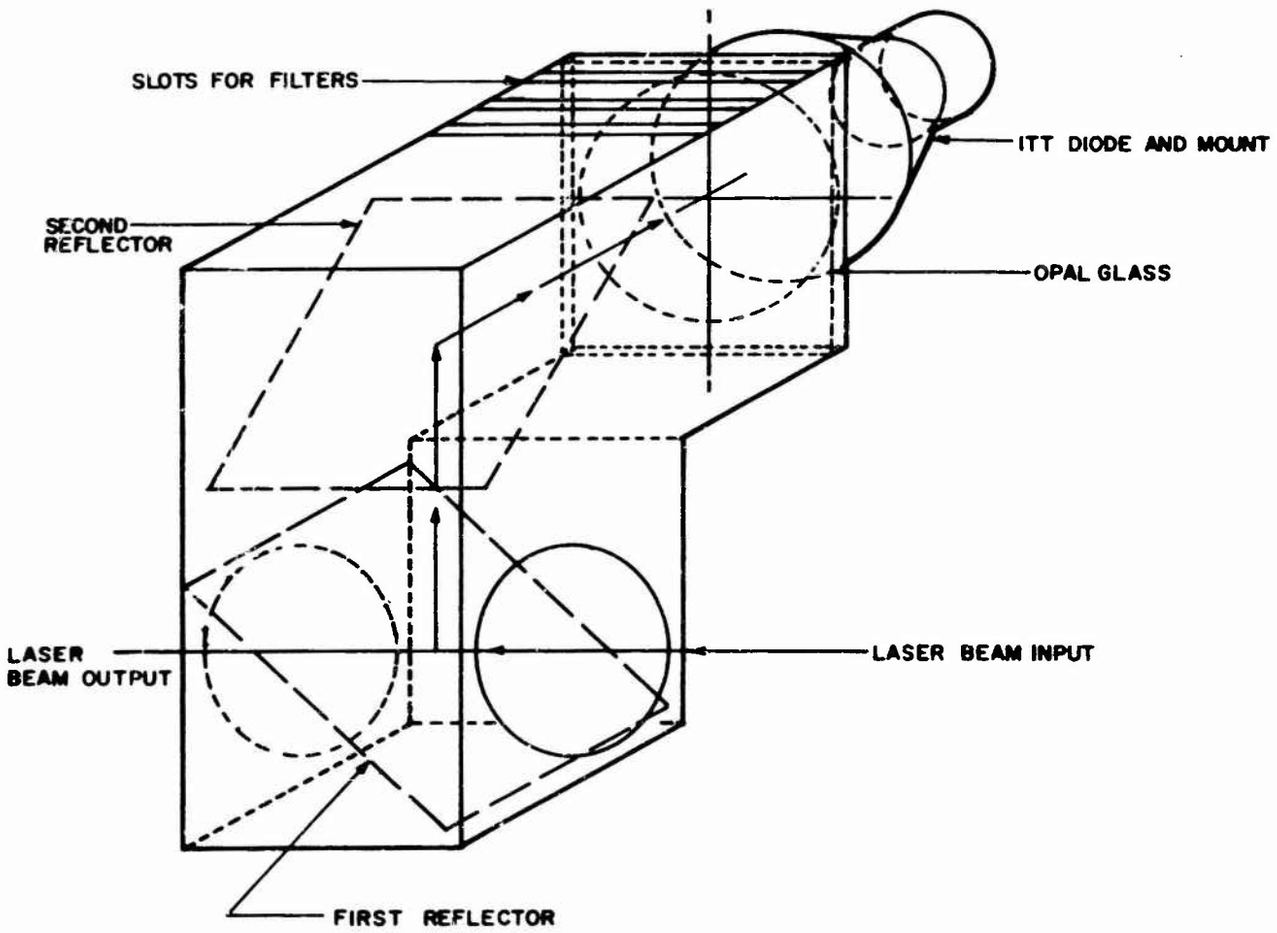

Figure 22 LASER BEAM POWER MONITOR

3.3.3 Combined Scattering and Attenuation Measurements

It is expected to be a straightforward procedure to make simultaneous measurements of attenuation and scattering. In fact, if the attenuation in the chamber is large, such measurements will be necessary if accuracy in the scattering measurements is to be attained. The experimental set up for the combined measurements is shown in Figure 23. Here we have made provision for calibration as well as measurement. The attenuation-measurement procedure is the same as that discussed in an earlier report, in which a signal representing the difference between the light power incident on the aerosol region, and emerging from it, is compared to the signal representing the power incident itself.

If the transmissivity through the aerosol-containing length, L_o , is measured, then the laser power at the point at which the beam is scattered into the scattering detector can be calculated by the equation

$$P = P_o \, T^{x/L_o} \tag{107}$$

where T is the transmissivity through the entire aerosol region, L_o the length, and x the distance traversed through the aerosol before arriving at the scattering region. If the attenuation is large, it may also be desirable to correct the scattered power received at the detector by the factor T^{d'/L_o}, where d' is the distance traversed, in the aerosol, by the scattered radiation. In most cases, however, this correction will not be necessary, since T should be fairly near unity. and d'/L_o should be much less than unity.

The effect of multiple scattering on the transmission measurement has also been considered. At first it was felt that a significant amount of the energy transmitted through the aerosol might be the result of multiple scattering, so that it would be necessary to restrict the field of view of the detector of the transmitted radiation. This restriction is inherently undesirable, since any beam-divergence effects might then introduce a spurious attenuation. However, by transmitting a gas laser beam through the aerosol, and restricting the field of the detector, it was found that there was no measurable difference in the transmission, as the field of view was changed. In the experiment, the detector was removed from the attenuation region by a distance of about 1 meter. Avco now feels that as long as the detector is removed from the aerosol region, there will be no need to excessively restrict the field of view.

3.3.4 Wave Front Changes

Two methods can be used to determine the effect of the laser radiation on the aerosol, and in turn, the effect of the aerosol changes on the optical path through the aerosol. The first of these is interferometric. At Avco, a Mach-Zehnder configuration with a helium-neon gas-laser source is used, along with an STL model 1D image-converter camera to observe index-of-refraction changes in the

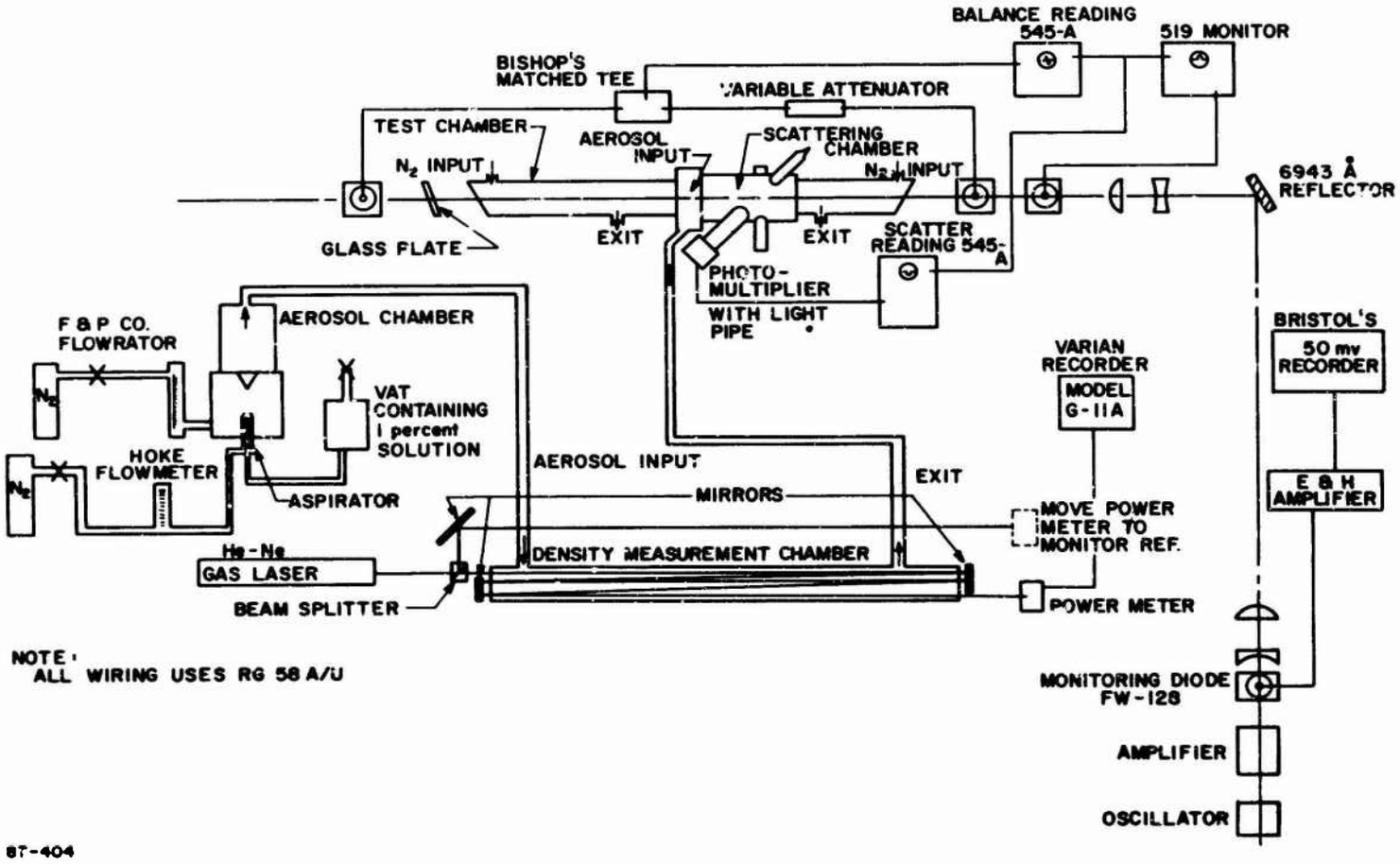

Figure 23 SCHEMATIC OF EXPERIMENTAL ARRANGEMENT

vapor created by the interaction of laser energy with solids. The basic arrangement is shown in Figure 24. Here the radiation from the gas-laser source is split into two equal fractions, and then after reflection from two mirrors, is recombined with a second beam splitter. One of the two beams created passes through the region to be investigated, and the other serves as a reference beam. By careful adjustment of the mirrors and beam splitters, the two beams can be made to recombine in such a manner that both beams form overlapping images, and yet arrive at slightly different angles of incidence. As a consequence, interference fringes appear in the image. Now, if there is a change in the index of refraction, then the fringes will shift by a small amount. The fractional shift (in terms of fringe separation) is then

$$\delta = \int \frac{n_o - n}{\lambda} \quad d_x \tag{108}$$

where n_o is the index of refraction in the indisturbed region, and n is the index in the disturbed medium. The integral is over the region where n differs from n_o.

In the system operated at Avco, the beam from the laser source was focused by means of a cylindrical lens to a line focus at the point of interest. This line was then focused onto the image plane of the STL 1D image converter. Since the reference beam also contained the line focus (the lens used to focus the laser beam was placed before the first beam splitter) it could be focused to a line at the image plane.

The mirrors could then be adjusted to make the images coincide and at the same time to produce a number of fringes which were perpendicular to the line. In the setup used at Avco, all of the mirrors and splitters were mounted on standard-optical bench components. Although some instability was apparent, the fringes were found to remain essentially stationary for a period of at least 1 millisecond. Because of the highly coherent nature of the gas laser used for the light source (a Spectra-Physics Model 116), there was no need to take extreme precautions to ensure that the optical path in each arm was precisely the same. The fringe pattern was oriented on the image plane so that the image was perpendicular to the direction of the sweep of the image, when the camera was operated in the streak mode. A typical interferogram is shown in Figure 25. The region where the fringe shift occurs represents a time of about 100 nanoseconds, with a resolution of about 10 nanoseconds.

In probing the aerosol, the same arrangement can be used, with the probe beam directed across the intense laser-beam path. Mirrors could be added to increase the number of passes through the aerosol. These should be added in both arms, to maintain an approximately equal path length. Again, a line focus of the probe and reference beams is required if a line image is to be formed at the detector surface. This arrangement is shown in Figure 26.

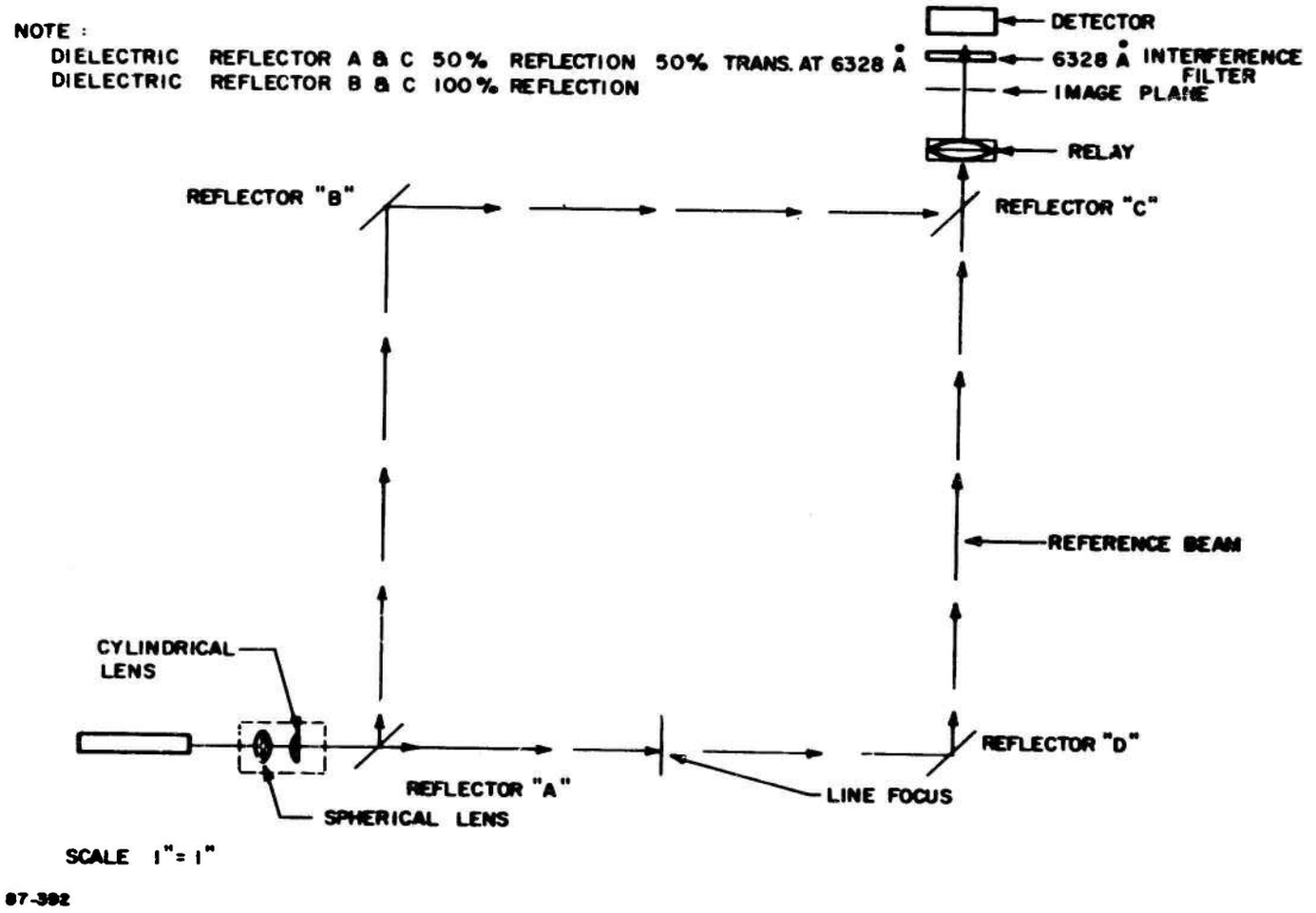

Figure 24 MACH-ZENHDER INTERFEROMETER

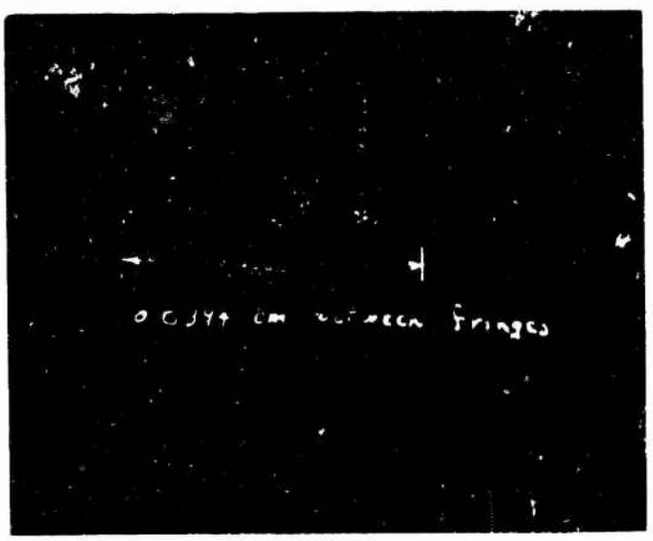

Figure 25 ENLARGEMENT OF INTERFEROGRAM

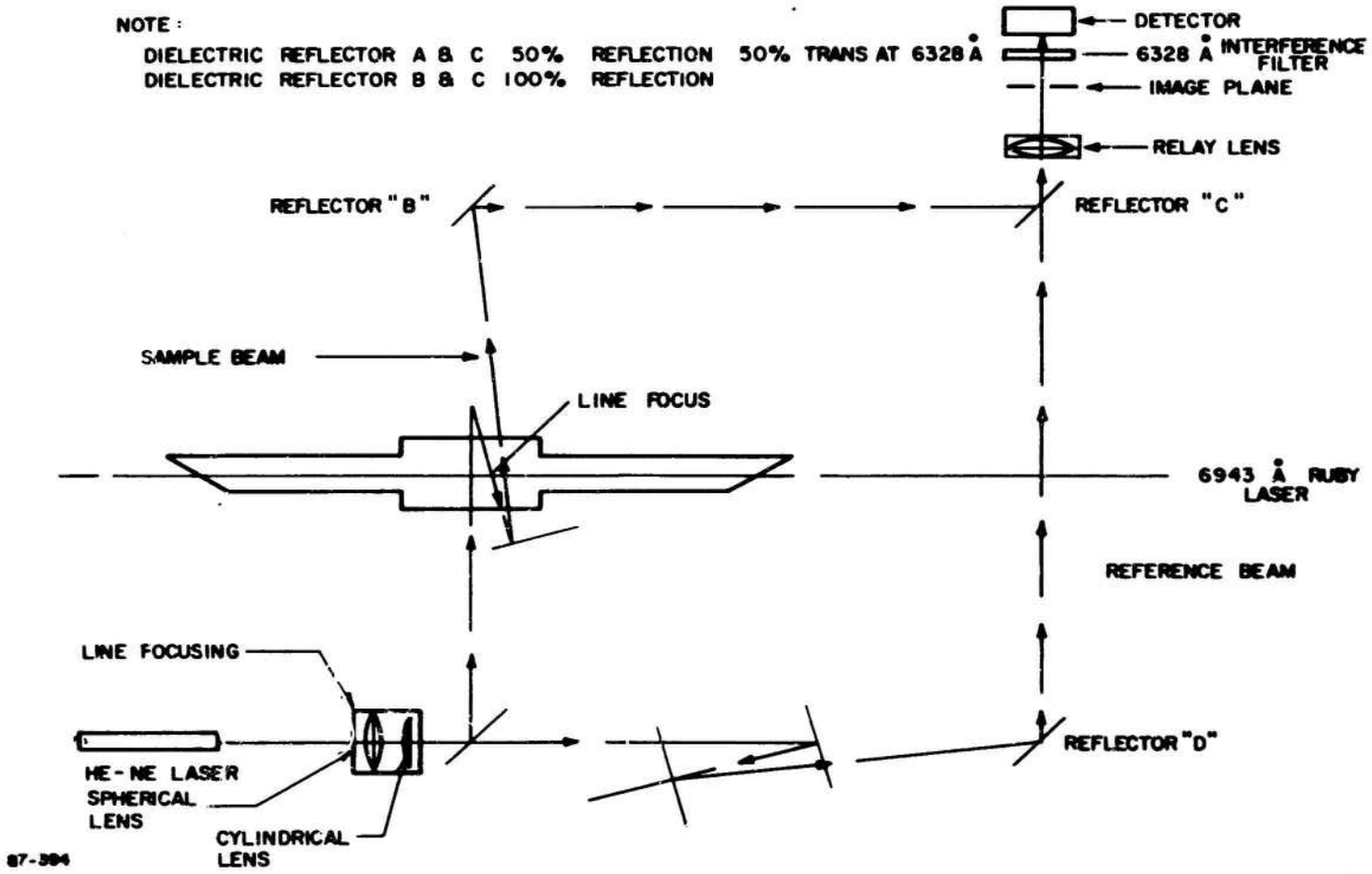

Figure 26 INTERFEROMETER ACROSS THE BEAM

The arrangement shown above is not very sensitive, since the path length traversed in the aerosol is short. A more sensitive arrangement is shown in Figure 27, where the probe beam follows the same path as the intense laser beam. Note that the probe beam passes through the aerosol in the opposite direction from the main beam. This is to avoid irradiating the detector with the intense laser radiation. The plane of polarization of the gas-laser-probe beam is rotated 90 degrees with respect to the plane of the intense laser radiation. This allows the use of a polarizer in the path from the gas-laser source, and essentially eliminates the possibility that the source can be damaged by the laser radiation which would otherwise reach it.

3.3.4.1 Alternative Method

An alternative method of measurement of fringe displacement is also possible. If, instead of the image converter, a photomultiplier is used, and this multiplier receives only the light corresponding to a portion of a single fringe, then the amplitude of the photocurrent will undergo oscillations as the index of refraction changes and the fringes pass across the multiplier aperture. The change in optical path length is now measured by the number of oscillations of the photomultiplier output. An ambiguity exists, however, since the direction of fringe motion will reverse once the index of refraction change has reached a maximum. In most cases, this reversal will be identifiable from the amplitude of the oscillation at that point, since it is not likely that the reversal will occur when the amplitude is either at the maximum, corresponding to complete constructive interference, or at the minimum, corresponding to complete destructive interference. This method will have a time resolution limited only by the multiplier response. An RCA 4459 multiplier would be quite adequate, since it has an S-20 response, a rise time of 2 nanoseconds, and a gain of 6.6×10^6.

If the image-converter-streak method is used, the resolution is limited by the amount of light available on the recording film. With Polaroid-type 47 film, a time resolution of 10 nanoseconds could be observed using a laser source of 10 milliwatts, and a Mach-Zehnder configuration which permitted about 50 percent of the laser light to arrive at the image plane. This configuration would be the same for the across-the-beam probe. However, the along-the-beam probe puts only about 7 percent of the gas-laser radiation onto the detector. Thus a 10 milliwatt laser would provide about 70 nanoseconds resolution. In most cases this would be adequate, since the thermal effects associated with a Q-switched laser pulse would require a longer time than this to become apparent. More of the energy of the gas laser could be sent into the detector, but only at the expense of a reduction of intensity of the main laser beam. In the arrangement shown, this reduction is only about 1 percent.

Also in this arrangement, a large fraction of the energy transmitted through the test chamber is directed toward the gas-laser source. However, the gas laser can be protected by distance (the main laser beam has relatively large divergence), by the addition of a filter, and by the polarizer indicated in Figure 27.

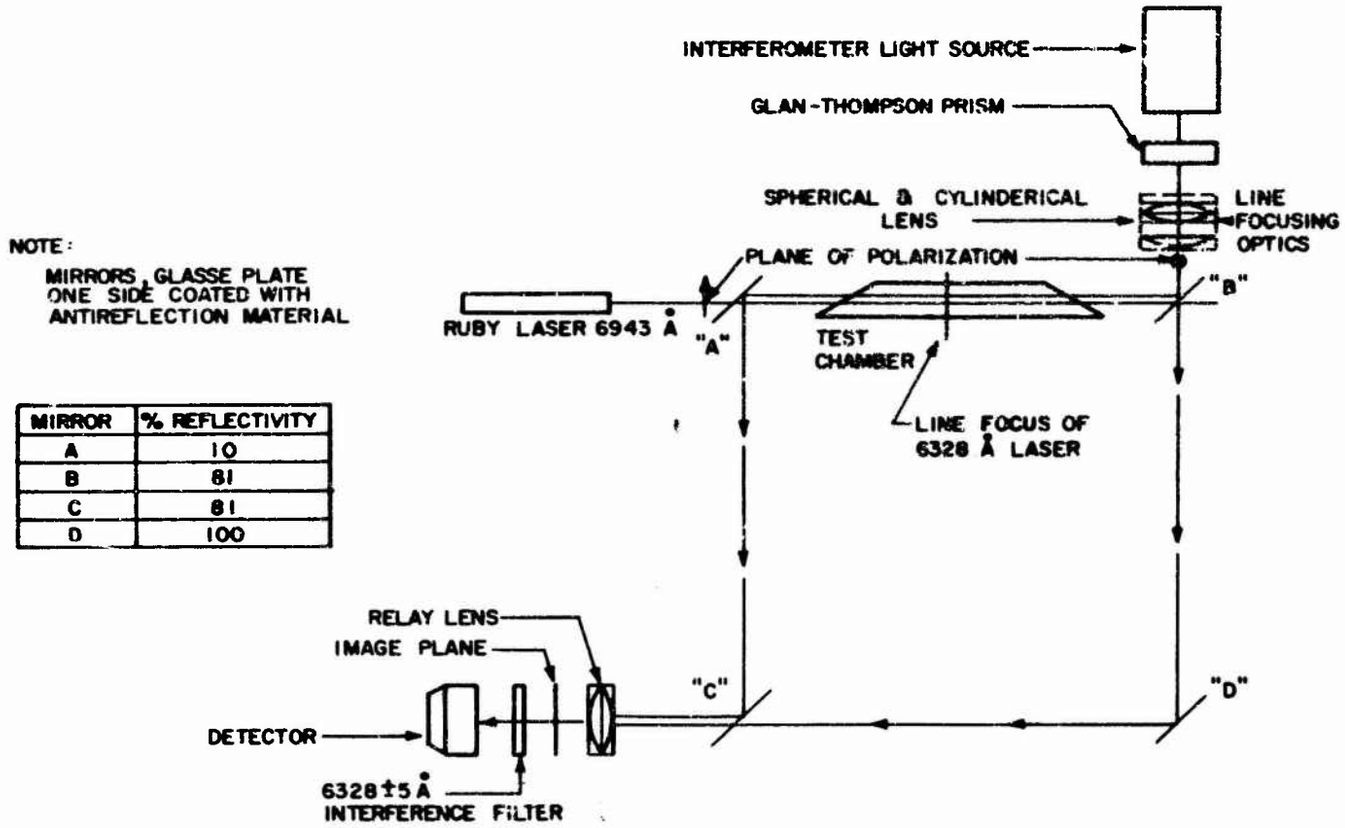

Figure 27 MORE SENSITIVE INTERFEROMETER

The other approach to the measurement of the optical-path change is to measure the effect on the beam itself, or on a beam sent down the same path at some time after the first beam. This type of measurement is not as sensitive as the interferometric measurement, but is a direct measure of the effect of an index-of-refraction change.

The suggested approach is the measurement of beam divergence, after the laser beam has emerged from the test chamber. Such a measurement can best be made by measuring the diameter in the far field of the laser beam. This is done by focusing the radiation, with a long-focal-length lens, onto a sensitive film, such as that EG&G X-R film. If necessary, an attenuater may be used to reduce the intensity at the film plane. The image of the beam is now accurately mapped with a profileometer, and a contour plot of the intensity is made. If the focal length of the lens is known, and the beam was initially parallel, the divergence corresponding to any point on the contour plot (the 1/2 intensity point is often used) can be determined from the size of the contour. This method can be used to determine the beam divergence for a short pulse. However, if the beam divergence changes during the pulse, as will probably be the case for a long pulse, then it will be necessary to use a time-resolved technique. One approach is to focus the radiation onto a screen, and photograph the screen with a framing camera.

It should be mentioned that this technique requires a certain amount of trial and error to find the minimum focal diameter of the beam. The focus of the laser radiation is not necessarily at the focal point of the lens, if the beam is not initially parallel.

Figure 28 shows a schematic of the suggested arrangement for time-resolved measurement of the divergence of the laser beam. The focal length of the lens should be sufficient so that the minimum focal diameter is large enough to prevent damage to the screen. For a beam with a divergence of 2 milliradians and an initial diameter of 1 centimeter, the focal length should be on the order of 500 centimeters. If the focal length is to be shorter, an attenuater should be used. The screen can be opal glass, or even ground glass. The camera is to be focused on the screen. If necessary, additional attenuation can be placed between the screen and the camera, although decreasing the aperture of the camera may be sufficient.

3.3.5 Beam Profile Measurements

Since the laser beam does not have constant energy density in its cross section, because of imperfections in the optics and ruby rods, it is necessary to measure the beam profile, if knowledge of the energy density is necessary to the understanding of an experiment. The beam profiles are reproducible as long as the components of the laser are not changed. This is especially true for the ruby-rod and flash-lamp positions. Typical beam profiles that were constructed by using a photographic technique are shown in Figures 29 and 30. A method by which the time history as well as the beam profile can be determined is presently being investigated.

Figure 28 DIVERGENCE MEASUREMENT

CONTOUR NO.	RELATIVE INTENSITY
1	1.0
2	0.98
3	0.91
4	0.86
5	0.81
6	0.76
7	0.72
8	0.67
9	0.62
10	0.52
11	0.40
12	0.3 to ZERO

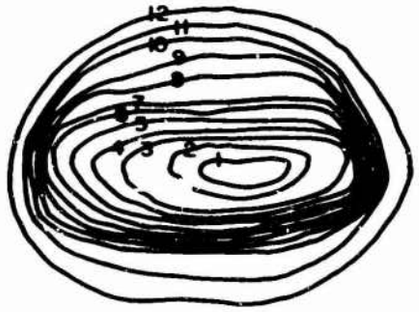

1 cm FILM
1.75 cm REAL SPACE
3.5 cm UNDIVERGED BEAM

87-397

Figure 29 BEAM PROFILE, SINGLE PULSE MODE

CONTOUR NO.	RELATIVE INTENSITY
1	1.0
2	0.96
3	0.92
4	0.86
5	0.80
6	0.74
7	0.69
8	0.62
9	0.57
10	0.46
11	0.36
12	0.25 to ZERO

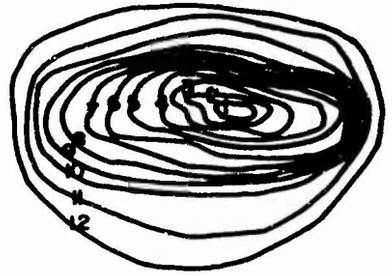

1 cm FILM
1.75 cm REAL SPACE
3.5 cm UNDIVERGED BEAM

Figure 30 BEAM PROFILE, MULTIPLE PULSE MODE

The apparatus used in the photographic approach is shown in Figure 31. A portion of the beam is diverted into a measuring system with a pellicle. Pellicles are manufactured by National Photocolor Corporation and consist of a clear plastic membrane stretched over a metal frame. The membrane has an index of refraction of 1.49 and a thickness of about 8 microns. With this type of reflector, the separation of images due to reflection from front and rear surfaces is extremely small. Pellicles are able to withstand very high intensities. The beam profile at any desired point is determined by focusing the desired portion of the test chamber onto the EG&G X-R extended-range film. The pellicle provides the necessary attenuation, since only about 2 percent of the beam is reflected (plane of polarization parallel to plane of incidence). This type of film has a relative exposure ratio of 10^8, which is accomplished by superimposing three emulsions of different sensitivity on one film base. The film is calibrated by exposing the film to laser radiation through a neutral-density step-wedge. The density of the various exposures are determined by using a microdensitometer. With this information, a calibration curve of density versus relative exposure can be drawn.

A density distribution of the laser-beam profile is determined by scanning the exposed film with a microdensitometer. From this, a three-dimensional relative-intensity distribution plot can be constructed.

Figure 32 is an experimental setup used for probing the cross-section of a ruby laser beam to determine if a relationship exists between the position within the cross-section and the time history of the laser pulse. Here an ITT, FW 114 Planar diode, using the collimating tube and lens system, "sees" a magnified portion of the laser beam in the far field. The planar diode response is recorded by a Tektronix 545 oscilloscope. Figure 33 and 34 show typical responses. The planar diode is mounted so that it can accurately scan the beam vertically and horizontally. In this way small portions of the beam cross-section can be sampled as to its position, relative intensity, and time history. So long as components of the system are not disturbed, it is known[3] that the beam profile does not change from shot to shot. Therefore a beam profile can be constructed from relative-intensity measurements made while scanning the beam cross-section so long as the laser output energy remains constant. All time measurements are made relative to a trigger pulse from an ITT FW-114 planar diode which "sees" a portion of the laser beam.

The time response of the present system is limited by the time response of the oscilloscope. Analysis of the preliminary data shows no measurable time variations with respect to position. The present optical system coupled with a Tektronix 519 oscilloscope will improve the time response to less than 1 nanosecond, which is necessary for a thorough analysis.

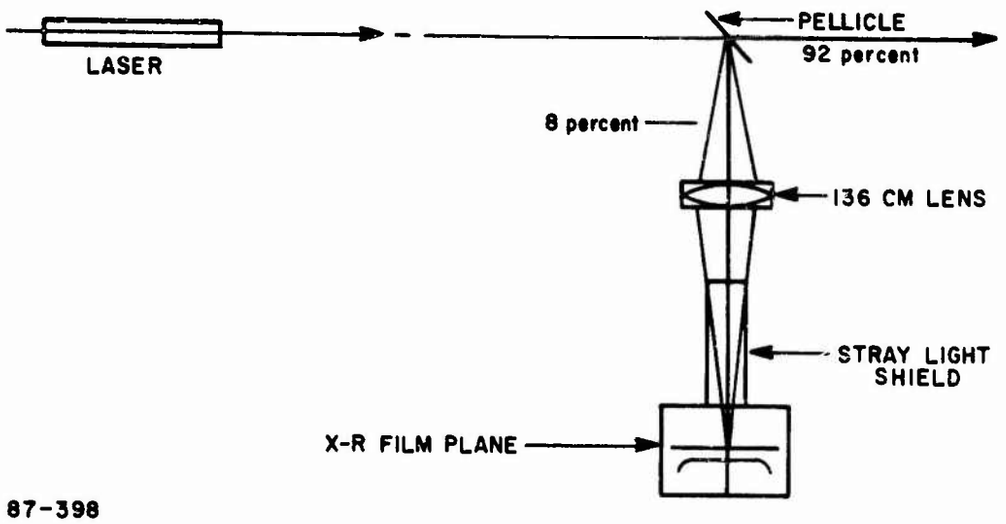

Figure 31 BEAM PROFILE MEASURING EXPERIMENT

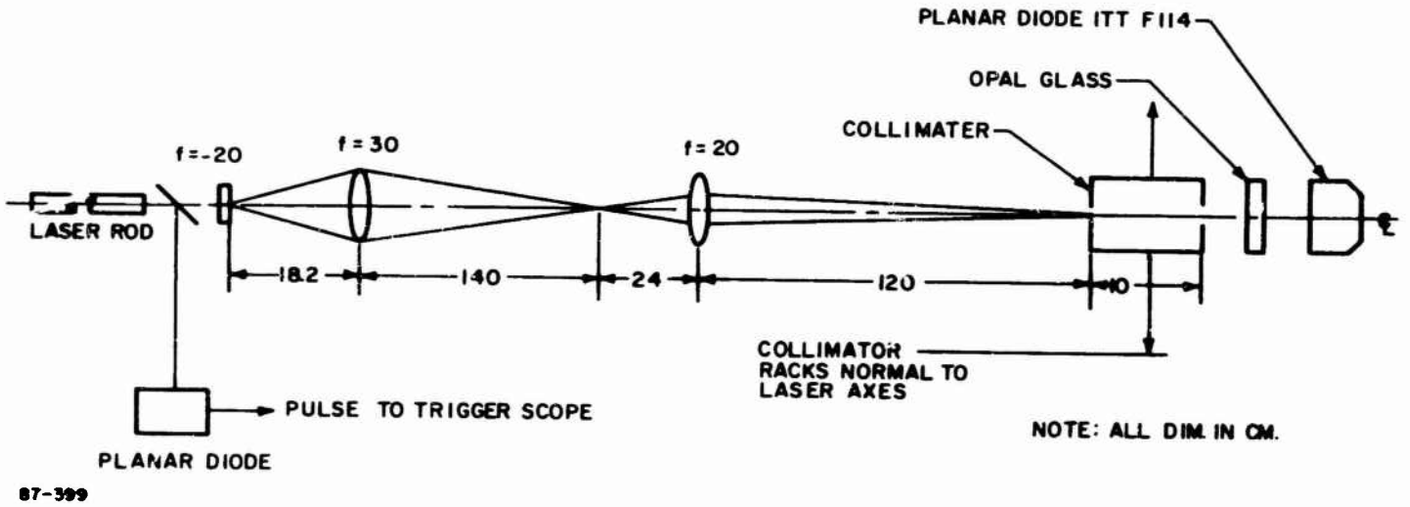

Figure 32 CROSS-SECTION PROBE OF LASER BEAM

Figure 33 PLANAR DIODE RESPONSE

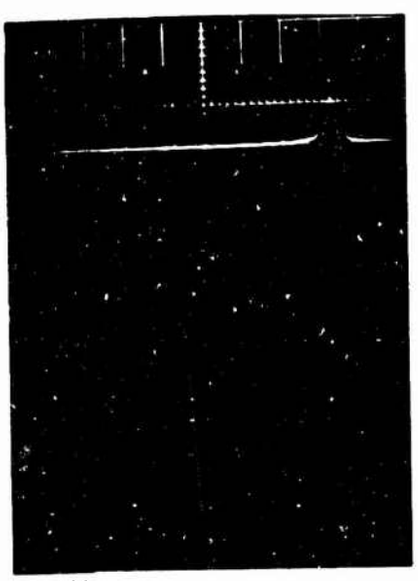

87-400

Figure 34 PLANAR DIODE RESPONSE

3.3.6 Laser Beam Calorimetry

The monitoring photodiode, which utilizes two reflectors so as to be independent of polarization and an interference filter, so as to eliminate any flash lamp pick up, was calibrated with a liquid calorimeter, Figure 35. This calorimeter has been operated successfully with incident energies up to 10 joules from the laser operating in the multiple-pulse mode, and with peak power of the order of 100 megawatts from the laser operating in the Q-spoiled mode. The calorimeter consists of a polished copper cell filled with an absorbing liquid. This liquid composition is one part Scripto blue-black ink and four parts distilled water. The front window is a disk of fused quartz cemented with epoxy to the copper cell. At the rear of the cell, a temperature-sensing iron-constantan thermocouple is soft-soldered to the copper back. The cell is wrapped with a felt material and inserted into a cardboard tube so that the quartz window is exposed. This has been found to be sufficient insulation against conductive and convective losses from the sides, since thermal equilibrium between the copper cell and the liquid occurs in less than 20 seconds. The output of the thermocouple is amplified by a Weston inductronic amplifier and recorded by a Sanborn recorder.

After weighing all components and using the specific heat equation, the calorimeter properties yield a response of 3.69 μ volts per joule with an iron-constantan thermocouple. With a strip chart recorder having a response of 4.10 divisions per μ volt, the response for the calorimeter is then 15.13 divisions per joule. This response of the calorimeter was plotted with the response of the photo-diode and its recorder.

Recalling that since 4 percent of the incident light is lost to reflection, the light received at a point in space will then be 1.1 the value of the calorimeter registers. Since the calorimeter doesn't have a response until a certain level of output is obtained, the slope of the resultant curve can be normalized to zero. Hence, the monitoring photodiode yields 26 divisions for every joule of laser energy output.

3.3.7 Miscellaneous Observations

In the course of the various experimental activities, a number of experimental effects occur which can obscure the results. The first and most obvious is a breakdown effect at the focal point of lenses. An air breakdown can occur, in the absence of any triggering matter, at laser intensities of approximately 10^{11} watts/cm^2. This means that, with a Q-switched laser of output power 10^9 watts and divergence 2×10^{-3} radians (half angle), that a breakdown can occur if the focal length of a condensing lens in the optical path is less than about 25 centimeters. If it is desired to limit the field of a detector which can see the entire output of the beam, care must be taken to avoid this breakdown.

The breakdown phenomena is particularly apparent in calorimetry of the beam, and effectively prevents the use of small aperture, black-body-type calorimeters, unless they are evacuated. Breakdown also prevents the use of open

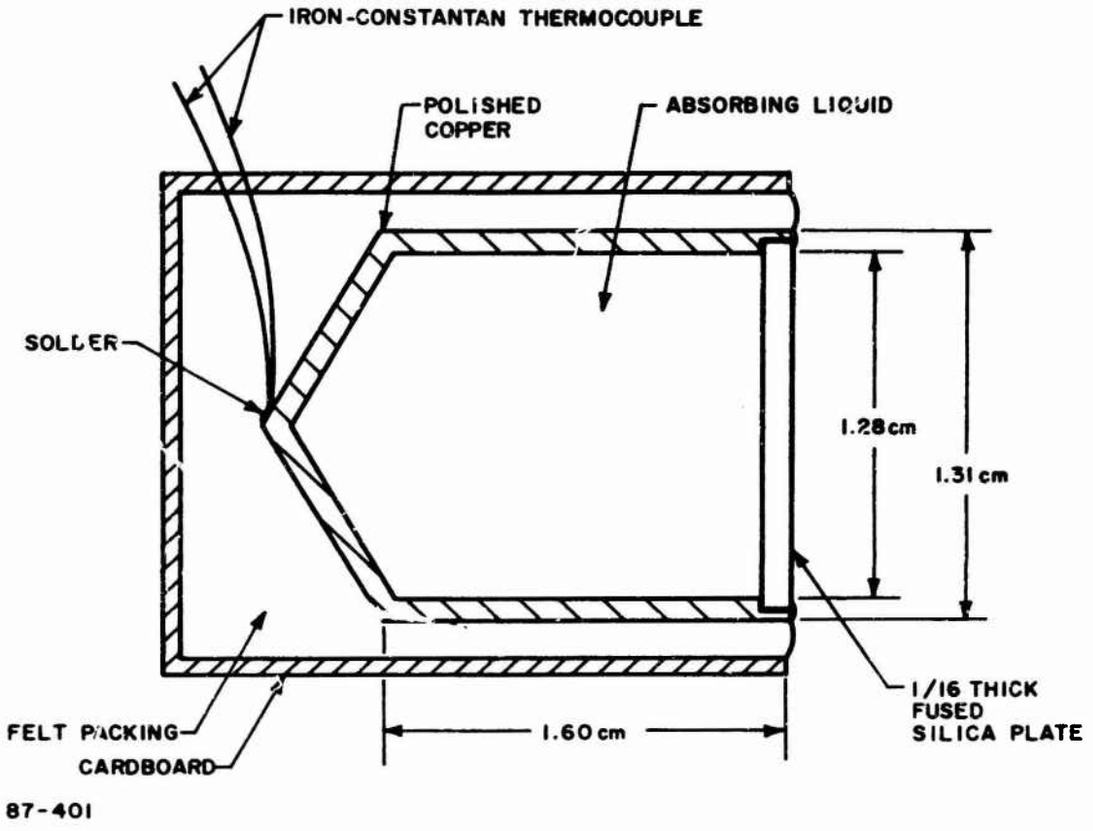

Figure 35 SCHEMATIC OF LIQUID CALORIMETER

calorimeters, because the vaporization of the surface carries away too much of the energy of the beam. Avco has found that the only suitable calorimeters for high-intensity laser beams are either the liquid calorimeter, which has been described, or an evacuated, small-aperature, black-body cavity.

Secondary reflections from optical surfaces can also cause some problems. If the optical surface is placed too close to the output end of a laser-amplifier system, enough radiation can be reflected back into the system to cause weak oscillation and consequent reduction of the population inversion. Secondary reflections can also lead to a breakdown on matter at the focus of the reflection. This will ordinarily not occur in air, but can occur if the secondary focus is inadvertently located at or near a solid surface.

As has already been mentioned, breakdown can occur at the air-window interface, if the laser beam intensity is in the vicinity of 10^9 watts/cm^2. If there are some absorbing contaminants on the window, the breakdown may occur at even lower levels. It may therefore be important to include additional space between the windows and the aerosol-containing region to eliminate too high an intensity at the windows.

Lens design for laser radiation is considerably simpler than for broadband radiation. The only aberration of significance is that of spherical aberration, and this is negligible, if the ratio of focal length to beam diameter is greater than 10. The lenses used should be of high quality. Such high-quality lenses can be obtained, ground to order, from such suppliers as Special Optics, Cedar Grove, New Jersey.

The only major problem is lens design is the prevention of internal focusing of radiation reflected from the surfaces. This is automatically done when thin lenses are used, if the focal length-to-diameter ratio is large. A problem could arise, however, if a lens of much greater diameter than necessary was used.

Cemented lenses must be avoided, since the laser radiation readily destroys the cement.

Dielectric coatings can be applied to lenses and other optical surfaces, either to reduce unwanted reflections or to attain the desired reflectivity. Avco has obtained highly resistant dielectric coatings from Optics Technology, Inc., 248 Harbor Boulevard, Belmont, California.

Timing of the laser pulse, when a Q-switched output is desired, poses some problems. Avco has found that there is the least jitter in a Kerr-cell Q-switch system, since the switching is deliberately triggered at a specified time. The saturable filter systems have the most jitter, since the pulsing occurs at a time which depends upon the exact firing level, rod temperature, etc. A rotating-prism system is intermediate in jitter, but timing can be done to fairly high

precision with the aid of a secondary light beam which reflects from the prism. In the attenuation and scattering measurements, timing problems are not serious, since the detectors can operate in an internal trigger mode. However, when a framing camera, such as the STL image-converter camera, is used, it may be necessary to trigger the camera before the arrival of the laser pulse, if the event is to be caught. This requires some means of triggering the camera fixed time before the onset of the laser pulse.

4.0 AEROSOL GENERATION

4.1 INTRODUCTION

Avco has investigated the different possibilities to produce aerosols by evaluating its own past experience; by studying papers from the fields of geophysics, industrial chemistry, protection against nuclear hazards, medical research, colloid chemistry, and others; and by visiting scientists working in the aerosol field and discussing this problem with them.

There are a number of possibilities to solve this problem. Among these are aerosol generators which are known by the name of the scientists who developed them, such as the LaMer Generator, the Lauterbach Generator, and the various Dautrebande Generators. These generators produce mostly liquid aerosols of a more or less monodisperse distribution, and some may also produce solid aerosols. The principle is either a mechanical disrupture of a surface of a liquid, or an evaporation and condensation process. The most elaborate generator of this type is the one designed by Whitby and Liu. A very promising type is the Vonnegut generator.

A number of possibilities to produce liquid aerosol or solid-dielectric aerosol in polydisperse distribution by some very simple means are also known. These are either again disruptures of surfaces or condensation of water or other vapor on nuclei. The surface disruptures can be made by a gas jet or by ultrasonic vibration.

The possibilities have been investigated to reduce the bandwidth of polydisperse aerosol, i.e., to make it almost a monodisperse one, by using filters, electrostatic precipitation or inertia precipitation.

Finally investigation of the possibilities of using hydrosol manufactured by industry in hopes of turning it into an aerosol was undertaken. Since these hydrosols come in the size range between 0.08 and 1.2 microns, which is of interest, and because of other reasons (very precise sizes, available both as uncoated spheres of nonconductive material and as spheres coated with different more or less conductive materials) these hydrosols are considered to provide the best material for producing solid aerosol for the purpose of the planned experiments. These aerosol particles are spheres. For this reason they may easily be measured according to size and number densities in the Goetz Aerosol Spectrometer*.

* Producer: Zimney Corporation, 160 Taylor Street, Monrovia, Calif., 91016, phone (213) 357-2291, TWX (213) 571-3050. Typical price for the Spectrometer about $5,500, for the Analyzer $6,700. Delivery time 6 months.

In the following, concentration is on this last-mentioned method: how to make a monodisperse, solid, dry aerosol consisting of spheres of a known material.

4.2 SOURCE FOR LATEX HYDROSOL

There are two sources for latex polystyrene spheres in the indicated size range: one a foreign manufacturer* . These spheres come with diameters which are accurately known, and all spheres in one package have but one diameter, but only a limited supply of spheres of one given diameter is available. Once this supply is exhausted, new spheres can and will be produced, but the diameters will be different.

The American source** offers, at present, the following sizes: 0.088, 0.126, 0.234, 0.357, 0.557, 0.796, and 1.099 microns. The polystyrene material includes some inorganic impurities, but this is of little or no concern for the present purpose. The hydrosol comes in packages of 15 milliliters of water with 10 percent polystyrene material in it.***

4.3 DEFINITION OF THE PROBLEM

The latex spheres come as hydrosol, i.e., immersed in water. When these are transformed into an aerosol, i.e., immersed in air or a gas, there are two problems:

a) The avoidance of clustering; in other words, at least 90 percent of the aerosol particles must consist of one sphere only.

b) When the water droplets are evaporating, other nuclei will be formed from the impurities in the water. This must be avoided, or a means must be provided to separate these undesired nuclei from the monodisperse latex aerosol.

4.4 BASIC SOLUTIONS

The following possibilities have been proven experimentally for the solution of the two problems indicated above:

For Problem (a): The amount of water in which the hydrosol is immersed must be increased to such an extent that all droplets that will form during a spraying process do not contain more than one sphere in the maximum. This means that there will be many droplets without a sphere (and this aggrevates problem b). To determine the amount of water to be added, a

---

* BASF (Badische Anilin und Sodafabrik), 6700 Ludwigshafen (Rhein), West Germany.

** Bio-Products, Dow Chemical, P. O. Box 512, Midland, Mich., telephone (517)636-5012, attention: Mr. Louis Lippe.

*** present price: $10.00 per package.

formula for the Poisson distribution derived by Greene and Lane[4] can be applied, which reads as follows:

$$P(n) = \frac{[x\,(d_o/d)^3]^n}{n!}\ exp\ [-x\,(d_o/d)^3]\ ; \qquad (109)$$

where

$P(n)$ is the probability to obtain n spheres per water droplet,

x is the volume ratio of the particles in the suspension,

d_o is the diameter of a water droplet in the spray,

d is the diameter of the latex spheres.

To obtain a probability that 90 percent of all aerosol particles are single spheres, the ratio P(2)/P(1) must be 0. 1. As can be seen from the formula, it is essential to know the diameter of the water droplets in the spray, and a means must be provided to measure them. If this is done, the degree of dilution, and (by this) the parameter x in the equation, may be determined.

For Problem (b): Two means must be applied here. (1) The water used for the dilution must be very clean (conductivity water), and (2) a size-selective filter for the dry aerosol must be applied.

4. 5 GENERAL CONCEPT FOR THE PRODUCTION OF THE AEROSOL

There will be three vessels constituting the aerosol generator. The first vessel will contain the diluted hydrosol. The second serves as a space for the evaporation of the droplets of hydrosol sprayed into it through a nozzle from the first vessel. The third contains a size-selective filter for the separation of the latex spheres from other nuclei.

Before the degree of diluting can be determined, according to the formula given in Section 4, the diameter of the spray droplets must be determined. After these droplets have been formed, by the same process to be applied during the aerosol generation proper. Then the degree of dilution is calculated, and the hydrosol is diluted according to this degree by extremely pure conductivity water. The proper nozzle is used for the spraying, and the proper pressure and volume of spray-air or spray-gas is applied. For the intended experiments, extremely clean nitrogen will be used. The second vessel is to be filled and constantly fed

by extremely clean and very dry nitrogen (relative humidity less than 10 percent). In this environment the spray droplets will evaporate in a fraction of a second[4]. Since there will be only a few (less than 10 percent) droplets containing more than one latex sphere, the aerosol will consist of 90 percent of single latex spheres, about 10 percent of double spheres (clusters) and to a small fraction (very small mass) of residuums of evaporated water droplets which did not contain any latex sphere. In terms of numbers, these residuums or nuclei are considerable, about 10^{11} of them per cm^3 have been counted in a similar experiment. For this reason these nuclei must be eliminated, and this is done by blowing the gas with the aerosol through a filter consisting of glass spheres with a diameter of about 1.5 millimeter. In the experiment quoted, this filter reduced the number of nuclei to about 10^2 cm^{-3}. Thus the gas coming out of the filter is a practically monodisperse aerosol consisting of latex spheres, uncovered or covered with conducting surfaces, etc., depending on the hydrosol applied. Figure 36 presents an overall scheme of this setup.

4.6. THE SPRAYING PROCESS

The best nozzle for this experiment is one of the type commonly used in medicine for the treatment of asthma and respiratory diseases. Figure 37 shows a cross section of a nozzle as used in such experiments.

This nozzle is operated by clean nitrogen at a superpressure of 1 atmosphere, using 15 liters of nitrogen per minute in order to spray an amount of 0.25 cm^3 per minute of the diluted hydrosol. This arrangement gave a spray consisting of droplets of about 2 micron diameter (d_o in the formula in Section 4).

The nitrogen is taken from pressurized bottles, containing bone-dry gas, and cleaned by a Cambridge Absolute Filter, which eliminates 99.97 percent of 0.5 micron particles, and more of smaller, as well as greater particles.

4.7. MEASUREMENT OF DROPLET SIZE

In order to measure the diameter d_o of the droplets, care must be taken that they do not evaporate prior to, or in the course of the measurement. To this end, the spray is made into an atmosphere with a high relative humidity, and the droplets are caught in oil. This oil must have such a consistency that the droplets do float just under the surface of the oil, so that they do not evaporate, but still are visible in a microscope. By mixing several mineral oils, this condition can be fulfilled. Since this is a rather tedious precedure, care must be taken that all parameters governing the spray process remain securely controlled, so that it can be expected that the droplets are of the size determined before.

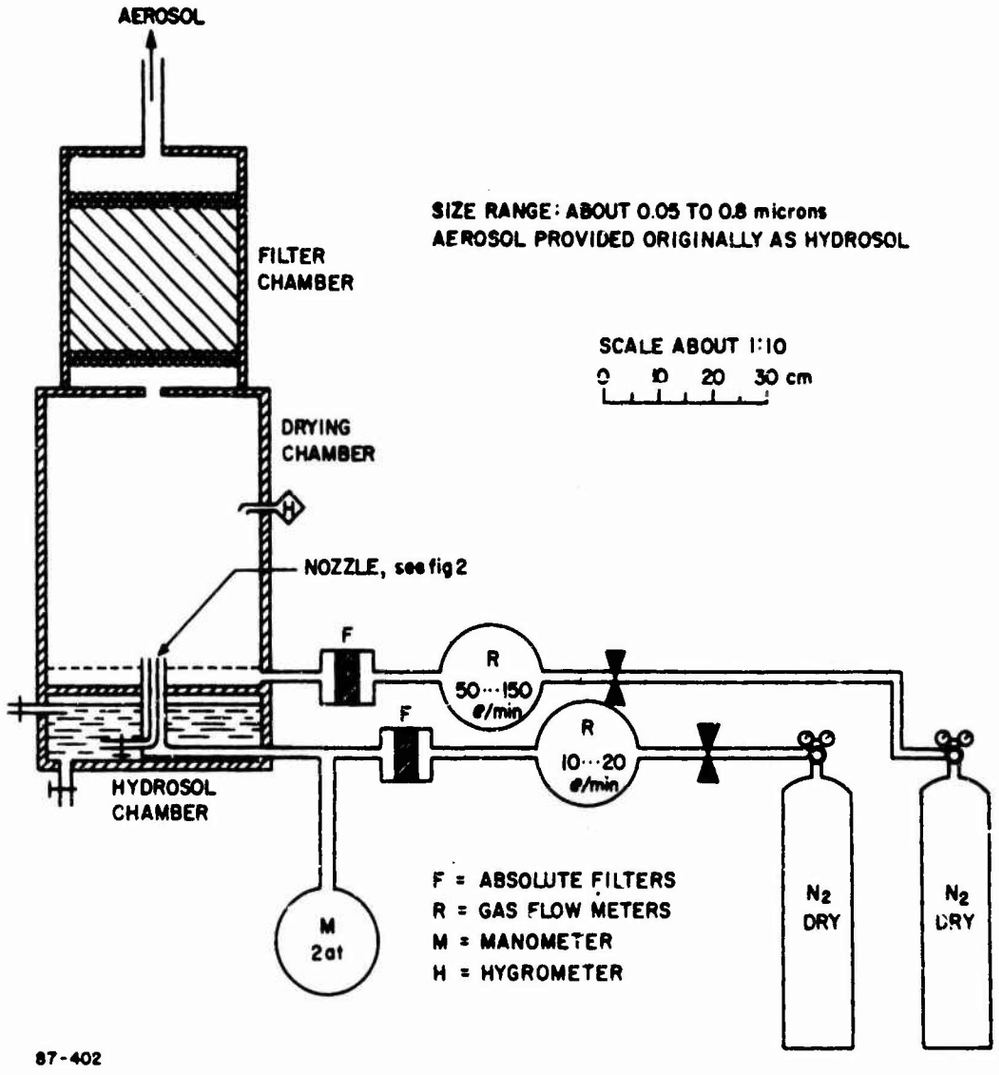

Figure 36 SOLID AEROSOL GENERATOR

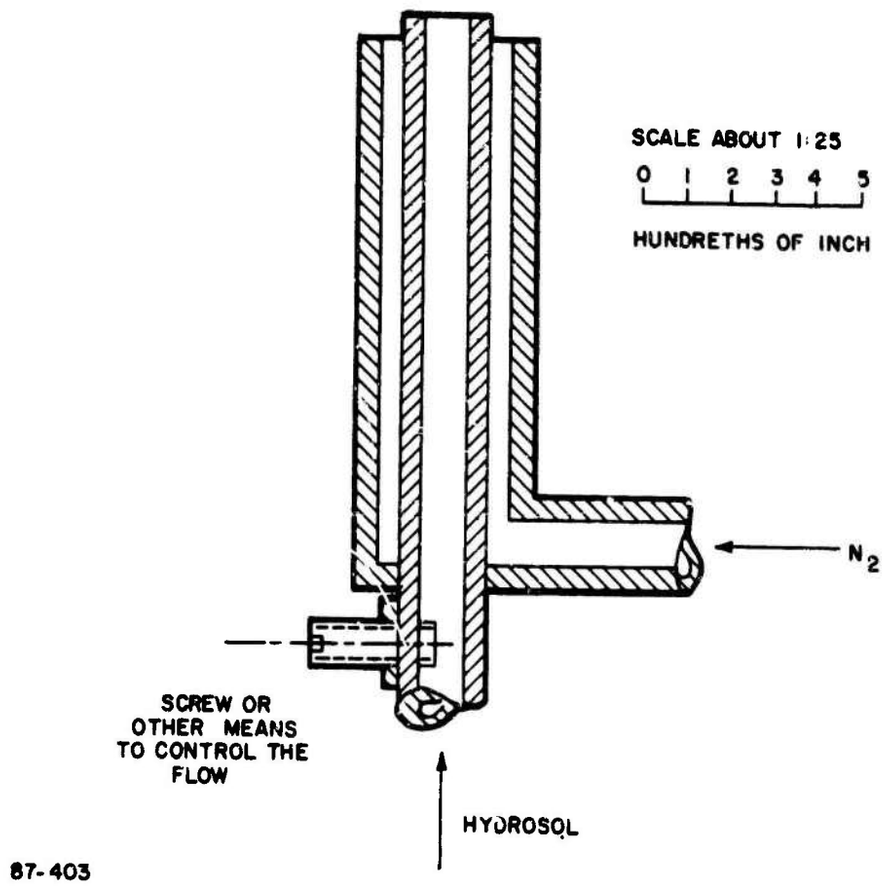

Figure 37 SPRAY NOZZLE

4.8 EVAPORATION OF DROPLETS

The nozzle ejects the spray into a cylindrical drying chamber, which has a diameter of 40 centimeters and a height of 52 centimeters, and a content of 65 liters. Into this chamber a steady flow of clean, dry nitrogen is maintained at a rate of 100 liters per minute. This gas is taken from a pressurized bottle containing bone-dry nitrogen and fed through an absolute filter (see above). Thus every minute , 115 liters of nitrogen enter the chamber, plus a very small amount of water (1/1000 liter per four minutes), which is quickly turned into water vapor.

4.9 REMOVAL OF THE SMALL NUCLEI

The nitrogen, containing the latex aerosol nuclei consisting of the residuums of fully-evaporated water droplets, and a minute amount of water vapor, streams out of the drying chamber through an orifice covered with a mesh grid of about 1-millimeter grid size into another vessel. This filtering vessel has a 30-centimeter diameter and is about 40 centimeters high, 30 centimeters of which are filled with glass spheres of a diameter of about 1.5 millimeter. The 115 liters passing this filter each minute correspond to a velocity of about 2.7 cm/sec. This filter is designed based on proposals by Lassen[5] and Langer[6]. As mentioned above, this filter reduces the content of nuclei from a rough 10^{11} cm^{-3} to about 10^{2} cm^{-3}. The maximum transparency of this filter is for particles with a radius between 0.3 and 0.4 micron. Particles smaller than 0.01 micron and greater than 0.9 micron are filtered out at a rate of better than 95 percent.

Thus the filter must be modified if the aerosol generator is to be used for particles of about a micron size or greater.

At the top of this filter, a pipe of about 1.5-centimeter inner diameter provides the monodisperse-spherical-solid aerosol at a rate of 115 liters per minute, immersed in nitrogen. The number density of these particles should be determined by experiment.

5.0 LABORATORY MEASUREMENTS

5.1 EXPERIMENTAL ARRANGEMENTS

During the last portion of the research period, the aerosol generator which has been described was set up and used to provide aerosols for some brief experimentation. A schematic of the overall experimental arrangement is shown in Figure 23. This system demonstrated the existence of several known phenomena and proved capable of detecting these phenomena to prescribed limits; a 1 percent difference in the signals from two phtodiodes, one before and one after the test chamber; a minimum noise signal of about 2.5 millivolts for the photomultiplier whose signal varies from 20 millivolts for low scattering intensities, to a high of 500 millivolts.

The system incorporated the standard oscillator-amplifier laser using new Czochralski ruby rods in order to improve on the beam profile, beam inhomogeneities, and beam divergence. The beam, upon leaving the amplifier, passes through the laser power monitor, Figure 23. This incorporates an ITT diode whose output (integrated by 0.01-millifarad capacitor) is fed into the 100-millivolt side of an E+H electrometer amplifier (Model 201C). This, in turn, is fed into a Bristol's 50-millivolt strip-chart recorder which displays the energy of each shot. The beam was expanded to two inches in diameter immediately after the monitor. It is then reflected by a dielectric reflector for 6943Å and focused through two lenses to a point 157 centimeters away from the last lens. The two lenses used were first, a plano concave (f = -28.4 cm) and second, a plano convex (f = 50 cm) in such a manner as to minimize spherical aberations. The distance between these two lenses was about 22 centimeters. The beam passed from the lenses through two-glass-plate beam splitters, through a Brewster-angled glass window on the front end of the test chamber, through the baffled chamber region containing the aerosol, out of the other Brewster window and finally through a verticle glass plate (rotation produced the final balance to 1 percent for the balancing diodes) and a second beam splitter. The glass beam splitters deflect approximately 2 percent of the beam into the ITT FW-114 photodiodes.

5.1.1 Actual Focal Point

The actual focal point of the laser beam was placed directly in the field of view of the RCA-6810A photomultiplier (3 nanosecond rise time with an S-11 spectral response) which measures the forward scattering at an angle of 45 degrees to the beam path. The beam was centered visually by observing its scatter through the aerosol and had a measured diameter of 2 millimeters. This means that the equation relating the power scattered into the multiplier with the input beam power

$$Pd = \frac{\pi r_1^2 r_2}{L(L+d) Si\,\theta} \quad P_o \qquad (110)$$

is better than 10 percent in accuracy. Figure 4 showed the geometric layout for this scattering chamber and Figure 38 shows it for the collimating tube labling all existing dimensions. Figure 38 is an improvement over the original version shown in Figure 5.

The signal from the first photodiode was a monitoring pulse that was sent to a 519 Tektronix oscilloscope and recorded by using a C-12 Tektronix camera system.

The 519, set on internal trigger, produces an output-trigger pulse when it triggers internally. This pulse triggers two other 545-A oscilloscopes set on external single-sweep mode. One 545-A monitors the pulse produced by the photomultiplier from the scattered light. The multiplier scans through the chamber into a light trap to minimize any spurious signals. The signal is sent through a Tektronix 53/54B type plug-in preamplifier which has a variable gain adjust ranging from 20 volts to 5 millivolts.

The other 545-A was modified so that a signal could be brought directly to the oscilloscope plates. This required the use of a Tektronix-deflection plate connector. The signal monitored by this system was produced by using two FW-114 IT+T diodes, one immediately before the chamber and one after, whose outputs were fed into a Bishop Instrument matched tee at 50 ohms. These outputs each had to be passed through a 100-foot cable which acted as a 100-nanosecond time delay. In the line from the first diode, an extra length of line had to be incorporated in order to time-balance the two signals. This amounted to 90 centimeters of cable in conjunction with a GR constant - Impedance Adjustable 20-centimeter line, No. 874-LK20L. At the match, this signal was also reversed as seen in Figure 39. Then the signal sent to the oscilloscope plates was the difference in amplitude of the two, both matched in time. The plates of the oscilloscope have a 2-nanosecond rise time with a 7.25 volt/cm deflection-screen constant.

By incorporating a Tektronix shutter-actuator power supply (Model 1, No. 016-211), one button is pushed which opens two camera shutters set for one second exposure and fires the laser simultaneously. The other camera was tripped just prior to pushing the actuator button. This yields three pictures of three pulses that have a definite time relationship among their pulse peaks.

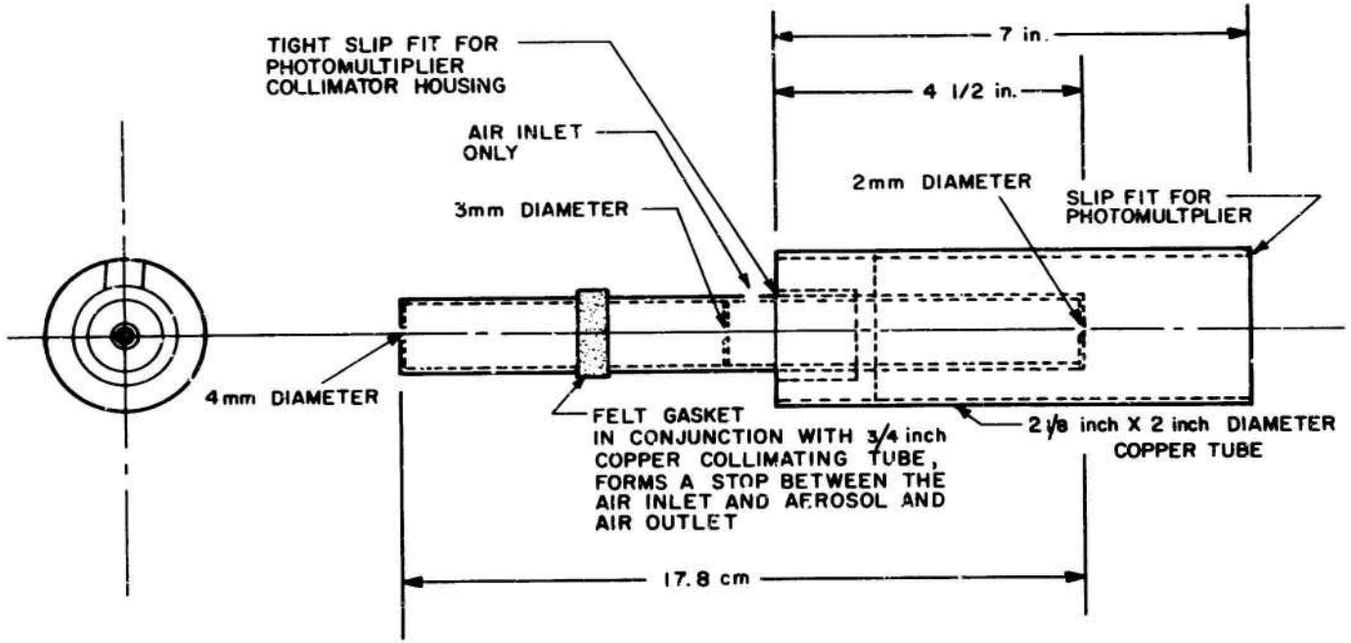

Figure 38 IMPROVED PHOTOMULTIPLIER HOUSING

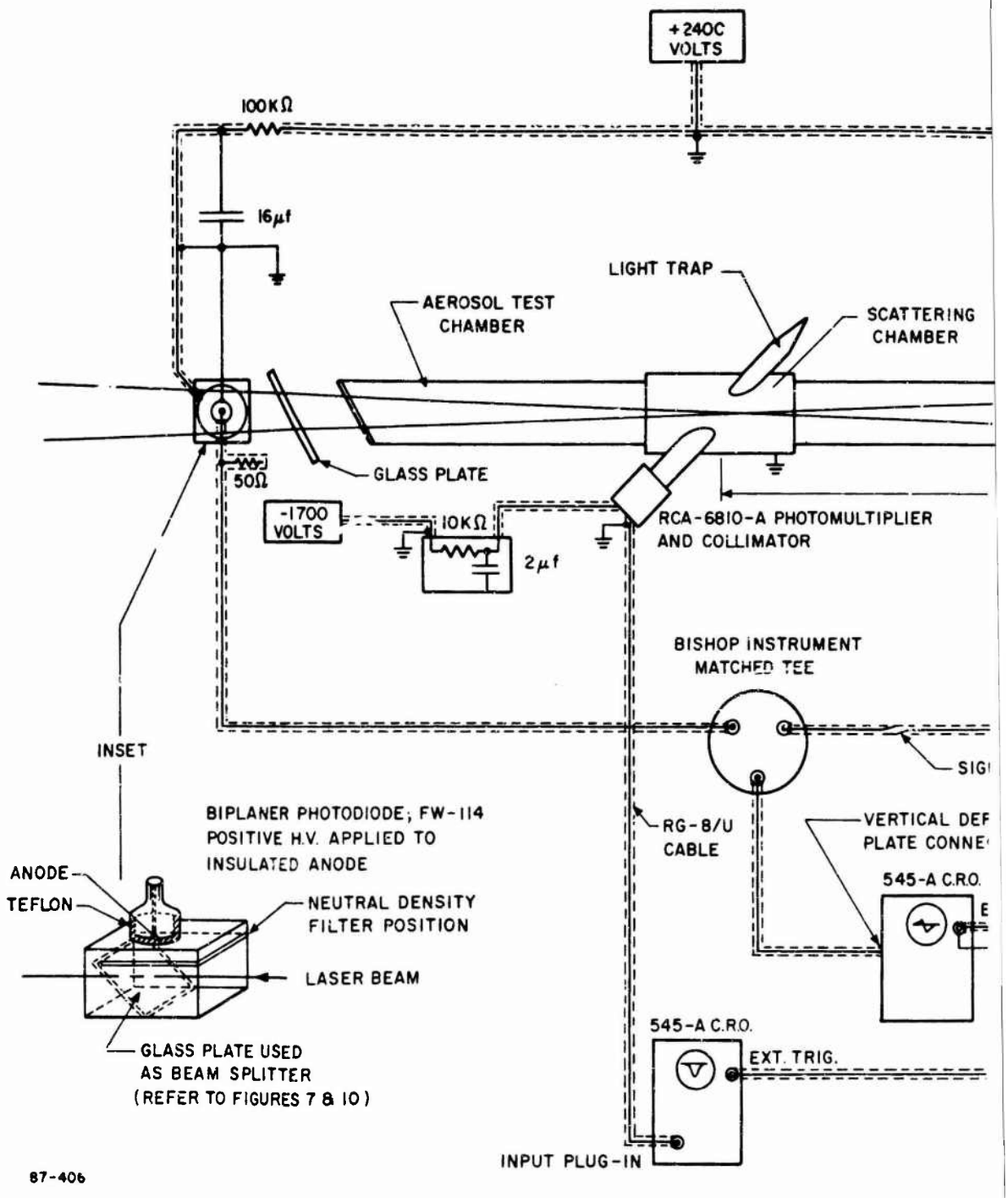

Figure 39 COMPLETE FINAL ELECTRICAL CIRC

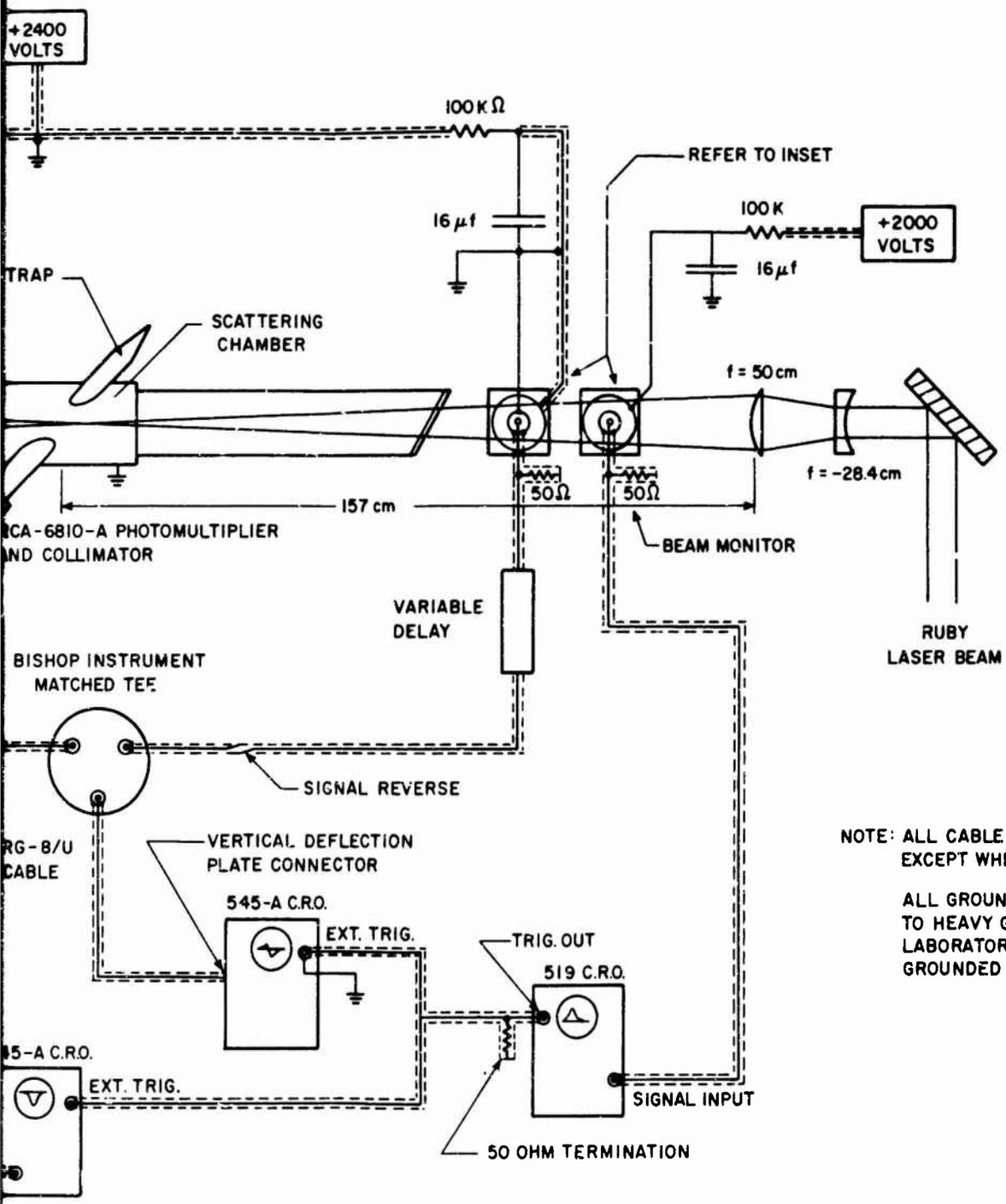

NOTE: ALL CABLE IS RG-58 A/U EXCEPT WHEN LABELED

ALL GROUNDS ARE CONNECTED TO HEAVY GROUND CABLE, LABORATORY BENCH ALSO GROUNDED

B

COMPLETE FINAL ELECTRICAL CIRCUITRY

5. 1. 2 Aerosol Generator

The aerosol generator described in Section 4. 0 of this report was used to produce the aerosols for this experiment. Figure 40 is a photograph of the generator. The upper and lower chambers were made from cast acrylic tubes. Originally, the upper chamber contained glass spheres to act as a filter. These, however, were found to be unnecessary. The aspirator used to inject the aerosol particles into the lower chamber was constructed from glass according to the dimensions shown in Figure 41. This proved to be superior to the design obtained originally. A dry (tank) nitrogen flow of about 10 liter/min was used to operate the aspirator. The hydrodisperse particle solution was introduced with the aid of the flask shown in Figure 40. Control of the flow of the solution was accomplished by adjusting needle valves in the path of the flow, and by controling the rate of air admission into the top of the flask.

With the 10-liter-per-minute-aspirator gas flow alone, the resulting aerosol was dominated by condensed water vapor. However, an additional flow of 10-cubic-feet-per minute of dry (tank) nitrogen was sufficient to prevent such condensation. The cone placed in the lower chamber collected any large water droplets which were formed, and prevented them from reaching the upper chamber. The upper chamber itself acted primarily as a diffusion chamber.

The gas flow from the generator then passed into a monitoring chamber, which is shown in Figure 42 and in the photograph, Figure 43. A 6328A He-Ne-laser beam is multiply reflected through this chamber to monitor the attenuation of the aerosol. This beam then emerges and is recorded with the aid of a Spectra-Physics power meter and a Varian G-11A recorder.

After leaving the monitor chamber, the aerosol enters the test chamber through 4 inlet tubes. These tubes are arranged in the approximate center of the chamber length, and the inlets are equally spaced about the circumference. These can be seen clearly in Figure 44. The 4-tube arrangement has been found to produce the least turbulence inside the chamber.

Figure 40 also shows the scattering chamber, which is located adjacent to the inlet chamber. Because a short aerosol-containing length was required for the experiment, the window-protective baffles are located next to the inlet and scattering chambers, and the windows themselves are a long distance from the aerosol-exit region. This arrangement was necessary to prevent the laser beam from attaining too high an intensity at the windows.

Figure 45 shows an overall view of the experimental set-up. The monitor chamber is in the center foreground, and the output monitor phototube is on the left. The laser beam enters the test chamber from the right.

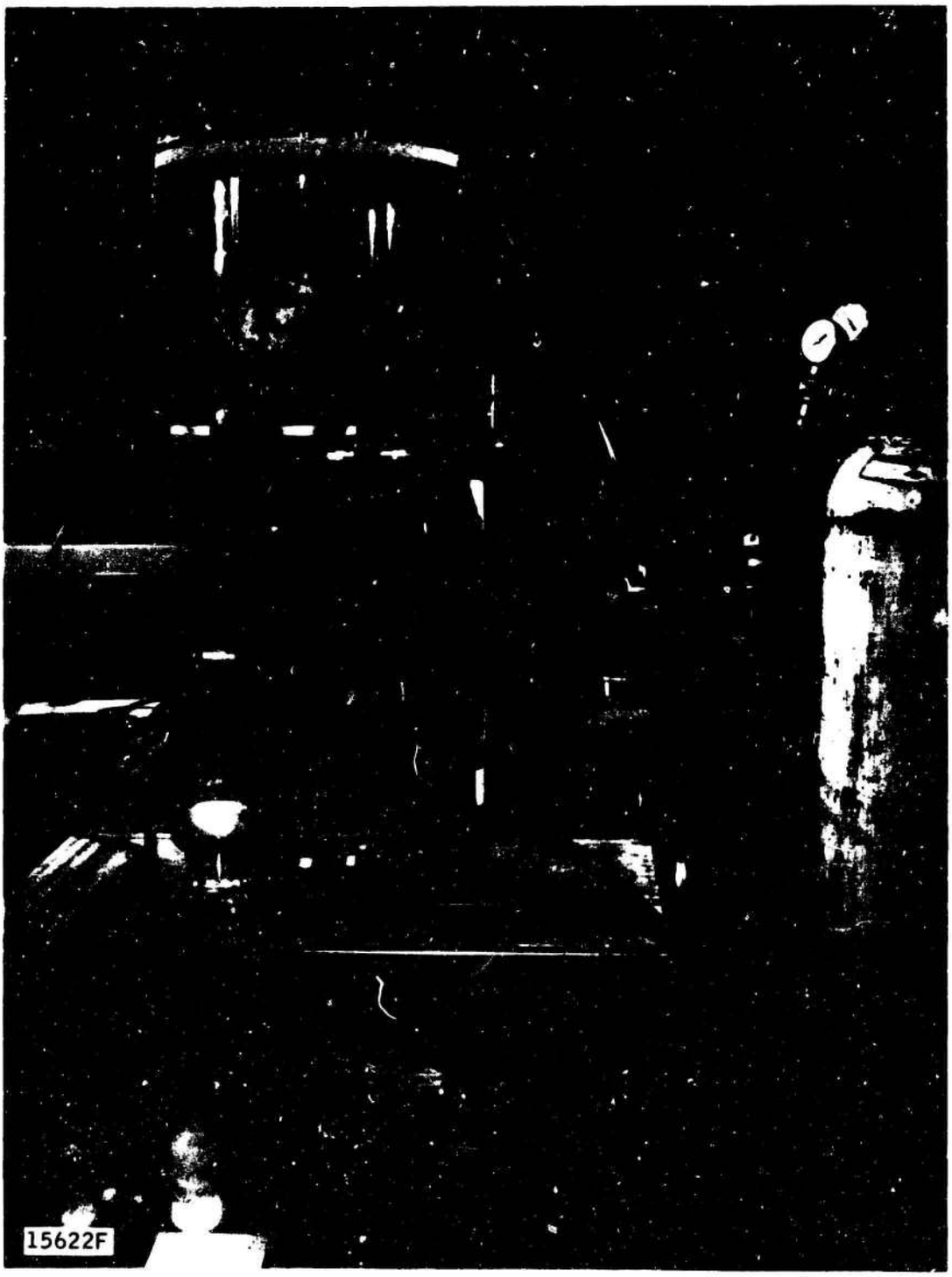

Figure 40 PHOTOGRAPH OF GENERATOR

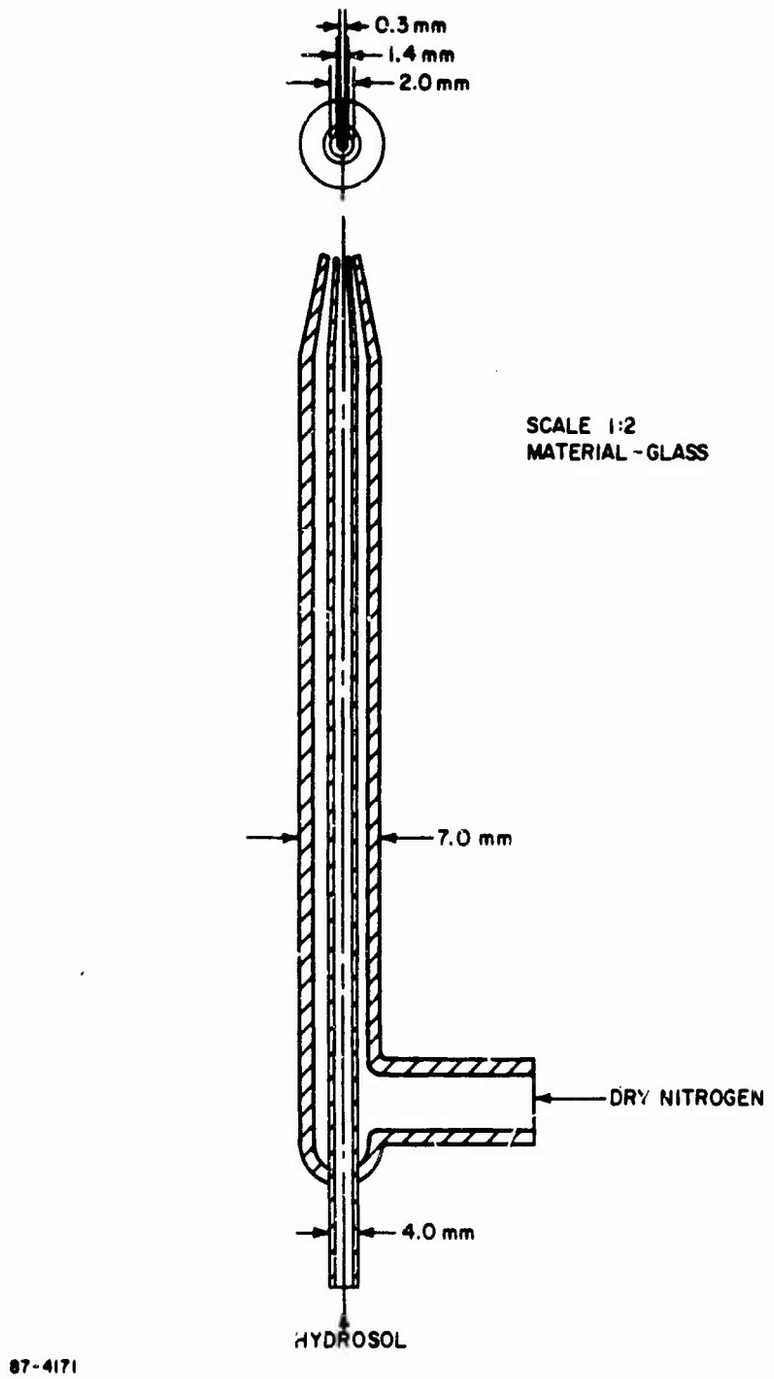

Figure 41 SPRAY NOZZLE USED

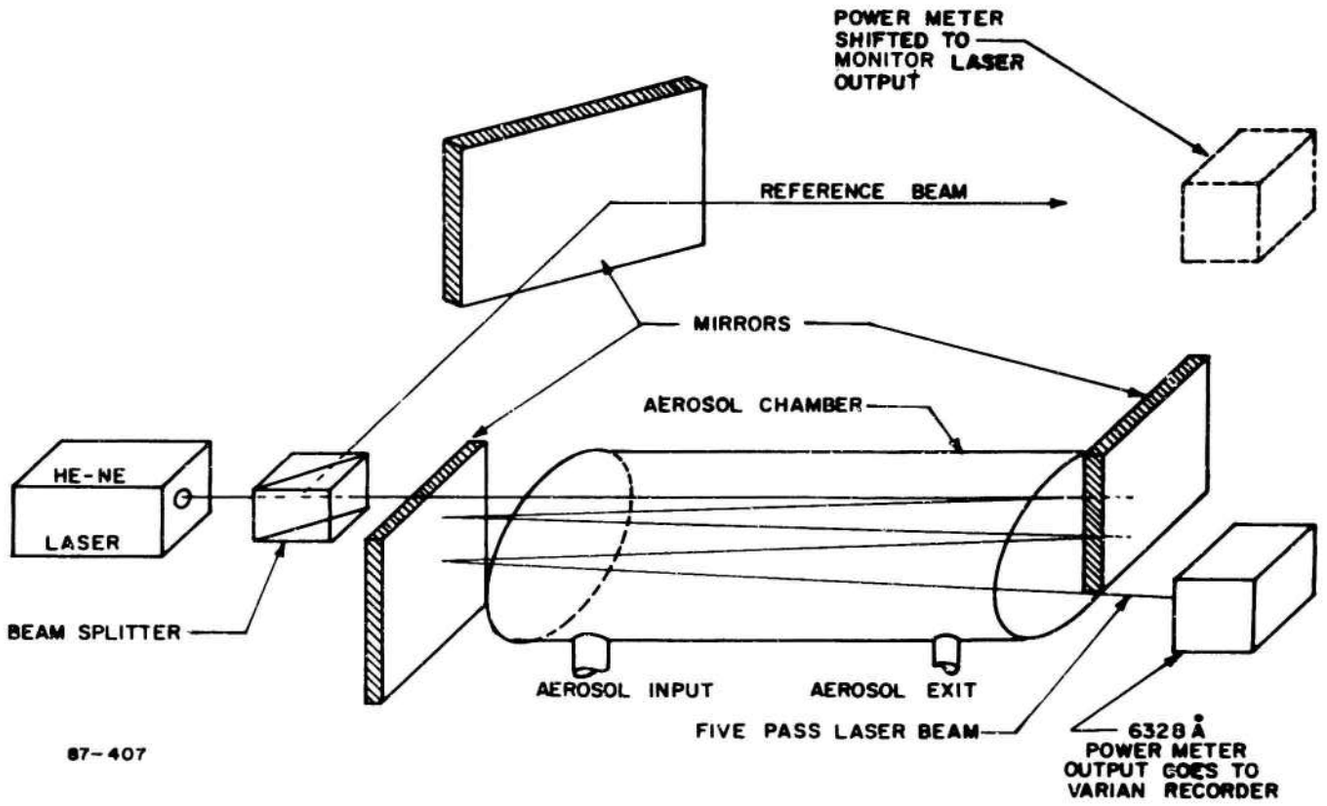

Figure 42 AEROSOL MONITOR SYSTEM

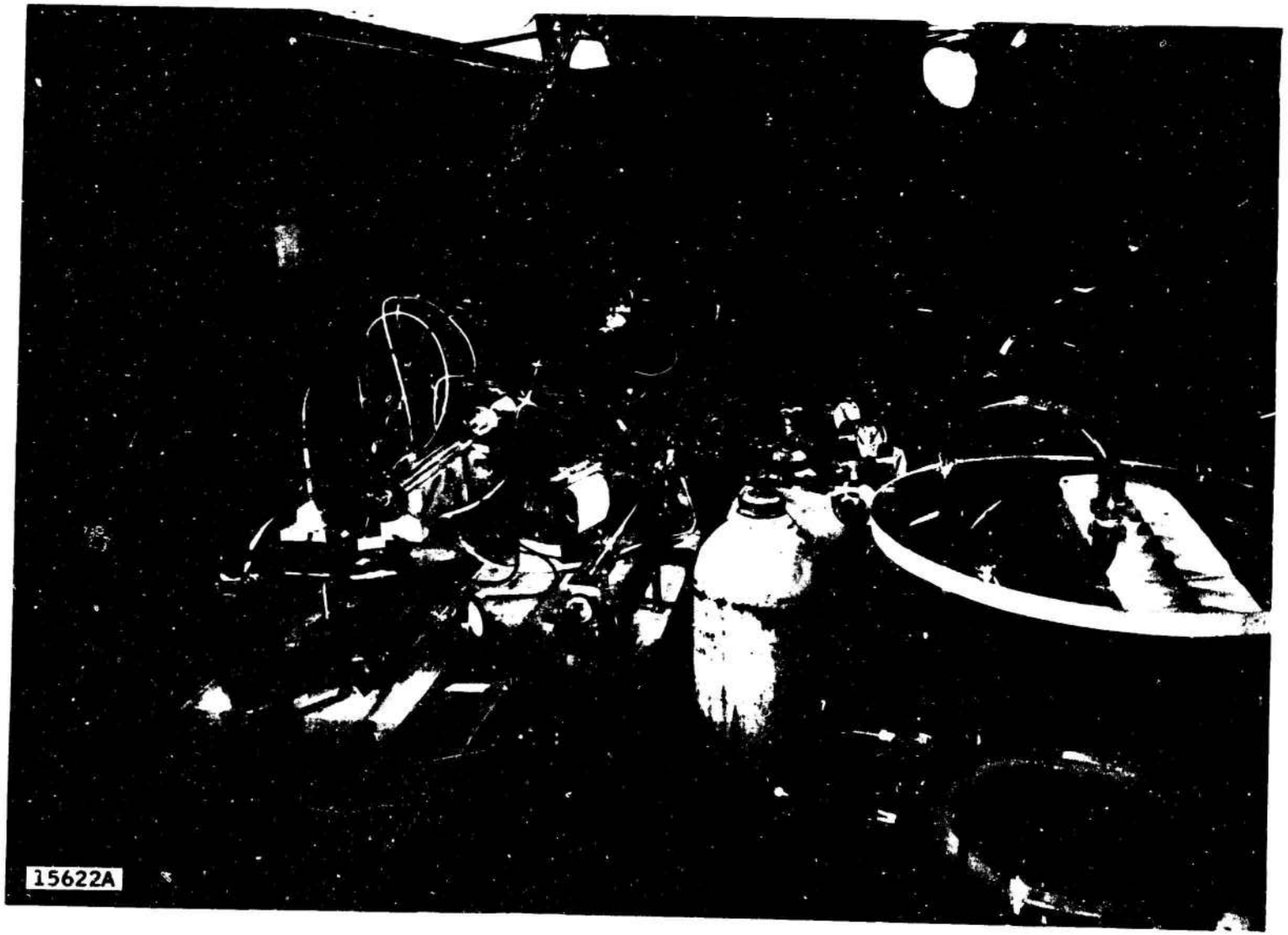

Figure 43 PHOTOGRAPH OF AEROSOL SYSTEM

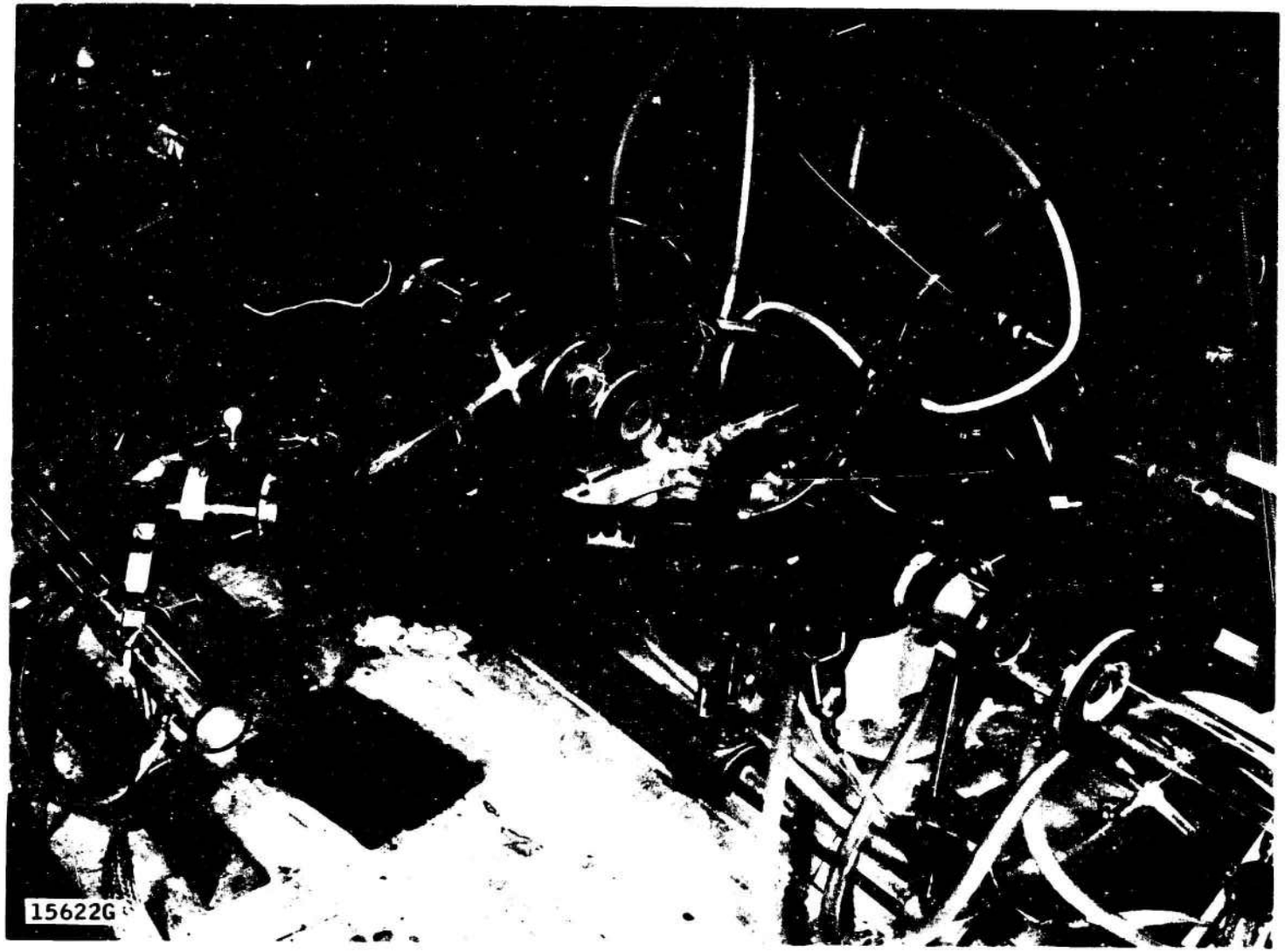

Figure 44 SCATTERING CHAMBER PHOTOGRAPH

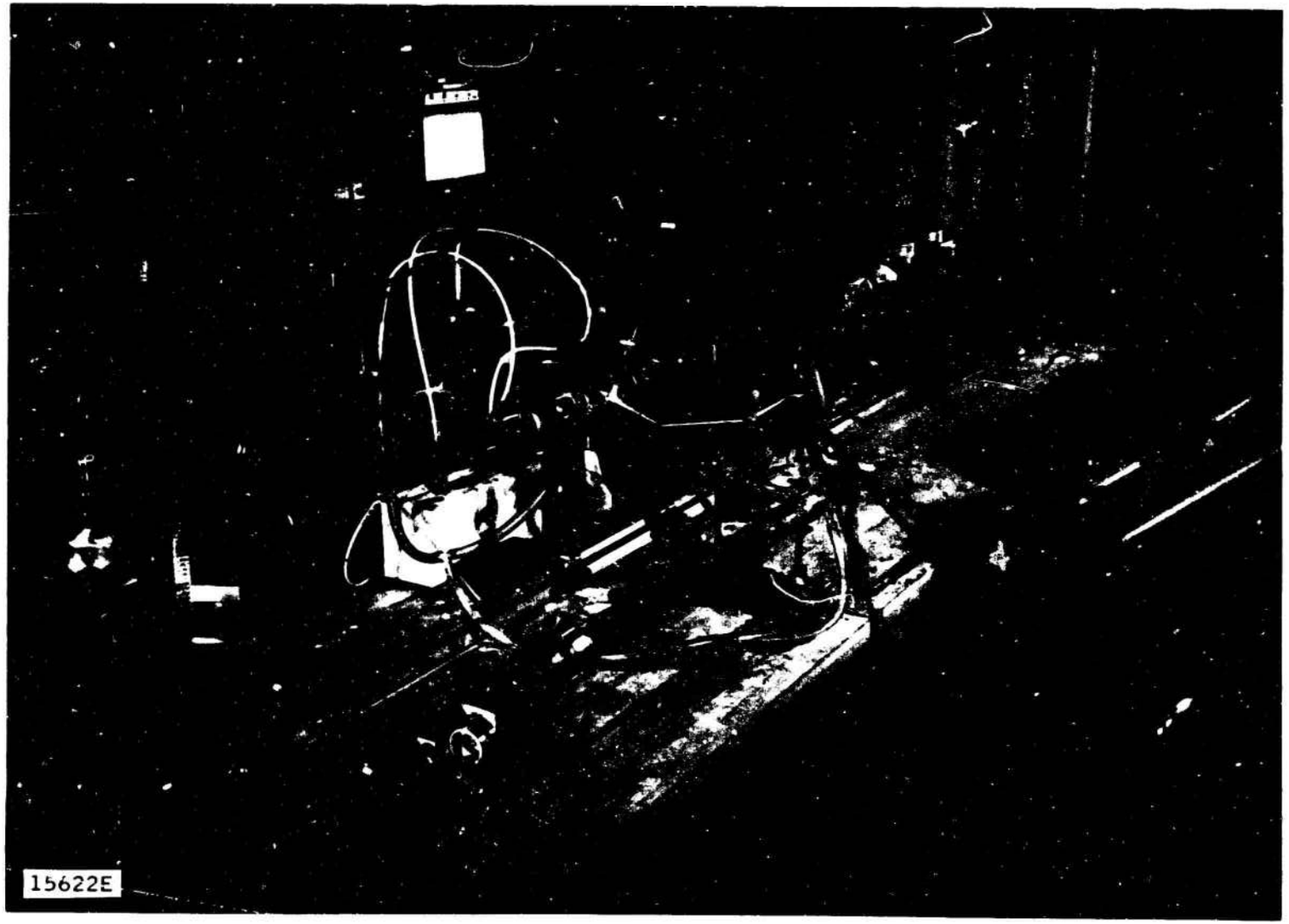

Figure 45 PHOTOGRAPH OF EXPERIMENTAL APPARATUS

The oscilloscopes were focused just prior to testing by using a pulse generator built from flip-chip modules made by Digital Equipment Corporation. The generator utilizes a variable clock (R401), a Schmitt Trigger (W501), and a pulse amplifier (W607). By using the clock to fire the trigger which free-runs the three amplifiers hooked in series, a 40-nanosecond, 7.5 volt pulse is produced with a megacyle repetition rate. By triggering the scope and observing the pulse on the single sweep mode, actual test conditions are approximated and a good focus can be obtained.

Once an aerosol of stable concentration had been created (and monitored by observing the constancy of the transmission through the monitor chamber), a series of laser firings were carried out at various different peak powers.

The instantaneous transmissivity (or optical density) of the aerosol under test was determined using the procedures described in Section 3.0. Some of the experimental results are shown in Figure 46. The upper curve is the optical density of the latex-sphere aerosol at the time of peak laser power. It is to be noted that, in the vicinity of 10^9 watts/cm^2, the optical density undergoes a sharp increase. This is precisely what is to be expected if the latex spheres become absorbing at this level as a result of non-linear effects. The latex spheres, at breakdown, produce an ionized vapor, Since this ionized vapor can trigger an air breakdown, the sharp increase in attenuation is to be expected. The oscilloscope trace for the balanced photodiode shows this breakdown dramatically. In Figure 47 and 48, photographs 1 to 3 show the breakdown increasing as the laser power increases.

The boron, on the other hand, indicated a decrease in attenuation as the power is increased. This is again to be expected. The boron particles are very small compared to a wavelength of light. They are also small enough so that they would be partially evaporated by the laser energy, but the vapor thus created would not become absorbing. Thus the attenuation would be expected to decrease. In Figure 48, photograph 4 shows no breakdown effect when the boron was used.

Figure 49 compares the optical density versus time for the latex and boron spheres. A time plot of the laser pulse for the latex spheres is superimposed.

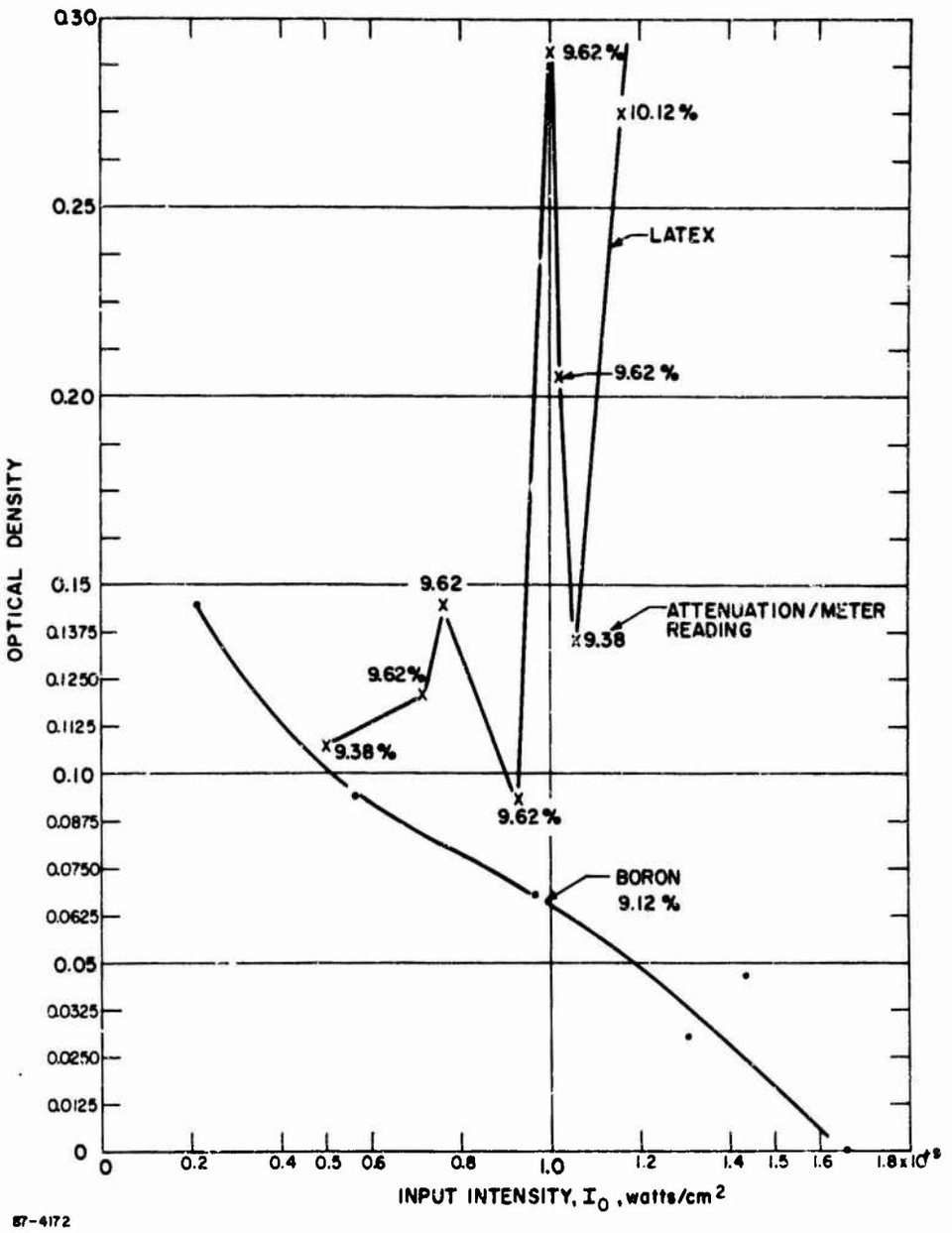

Figure 46 GRAPH OF OPTICAL DENSITY VERSUS INPUT INTENSITY

Figure 47 OSCILLOSCOPE TRACE 1 & 2

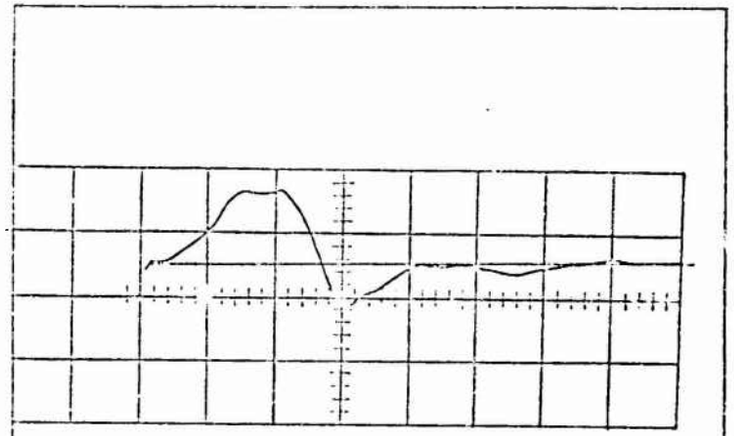

FIGURE 47 : TRACE 1
20 NS/CM SWEEP

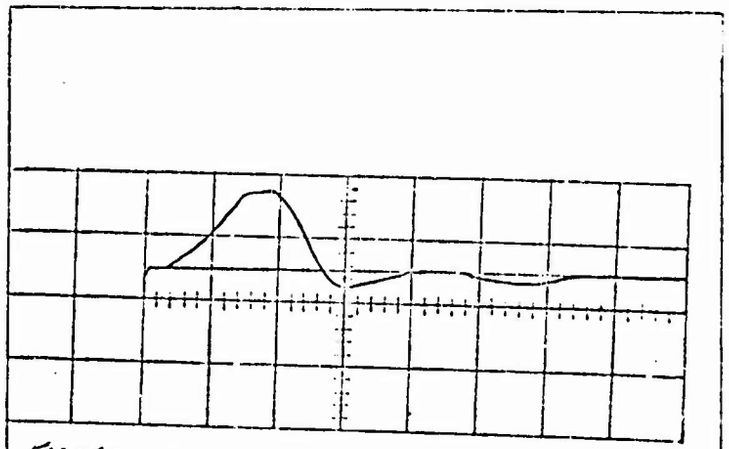

FIGURE 47 : TRACE 2
20 NS/CM SWEEP

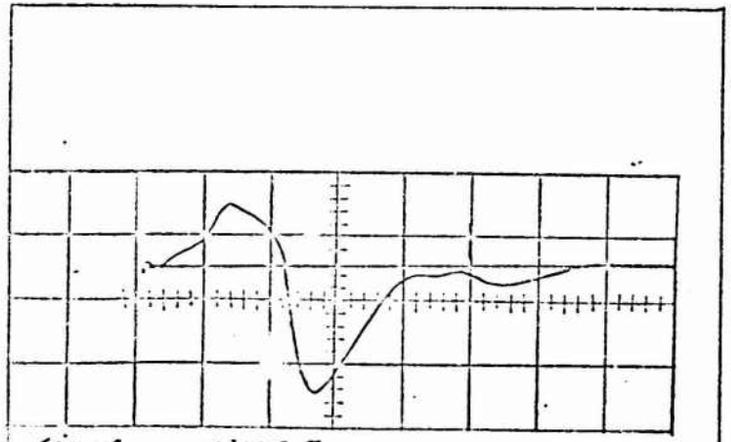

FIG. 48 TRACE 3
20 NS/CM SWEEP

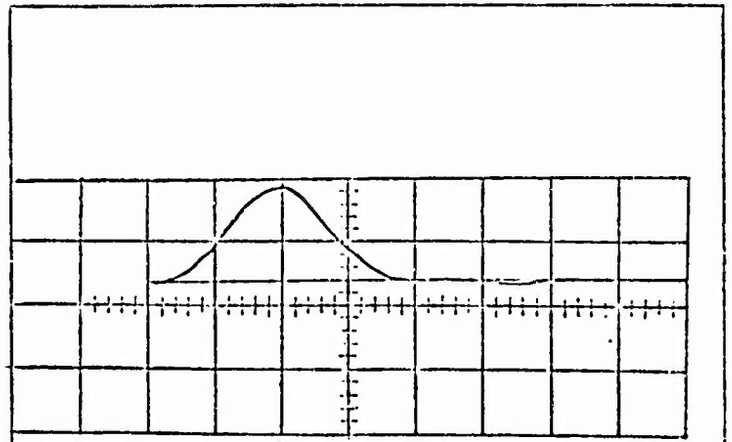

FIG. 48 TRACE 4
20 NS/CM SWEEP

FROM PAGES 108 & 109
CONTRACT DA-18-001-AMC-957(X)

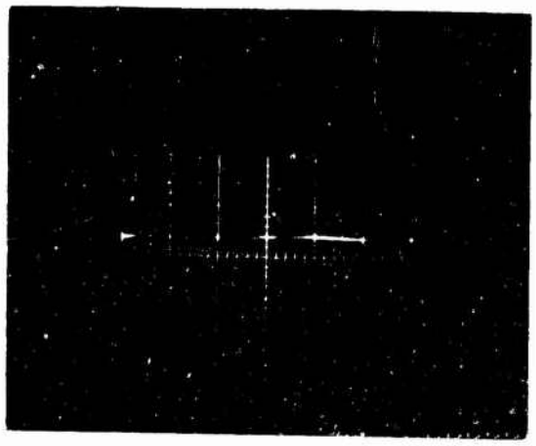

Figure 48 OSCILLOSCOPE TRACE 3 & 4

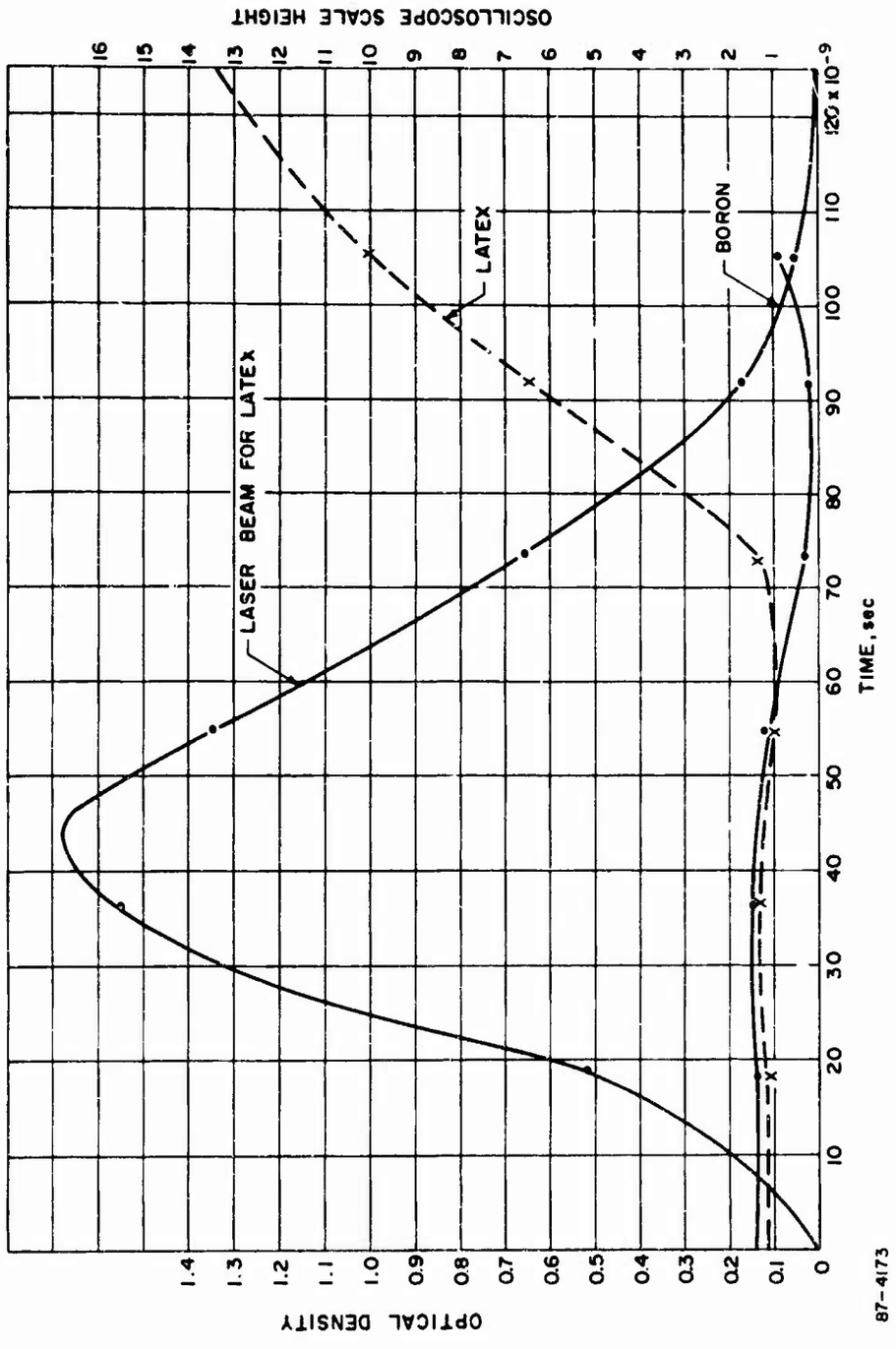

Figure 49 OPTICAL DENSITY VERSUS TIME

6.0 SUGGESTED CHAMBER DESIGN

6.1 CHAMBER CONSTRUCTION

The glass-and-metal construction that has been used for the experimental work described is adequate for work carried out at atmospheric pressure and below. The method of construction - that is, the use of segments - allows a large degree of versatility, since the overall length of the chamber, and the type of experiments, can be varied at will. Avco feels that this is superior to the approach involving multiple reflections within the chamber, although the latter is a useful approach, especially for attenuation measurements.

If operation at higher pressures is desired however, the method of chamber construction used is no longer adequate. Accordingly, chamber designs which are conservatively estimated to be adequate at 10 atmospheres (150 psi) have been prepared and will be discussed in the following pages.

6.1.1 Basic Design

The basic chamber design incorporates simple, smooth-surfaced flanges. These flanges are to be bolted together, with Consolidated Vacuum Corporation "Con-O-Rings" serving as a hermetic seal. Figure 50 shows the aerosol generation chamber. This is constructed with the standard 15 1/2-inch flanges shown in Figure 51. This flange is welded to 0.065-inch wall-thickness type 304 stainless steel. (Stainless steel is chosen because the aerosol generation technique most suited for experimentation uses a hydrosol, and rusting of ordinary steel might be a problem). The viewing ports are constructed in the same manner as the ports on the export chamber, Figure 57. The top of the upper chamber is capped with a 1/2-inch thick plate containing a 1/2-inch-diameter pipe fitting for the exit. The bottom plate of the lower chamber is fastened to the chamber with a standard flange. This plate, Figure 52, contains a 1/2-inch threaded hole in the center for acceptance of the aspirator, shown in Figure 53.

The remaining parts of the apparatus are constructed of the standard 9, 3 1/2, 3, and 2 1/2 inch flanges shown in Figures 54 and 55. These flanges can be welded to 0.065 inch wall-thickness stainless steel of 4, 2, 1, and 1 1/2 inch optical density, respectively (note that the 3-inch flange has a 1-inch hole).

Figure 56 shows the chamber entrance and exit windows. Because of the sizes and thicknesses required, the use of Brewster angle windows has been discarded. Instead the windows are anti-reflection coated on both sides. This design allows a chamber of 4-inch diameter, and hence provides adequate space to allow multiple paths through the chamber. The length of the exit window is not shown, since it can be any length desired. A nominal length would be 3 inches overall. A 1/2-inch fitting is attached to the side wall to act as a gas inlet.

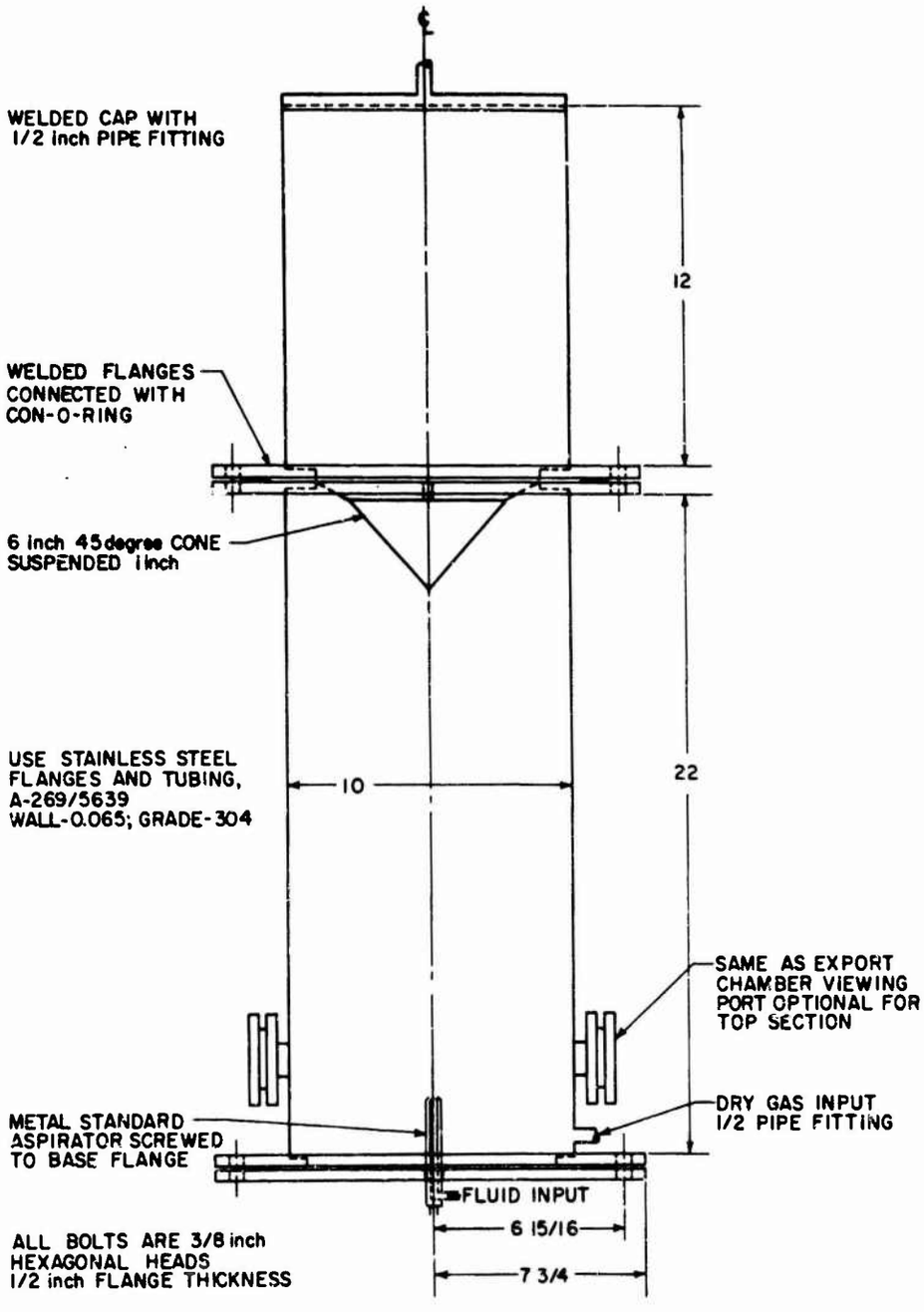

Figure 50 PROPOSED AEROSOL GENERATION CHAMBER

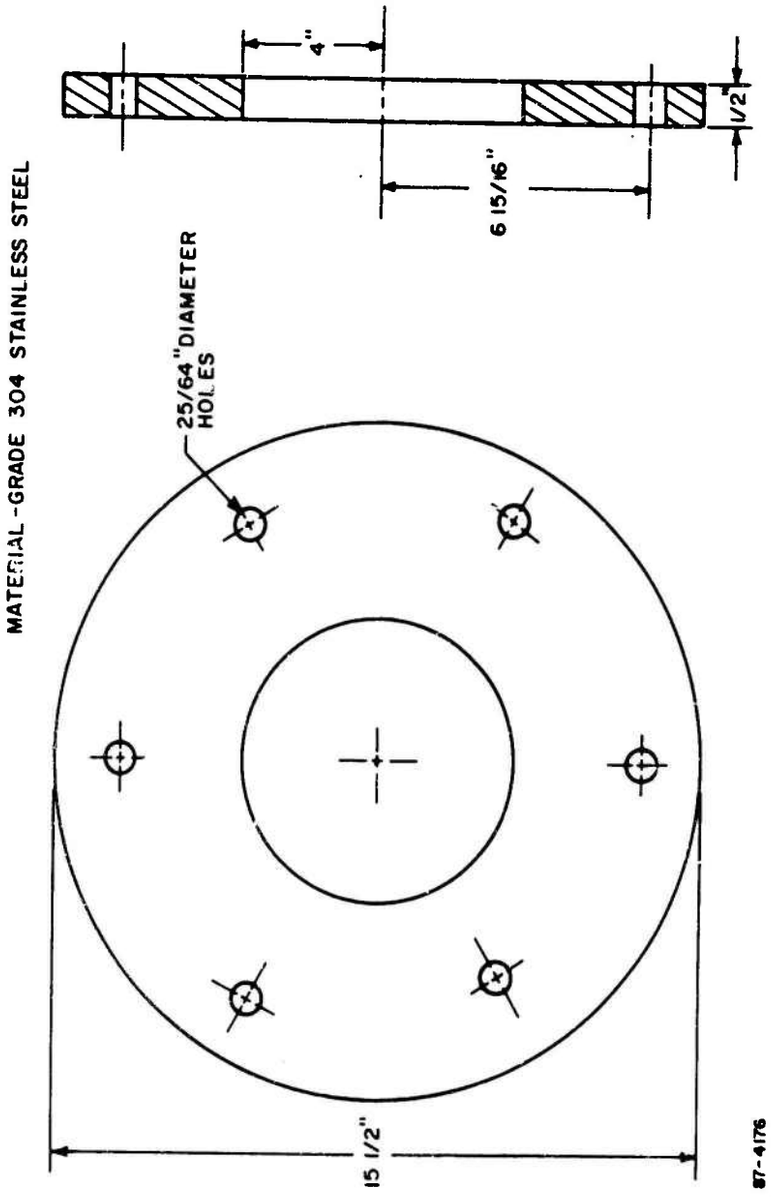

Figure 51 15 1/2 INCH FLANGE-WELDED

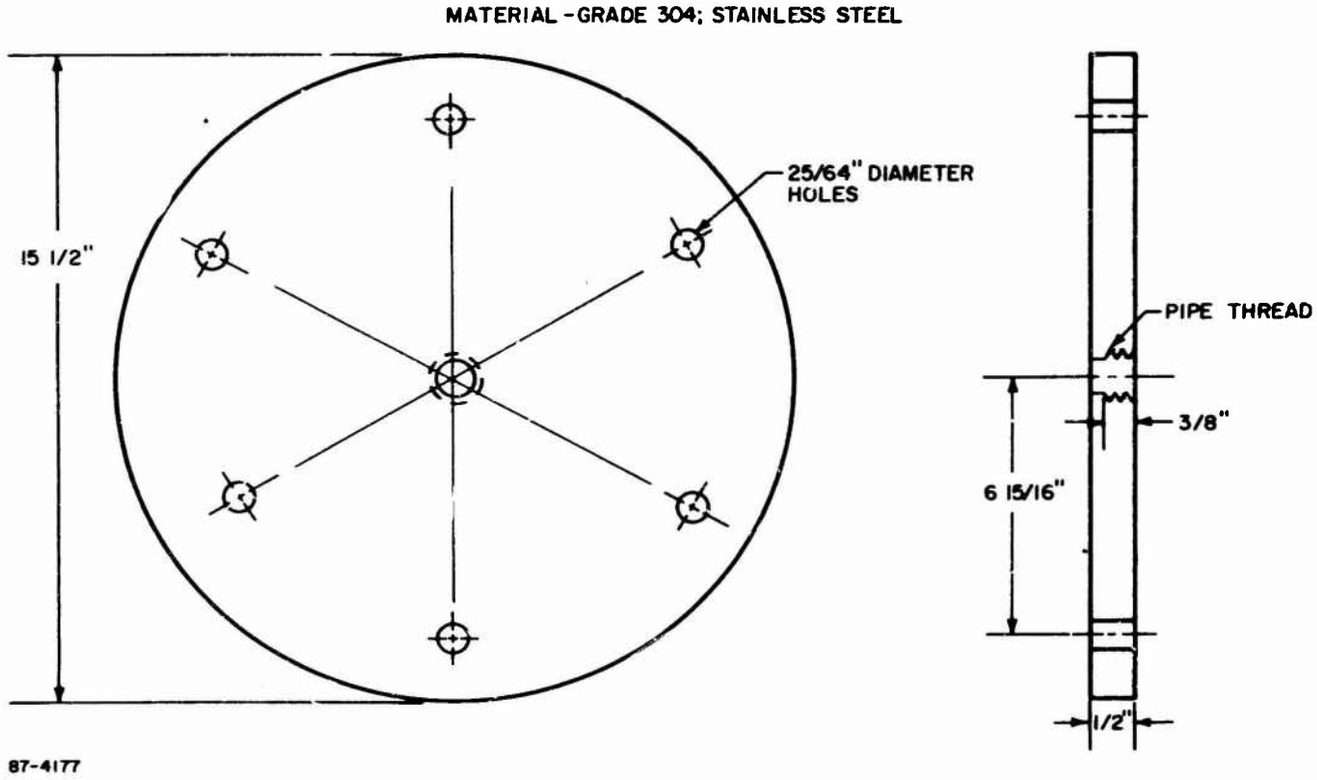

Figure 52 15 1/2 INCH FLANGE-ASPIRATOR HOLDER

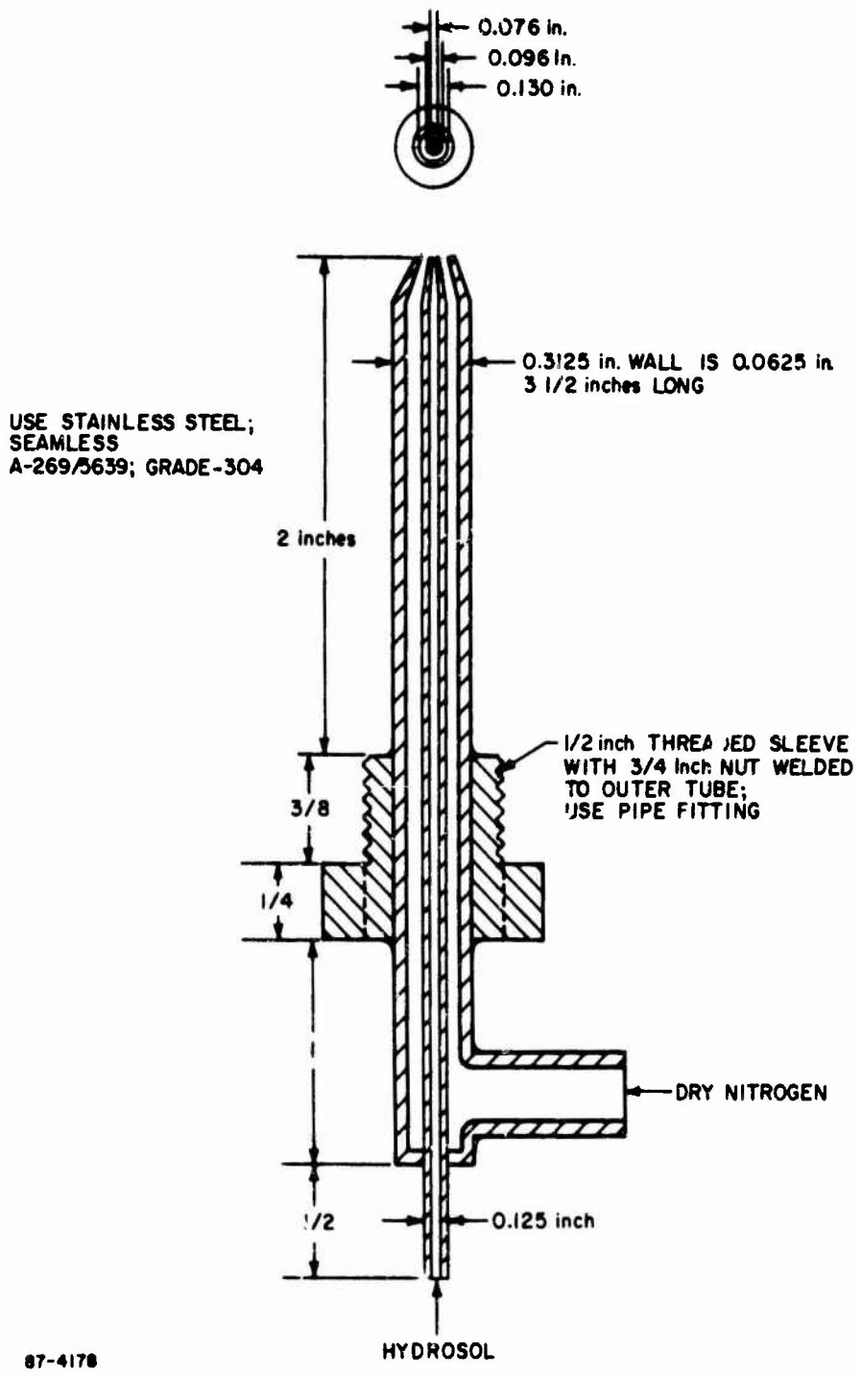

Figure 53 ASPIRATOR

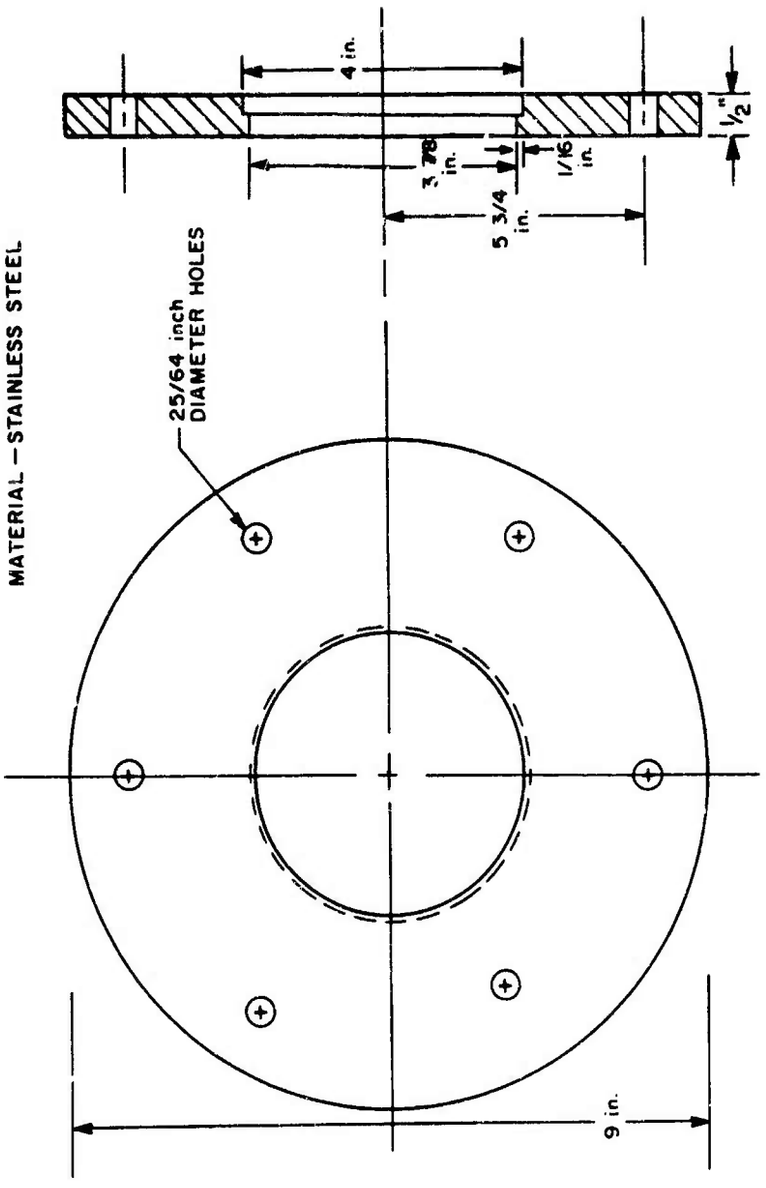

Figure 54 STANDARD 9 INCH FLANGE

NOTE:
ALL BOLTS USE 1/4 x 28 in. HEXAGONAL HEADS;
ALL WELDED TO TUBING WHEN SHOWN ATTACHED

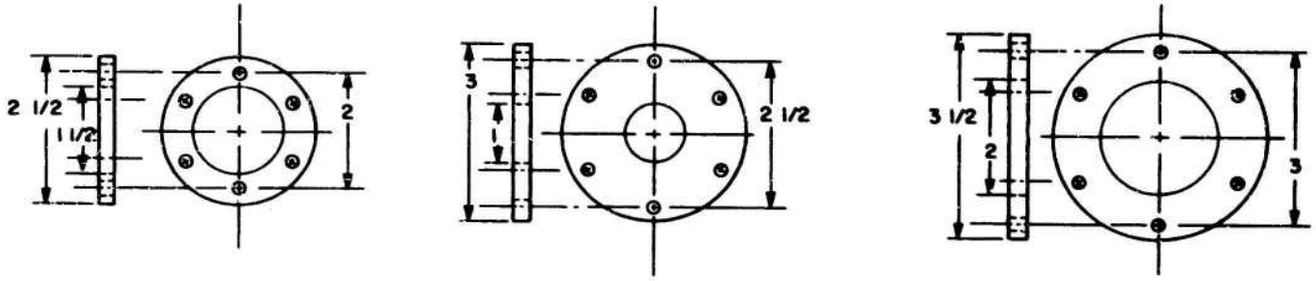

USE STAINLESS STEEL; A-269/5639
WALL - 0.065 in.; GRADE - 304
WIDTHS ARE ALL 3/8 inch

87-412

Figure 55 STANDARD 2 1/2, 3, 3 1/2 CHAMBER FLANGES

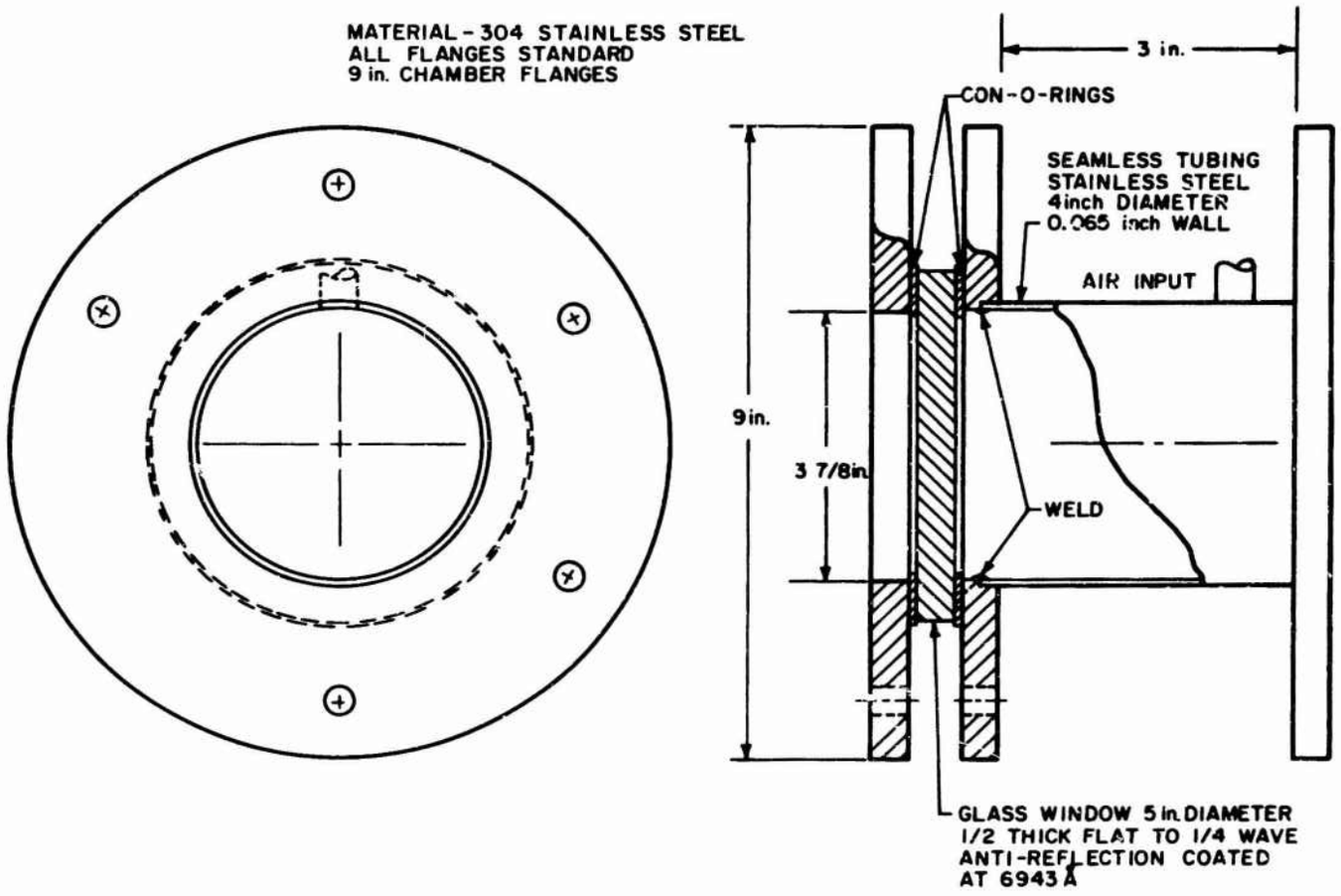

Figure 56 ENTRANCE AND EXIT WINDOWS

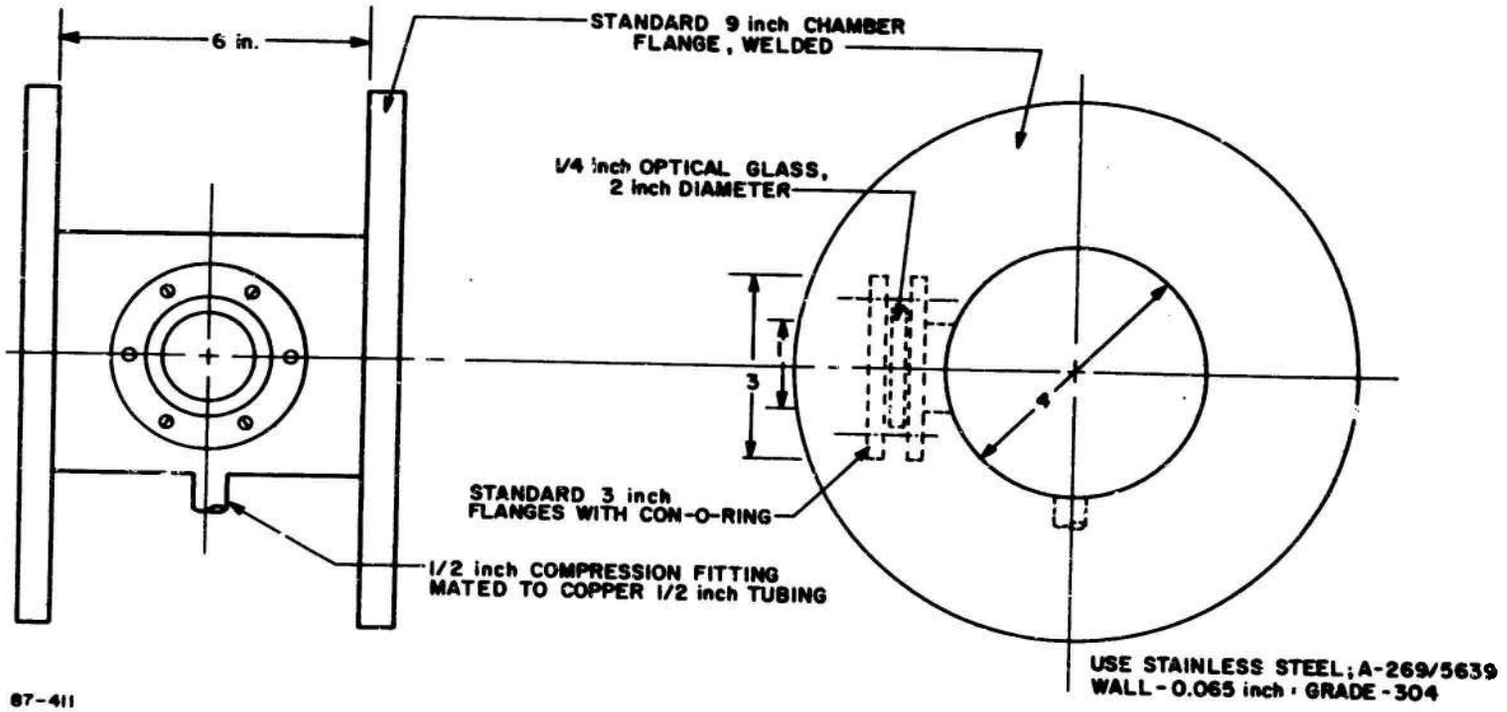

Figure 57 EXPORT CHAMBER

The export chamber is shown in Figure 57. This contains a small window through which the mixing of the aerosol can be observed. Its overall length is 6 inches.

Figure 58 shows the scattering chamber. The overall length is 20 inches, and the long side arms are 10 inches long. The short arms are 4 inches (from the center of the chamber). Figure 59 is a view of the collimating tube and the light trap which are to be attached to the chamber.

The chamber section for across-the-beam interferometry is shown in Figure 60. Figure 61 shows the aerosol inlet section. Figure 62 is a drawing of a photodiode holder which should greatly aid in the reduction of unwanted electromagnetic radiation from the holder, when short, intense laser pulses are monitored. The holder includes the capacitor which maintains the anode voltage during the photoelectric emission. Furthermore, the optical entrance to the diode also contains a screen which provides additional shielding.

This type of holder should be a marked improvement over the holder presently used, in so far as noise is concerned. It can be used in place of the holder shown in the monitor system of Figure 22.

The chamber length can be varied depending on the length of the section between the aerosol input section and the export section. The sections are simply any desired length of pipe having the standard chamber flanges welded to both sides. In this way the length of aerosol the laser beam sees for any particular experiment can be varied.

When using the scattering chamber, which is placed on the incident-laser-beam side of the aerosol input section, another section which is just as long should be placed on the opposite side. This is to ensure easier balance of flow rates at any desired operating pressure and to ensure that the aerosol is in a drifting state in the scattering chamber; that there is no turbulence which will introduce discrepancies in the data taken. Two port windows were placed at the top and bottom of the scattering chamber in order to verify this. All that is needed is a laser beam passing down the test chamber with enough power to illuminate the particles so that they can be seen. In this way, any turbulence can be easily noted.

Port windows are also provided in the aerosol export section. Using the gas laser, turbulence in the section can be noted and the flow can be adjusted in order to minimize this condition. It also provides for a quick check to ensure that the end windows are protected.

The baffles to be used between the aerosol input section and extension section, between the extension section and the export section, and between the export section and end window should be made out of light aluminum 1/16-inch thick,

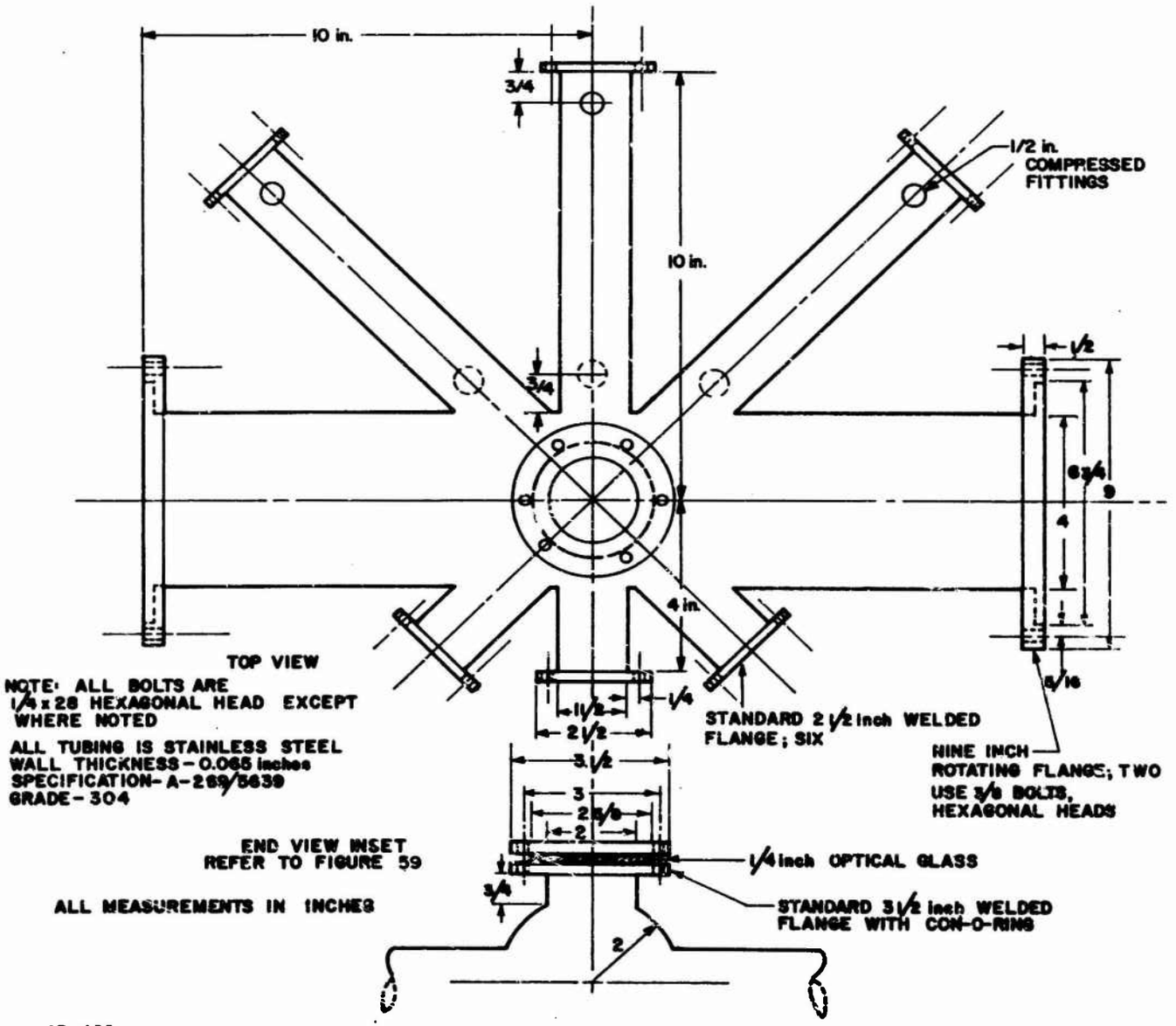

Figure 58 AEROSOL SCATTERING CHAMBER

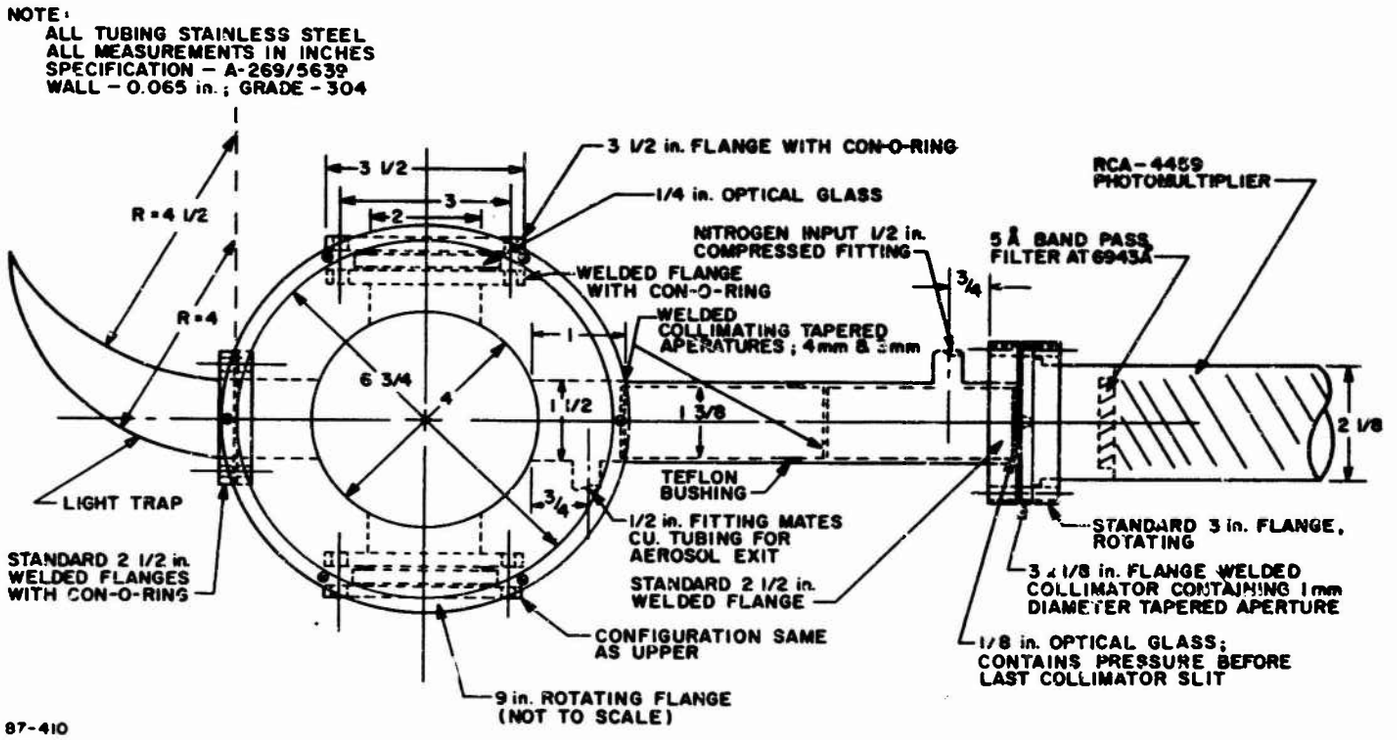

Figure 59 COLLIMATING TUBE AND LIGHT TRAP

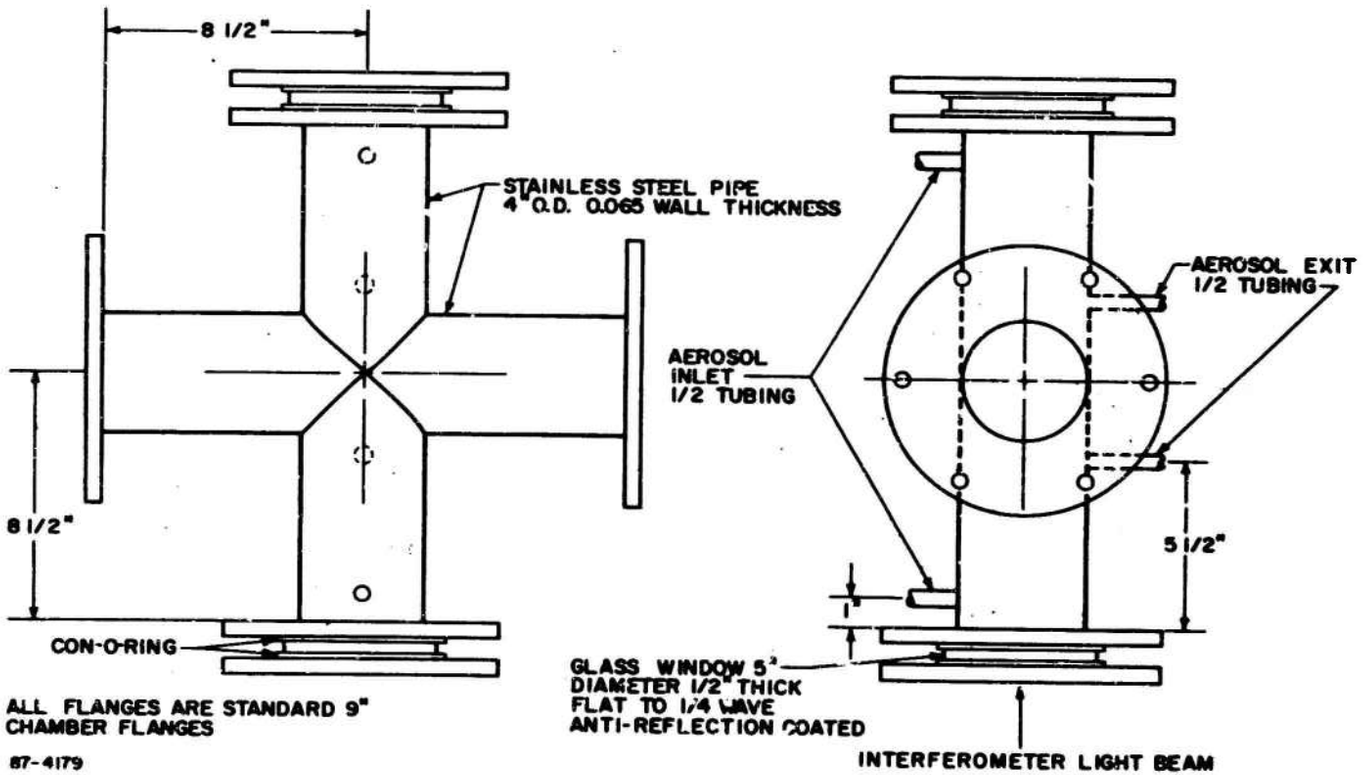

Figure 60 CHAMBER SECTION FOR INTERFEROMETRY

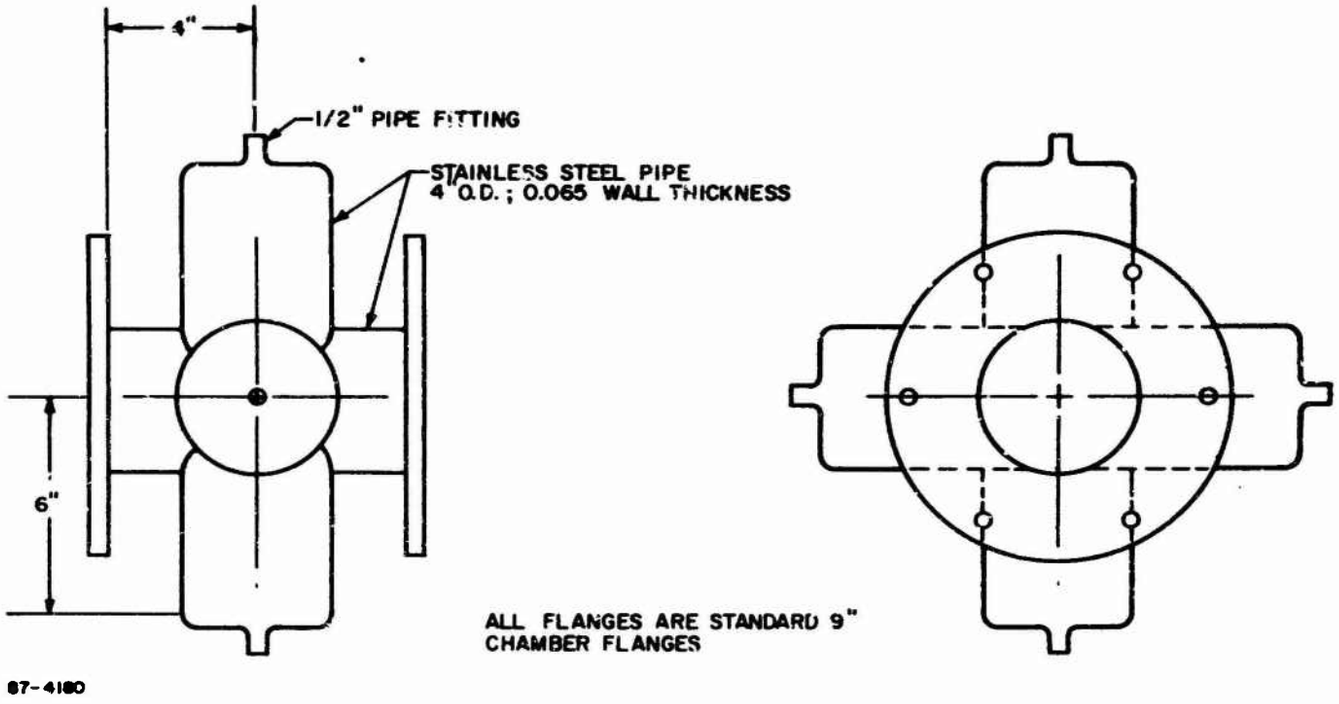

Figure 61 AEROSOL INLET SECTION

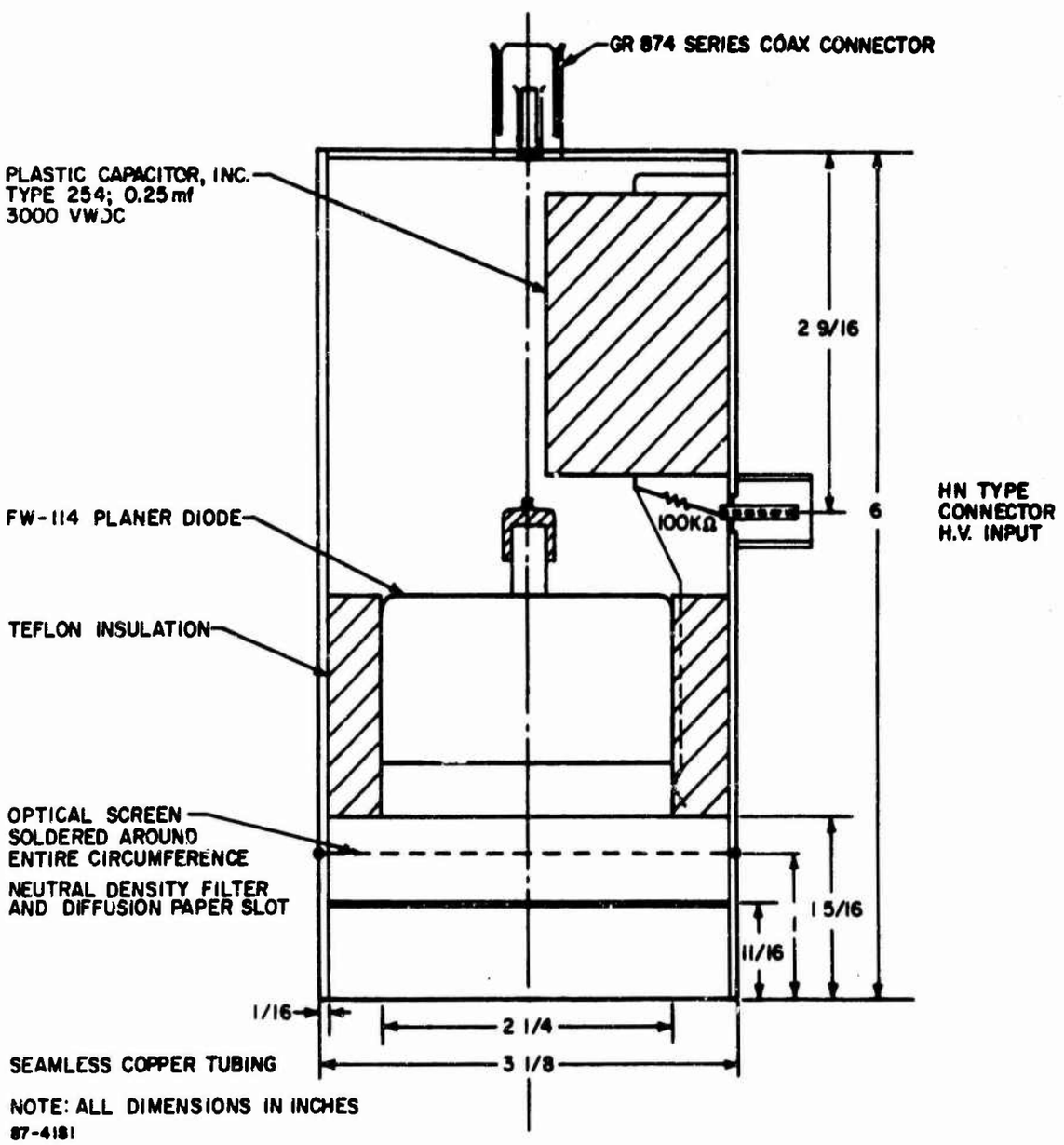

Figure 62 PHOTODIODE HOLDER

such that their overall diameter will fit inside the Con-O-Rings inside diameter; namely, 5 1/4 inches for those used on the test chamber. The actual hole in the baffle which regulates the air flow is variable and only by testing will the correct size be obtained. For a 2-inch-diameter test chamber running at a atmospheric pressure, a 1 1/4-inch opening was used for the baffle between the input section and the extension section, a 3/4-inch opening between the extension section and the export section, and a 1-inch opening between the export section and the end window. Whether, for a 4-inch-diameter chamber, the holes should be increased by twice the diameter or by twice the area to match conditions should best be answered in the laboratory.

REFERENCES

1. Wright, J. K., Proc. Phys. Soc. 84, 4, (1964).

2. American Institute of Physics Handbook, p 7-174.

3. Thompson, B. J. et al paper presented to a meeting of the American Meterological Society, April, 1965

4. Greene, H. L. and W. R. Lane. Particulate Clouds, Dusts, Smokes and Mists, London, 1957

5. Langer, G. and J. M. Pierrard, J. Colloid Sci. 18 (1963) p 95

6. Lasser, L., Zs. Angew. Physik, 12 (1960) p 157

APPENDIX

APPENDIX

A SIMPLE ANALYTICAL MODEL OF THE LASER-INDUCED BLOWOFF

1.0 Introduction

The information presently available on the interaction of laser energy with solids, at high incident fluxes and short pulse durations, is limited in scope. This is because the numerical theories of the interaction are extremely complex, and because the available experimental results are limited to relatively low energies concentrated on small areas. The following discussion involves the application of some simplifying assumptions to the problem, and the results, which are analytical, provide scaling laws which can be used to correlate more exact theoretical treatments and applicable experiments.

2.0 The Assumed Model

The present understanding of the laser interaction is that at relatively high incident fluxes, the bulk of the incident laser energy is absorbed in the vapor evaporated from the solid, rather than in the solid itself. The absorption process is primarily that of inverse Bremsstrahlung, and it is therefore not unreasonable to assume that the absorption coefficient is proportional to the square of the density of the vapor. Because the vapor formed at high intensities is essentially fully ionized, the absorption coefficient is not highly temperature dependent, so that, as a first approximation, temperature effects can be neglected.

Now, for the case in which a laser beam is incident on a plane surface at an angle of incidence θ (measured from the normal), and both the beam and the surface are infinite in extent, the intensity of the beam at a distance h from the surface is

$$' = I_o \exp - a \int_h^\infty \rho^2 \, dh' / \cos \theta \qquad (1)$$

where a is a coefficient, ρ is the density, and I_o is the intensity of the laser beam before any absorption occurs.

Under most conditions, the rate of evaporation from the surface is slowly varying, so that steady-state conditions can be assumed to prevail at the surface. If reradiation effects are neglected, then the rate of evaporation at the surface is

$$\dot{m}_o = \frac{A I_o \cos\theta \exp - a \int_0^\infty \rho^2 \, dh'/\cos\theta}{(L + 1/2\, v_s^2)} \tag{2}$$

where A is the absorptivity of the surface for optical radiation, l is the heat of vaporization per unit mass of the solid, and v_s is the velocity at which the mass leaves the surface; v_s is a function of the surface temperature, which again is not greatly dependent upon the intensity at the surface, so that v_s can be considered as essentially constant.

If it is assumed that a fraction β of the energy absorbed by the vapor is effective in accelerating the vapor in the direction normal to the surface, then the rate of change of the kinetic energy of the vapor as it moves away from the surface is

$$\frac{\partial}{\partial h} (1/2\, \rho v^3) = a \beta \rho^2 I$$

$$= a \rho^2 I_o \exp - a \int_h^\infty \rho^2 \, dh'/\cos\theta \tag{3}$$

if we neglect the contribution from the intensity reflected from the surface and from reradiation from the vapor. The former is only significant near the surface, at high laser intensities, and the latter is not as effective in heating or accelerating the vapor, because it occurs at a very short wavelength. Reradiation would affect the energy arriving at the surface, but this can be included in an effective absorptivity A.

Now, in order to integrate Equation (3), it is necessary to assume something about the flow. The simplest assumption is that the mass flow away from the surface is not a function of position. This assumption is not unreasonable, since the decrease in mass flow, with time, from the surface, as the laser beam is attenuated by the vapor layer, is compensated by the higher velocity as the vapor moves away from the surface. Under this assumption, the mass flow is

$$\dot{m} = \dot{m}_o = \rho v \tag{4}$$

and Equation (3) becomes

$$v^3 \, dv/dh = a \beta I_o \dot{m}_o \exp - a \dot{m}_o^2 \int_h^\infty \frac{dh'}{v^2 \cos\theta} \tag{5}$$

Equation (5) can be differentiated, and the exponential eliminated between the equation and its derivative, to produce the differential equation

$$d/dh\ (v^3\ dv/dh) = (a\ \dot{m}_o^2/\cos\theta)\ v dv/dh \tag{6}$$

which can be integrated once to give

$$v^3\ dv/dh = a + a\ \dot{m}_o^2\ v^2/2\cos\theta. \tag{7}$$

Now, if the laser pulse is of finite duration t, the vapor layer will expand to a distance h_m, and the velocity of the vapor at that distance will be v_m. Then, at time t, Equation (5) becomes

$$v^3\ dv/dh = I_o\ \dot{m}_o\ exp - a\ \dot{m}_o^2 \int_h^{h_m} dh'/v^2\cos\theta. \tag{8}$$

But, from Equation (7),

$$dh/v^2 = v dv/(a + a\ \dot{m}_o^2\ v^2/2\cos\theta) \tag{9}$$

so that the integral

$$a\ \dot{m}_o^2 \int_h^{h_m} dh'/v^2\cos\theta = \ln\,(a + a\ \dot{m}_o^2\ v_m^2/2\cos\theta)/(a + a\ \dot{m}_o^2\ v^2/2\cos\theta). \tag{10}$$

Thus Equation (5) becomes

$$v^3\ dv/dh = a\beta I_o\ \dot{m}_o\,(a + a\ \dot{m}_o^2\ v^2/2\cos\theta)/(a + a\dot{m}_o^2\ v_m^2/2\cos\theta), \tag{11}$$

and, from Equation (7), is obtained

$$\dot{m}_o I_o = a + a\ \dot{m}_o^2\ v_m^2/2\cos\theta. \tag{12}$$

From Equation (2) is obtained, using the integral of Equation (9) and Equation (12),

$$\dot{m}_o = \frac{A I_o\cos\theta\,(a + a\dot{m}_o^2\ v_s^2/2\cos\theta)}{(L + 1/2\ v_s^2)\ a\beta I_o\ \dot{m}_o}\ . \tag{13}$$

By elimination of "a" from Equations (12) and (13), an expression for $\dot{m}_o$ is obtained

$$\dot{m}_o = 2\beta I_o\cos\theta/\,[\,v_m^2 - v_s^2 + (2\beta/A\rho L + 1/2\ v_s^2)\,]. \tag{14}$$

Also, from Equation (13), Equation (7) can be written as

$$v^3 \, dv/dh = (a \, \dot{m}_o^2 / 2 \cos\theta) \, [v^2 - v_s^2 + (2\beta/A)(L + 1/2 \, v_s^2)] \, . \tag{15}$$

An expression for v_m in terms of the pulse duration t is still required. By applying conservation of energy, the total energy attained by the vapor, by absorption from the incident beam, is found to be:

$$E = \int_0^t \beta I_o \cos\theta \, (1 - \exp - a \, \dot{m}_o^2 \int_0^{h_m} dh'/v^2 \cos\theta) \, dt'$$

$$= 1/2 \int_0^{h_m} \rho \, (v^2 - v_s^2) \, dh' = 1/2 \, \dot{m}_o \int_0^{h_m} (v - v_s^2/v) \, dh'. \tag{16}$$

Equation (16) can be integrated with the aid of Equations (2) and (15), with the results:

$$3 \, a \, \beta \, I_o \, \dot{m}_o \, t = v_m^3 - v_s^3 \tag{17}$$

Then, by inserting the value for $\dot{m}_o$ from Equation (14), we obtain

$$I_o^2 \, t \cos\theta = (v_m^3 - v_s^3) \, [v_m^2 - v_s^2 + (2\beta/A)(L + 1/2 \, v_s^2)] \, / 6 \, a \beta^2 \tag{18}$$

as the equation relating v_m with I_o, t, and θ.

The impulse on the surface can be determined by determining the momentum of the vapor

$$J = \int_0^{h_m} \beta \, v dh' = \dot{m}_o \int dh'$$

$$= \dot{m}_o \int_{v_s}^{v_m} v^3 \, dv/(a \, \dot{m}_o^2 / 2 \cos\theta) \, [v^2 - v_s^2 + (2\beta/A)(L + 1/2 \, v_s^2)]$$

$$= (\cos\theta / a \, \dot{m}_o) \left\{ v_m^2 - v_s^2 + [v_s^2 - (2\beta/A)(L + 1/2 \, v_s^2)] \ln \left[1 + \frac{v_m^2 - v_s^2}{(2(\beta/A)(L + 1/2 \, v_s^2)} \right] \right\}. \tag{19}$$

On insertion of the value for $\dot{m}_o$ from Equation (17);

$$J = \frac{3_T \beta I_o t \cos\theta}{v_m^3 - v_s^3} \left\{ v_m^2 - v_s^2 + \left[v_s^2 - \frac{2\beta}{A} (L + 1/2\, v_s^2) \right] \ln \left[1 - \frac{v_m^2 - v_s^2}{(2(\beta/A)(L + 1/2\, v_s^2)} \right] \right\} \quad (20)$$

Equations (18) and (20) are sufficient for the determination of the impulse for all values of I_o, t, and θ. However, the assumptions used should only be valid when v_m is large compared to v_s. In this case, Equation (18) reduces to

$$I_o^2 \cos\theta\, t = v_m^{5/6}\, \alpha\, \beta^2 \quad (21)$$

and Equation (20) becomes

$$J = 3 \beta i_o t \cos\theta / v_m \quad (22)$$

from which is obtained

$$J = \frac{3 \beta^{3/5} I_o^{3/5} t^{4/5} \cos^{4/5}\theta}{6^{1/5}\, \alpha\, 1/5} \quad (23)$$

Equation (23) is the expression for the impulse per unit area as a function of pulse intensity, duration, and angle of incidence. It contains only the parameters α and β, and does not contain the absorptivity A, or the energy of vaporization $L + 1/2\, v_s^2$. This result justifies the neglect of the effect of reradiation on the rate of mass loss, and also implies that the vapor properties dominate the interaction process.

It should be pointed out that the analytical expressions in Equations (18) and (20) approach the expected value of the impulse as the pulse intensity and duration are decreased to the point that vapor absorption is negligible. In this case v_m approaches v_s, and

$$J = A\, v_s\, I_o \cos\theta\, t / (L + 1/2\, v_s^2) \quad (24)$$

as is to be expected.

3.0 Finite Beam Size

The preceding derivation is applicable to the case in which the distance traversed by the vapor, h_m, is small compared to the size of the incident laser beam. The h_m can be found by integration of Equation (15), and is

$$h_m = J/\dot{m}_o = \frac{1.5\, t}{v_m^3 - v_s^3} \left\{ v_m^2 - v_s^2 + \left[v_s^2 - \frac{2\beta}{A} (L + 1/2\, v_s^2) \right] \ln \left[1 + \frac{v_m^2 - v_s^2}{(2\beta/A)(L + 1/2 v_s^2)} \right] \right\} \left[v_m^2 - v_s^2 + \frac{2\beta}{A} (L + 1/2\, v_s^2) \right] \quad (25)$$

which approaches

$$h_m = 1.5\, v_m t = \frac{3(6)^{1/5}\ a^{1/5}\ \beta^{2/5}\ I_o^{2/5}\ t^{6/5}\ \cos^{1/5}\theta}{2} \tag{26}$$

as v_m becomes large.

Now, it is assumed that the pressure on the surface remains unchanged once h_m exceeds the beam radius. This pressure is defined by the product

$$p = \dot{m}_o\ v_m \tag{27}$$

where $\dot{m}_o$ and v_m are defined at the time when $h_m = r$.

When the expressions for the asymptotic values of v_m and $\dot{m}_o$ are used, together with Equation (26), the resultant pressure is

$$p = 3^{5/6}\ \beta^{2/3}\ I_o^{2/3}\ \cos^{5/6}\theta/2^{1/6}\ a^{1/6}\ r^{1/6} \tag{28}$$

It should be noted that changing the value of the cut-off point has only a slight effect on the pressure, since the pressure is not a strong function of r. The impulse is then

$$I = pt$$

$$= 3^{5/6}\ \beta^{2/3}\ I_o^{2/3}\ t\ \cos^{5/6}\theta\ a^{-1/6}\ r^{-1/6}\ 2^{-1/6} \tag{29}$$

4.0 Low Energy Case

At low energies, the impulse follows Equation (24). However, a finite length of time is required for evaporation to occur. This time is inversely proportional to the square of the incident intensity, so that the term t in the equations should be replaced by the term $t - t'$, where

$$t' = B/I_o^2\ \cos^2\theta \tag{30}$$

In most cases, this correction is necessary only for relatively low incident intensities and short pulse durations.

5.0 Summary

The equations that have been developed contain parameters that are best determined from either experiment or from relatively exact theoretical analyses. Since it is more convenient to work either with impulse per unit area or with coupling coefficient (impulse per unit area divided by energy incident per unit area), the results will be summarized in both these forms, for the various ranges of interest.

a. Low energy regime

Coupling coefficient

$$C = 0, \qquad t < t' \tag{31a}$$

$$C = a(1 - t'/t) \qquad t > t' \tag{31b}$$

$$t' = B/I_o^2 \cos^2 \theta \tag{31c}$$

Impulse/unit area

$$J = 0 \qquad t < t' \tag{32a}$$

$$J = a I_o \cos \theta (t - t') \qquad t > t' \tag{32b}$$

b. Short pulse regime

$$C = b(I_o^2 \, t \cos \theta)^{-1/5} \qquad h_m < r \tag{33a}$$

$$J = b I_o^{3/5} \, t^{4/5} \cos^{4/5} \theta \tag{33b}$$

c. Long pulse regime

$$C = c(I_o^2 \, r \cos \theta)^{-1/6} \qquad h_m > r \tag{34a}$$

$$J = c I_o^{2/3} \cos \theta^{5/6} \, r^{-1/6} \, t \tag{34b}$$

The constants B, a, b, and c, in the equations are to be evaluated from theoretical or experimental results. In general, the regions of validity of the equations, with increasing pulse duration or intensity, are in the order given. Figure 1 illustrates this, for constants arbitrarily chosen as B = 10^7, a = 10, b = 1000, and c = 100. These are chosen to give impulse in dyne-sec/cm^2, coupling coefficient in dyne-sec/joule, and time in seconds, with intensity in watts/cm^2. The different curves are for different radii in centimeters for an angle of incidence θ of 0 degree. In Figure 1, coupling coefficient is plotted as a function of time, for an incident intensity of 10^8 watts/cm^2.

The curve labelled $r = 0$ is Equation (31b), and labelled $r = \infty$ is (33a). Equation (33a) is also corrected for the evaporation time t'. If, for example, the beam had a 10 centimeter radius, then the coupling coefficient would follow the $r = 0$ curve for durations less than 1.5 nanoseconds. It would then follow the $r = \infty$ curve until this curve intersected the $r = 10$ curve at a pulse duration of about 500 nanoseconds. For longer pulses the $r = 10$ curve would be followed.

Unclassified
Security Classification

DOCUMENT CONTROL DATA - R & D

(Security classification of title, body of abstract and indexing annotation must be entered when the overall report is classified)

1. ORIGINATING ACTIVITY (Corporate author) AVCO Missiles, Space and Electronics Group Space Systems Division Wilmington, Massachusetts	2a. REPORT SECURITY CLASSIFICATION Unclassified 2b. GROUP

3. REPORT TITLE

A STUDY OF METHODS TO MEASURE THE EFFECTS OF A CONTAMINATED ATMOSPHERE ON THE TRANSMISSION OF A HIGH ENERGY LASER BEAM

4. DESCRIPTIVE NOTES (Type of report and inclusive dates)

5. AUTHOR(S) (First name, middle initial, last name)

Robert Schlier, Rudolf Penndorf, H. Ceccon, E. Neister, H. Dolazalek, and J. Culbert

6. REPORT DATE	7a. TOTAL NO. OF PAGES	7b. NO. OF REFS
May 1967	143	6

8a. CONTRACT OR GRANT NO.	9a. ORIGINATOR'S REPORT NUMBER(S)
DA-18-001-AMC-957(X) b. PROJECT NO.	AVSSD-0183-67-RR
c. d.	9b. OTHER REPORT NO(S) (Any other numbers that may be assigned this report)

10. DISTRIBUTION STATEMENT

Distribution of this document is unlimited.

11. SUPPLEMENTARY NOTES	12. SPONSORING MILITARY ACTIVITY
	U.S. Army Ballistic Research Laboratories Aberdeen Proving Ground, Maryland

13. ABSTRACT

This report is concerned with the transmission of a high energy laser beam through an atmosphere containing aerosols. The experimental approach consists essentially in firing a high energy laser beam through an instrumented test chamber in which various known aerosols can be introduced. Various analyses are presented of the effects which may be expected, and experiments are described to demonstrate these effects. Breadboard experiments have been performed to verify certain experimental techniques and their description with some experimental results indicating a non-linear interaction are included in this report. Finally, the specifications of an experimental test chamber in which laser beam experiments (at pressures up to 10 atmospheres) can be performed are included.

DD FORM 1 NOV 65 1473 REPLACES DD FORM 1473, 1 JAN 64, WHICH IS OBSOLETE FOR ARMY USE.

Unclassified
Security Classification

14. KEY WORDS	LINK A		LINK B		LINK C	
	ROLE	WT	ROLE	WT	ROLE	WT
High Energy Laser Beam						
Aerosols						
Test Chamber						
Aerosol Generation						
Aerosol Measurement						
Attenuation						
Scattering						
Absorption						
Time Resolved Nanosecond Pulses						
Aerosol Vaporization						
Aerosol Interaction with Laser Beam						
Differential Pulse Measurement						